Title
Investigation of Dispersion and Micrometeorology Under Spatially Inhomogeneous Conditions

Author
Qian, Wenjun

Publication Date
2010

UNIVERSITY OF CALIFORNIA
RIVERSIDE

Investigation of Dispersion and Micrometeorology Under Spatially Inhomogeneous Conditions

A Dissertation submitted in partial satisfaction
of the requirements for the degree of

Doctor of Philosophy

in

Mechanical Engineering

by

Wenjun Qian

August 2010

Dissertation Committee:
Dr. Akula Venkatram, Chairperson
Dr. Marko Princevac
Dr. Chris Dames

The Dissertation of Wenjun Qian is approved:

Committee Chairperson

University of California, Riverside

ACKNOWLEDGEMENTS

I would like to express my greatest thanks to Professor Akula Venkatram, advisor of this work, for not only the guidance of my research, but also encouragement and inspiration in every aspect of my life. After five years of PhD study with Professor Venkatram, I feel prepared to enter the next stage of my professional life.

I appreciate my committee members, Professor Marko Princevac and Professor Chris Dames, for their insightful comments and recommendations on my dissertation. Special thanks should go to Professor Marko Princevac and his research group, who made major contributions in collecting and preparing the data sets I have been using for my research. Professor Marko Princevac also patiently revised my journal papers with his expertise.

I am grateful to the former colleagues in University of California at Riverside, Dr. Sang-Mi Lee, Dr. Tao Zhan, Dr. Xiangyi Li, and current colleagues Qiguo Jing, Si Tan, Karim Alizad, Hansheng Pan, and Sam Pournazeri, for their constant help and contribution to my research. I am thankful to all the other graduate students in the Mechanical Engineering Department, especially Xin Xue, with whose company my five years PhD study is enjoyable and memorable.

Finally and most importantly, I would like to thank my parents for their endless love and greatest support, which always encourage me to conquer the difficulties and pursue higher goals everyday.

DEDICATION

To my father Cailong Qian,

and my mother Jianying Jiao.

ABSTRACT OF THE DISSERTATION

Investigation of Dispersion and Micrometeorology Under
Spatially Inhomogeneous Conditions

by

Wenjun Qian

Doctor of Philosophy, Graduate Program in Mechanical Engineering
University of California, Riverside, August 2010
Dr. Akula Venkatram, Chairperson

This dissertation summarizes the results from a study to develop and evaluate models to estimate dispersion of pollutants in boundary layers whose properties change with downwind distance. Such boundary layers occur at the interface between rural and urban areas, and water and land bodies.

I first developed a method to estimate the meteorological inputs required to apply the current generation of dispersion models, such as AERMOD, to urban areas. This method uses measurements made at a single level on a tower located in an urban area, and is based on the assumption that similarity methods applicable to spatially homogeneous conditions are locally valid even in an inhomogeneous urban area. I show that under unstable conditions, measurements of temperature fluctuations improve upon commonly used energy balance methods to estimate heat flux. Also, any bias in heat flux estimates has a minor effect on the prediction of surface friction velocity and turbulent velocities.

I examined a method to estimate urban micrometeorology using measurements made on a tower located in an upwind suburban area. I applied an internal boundary layer model to trace the evolution of the boundary layer as it traveled from the suburban measurement location to the urban location of interest. Estimates from the model were observations made during a field study conducted in Riverside, CA. Estimates of friction velocity compare well with urban measurements only when the variation of friction velocity with height within the urban canopy was accounted for.

I examined the performance of two steady-state dispersion models in explaining concentrations measured during field studies designed to study low wind speed conditions typical of urban areas. One model is based on the numerical solution of the two-dimensional mass conservation equation and the other is AERMOD, which accounts for low wind speeds by including wind meandering. The numerical method performs better than AERMOD through a justifiable description of the interaction between dispersion and the gradient of the wind speed near the surface. Including wind meandering, which occurs under low wind speeds, improves the performance of the numerical model. As part of this study, I developed a method to improve estimates of surface friction velocity during low wind speeds.

The last model is applicable to elevated sources, such as power plants, situated close to shorelines. It is designed to be compatible with AERMOD (Cimorelli et al., 2005), the USEPA's regulatory model that is currently designed for spatially homogenous conditions. The semi-empirical shoreline dispersion model accounts for plume entrainment by the thermal internal boundary Layer (TIBL), whose height increases with distance from the shoreline. I show that AERMOD can be modified to account for two-dimensional shoreline effects, and this modified model performs as well in explaining observations as dispersion models specifically designed for shoreline sources. I also developed a method to generate meteorological inputs that are compatible with the current structure of AERMOD's inputs.

TABLE OF CONTENTS

LIST OF FIGURES

1. INTRODUCTION AND OBJECTIVES

1.1 Problem Area

Worldwide urbanization has inspired many studies on the meteorology and air quality of urban areas (McElroy and Pooler, 1968a and 1968b; Rotach, 1995; Allwine et al. 2002; Allwine et al. 2004; Grimmond et al. 2004; Rotach et al. 2005; Mestayer et al. 2005; Hanna et al. 2006). Urban buildings exert drag on the air flow, which decreases the wind speed and increases the turbulence levels (Britter and Hanna, 2003) relative to those in the upwind rural boundary layer. The buildings and pavements in urban areas with higher thermal conductivities and heat capacities store more energy and also cool down more slowly than rural surfaces (Mitchell, 1961), Anthropogenic heat production is also higher in urban areas than in rural areas (Bornstein, 1968). These processes result in the urban area being warmer than its surroundings, which is widely known as the heat island effect (Oke, 1988). The upward heat flux that results when rural air flows onto the warmer, rougher urban surface increases the turbulence levels that are already enhanced by urban roughness elements. . The dispersion of pollutants over the urban area is affected by the decreased wind speed and increased turbulence relative to upwind rural area. The presence of buildings also affects the mean flow through channeling effects. The major objective of the research described in this thesis is to study these urban induced effects on the atmospheric boundary layer in the context of dispersion of pollutants. The second objective of this thesis is to understand the effects of horizontal spatial inhomogeneity on flow and dispersion.

Most of our current understanding of the atmospheric boundary layer and dispersion is based on field studies designed to ensure homogeneous surface conditions. The flow is independent of horizontal position but varies with vertical height so that the advection terms can be neglected in the governing equations (Kaimal and Finnigan, 1994). The height of the atmospheric boundary layer and the turbulence levels are controlled by the shear stress and heat flux at the surface. In the surface layer, which lies in the lowest 10% of the atmospheric boundary layer over homogenous surface, the decrease of the turbulent fluxes and stresses with height is assumed to be negligible. Meteorological variables such as wind speed and temperature only vary in the vertical direction. Under these conditions, simple "similarity" theories have been developed to describe profiles of the mean variables and turbulence statistics as a function of height and a few key parameters such as the roughness length, the surface shear stress, and the surface heat flux.

This thesis examines the applicability of these similarity theories to the horizontally inhomogeneous urban area. It also examines dispersion in the internal boundary layer that forms when a boundary layer in equilibrium with one surface flows over another surface with different surface characteristics. The next section describes the background and terminology required to understand my research in this dissertation.

1.2 Background

1.2.1 Vertical structure of the urban boundary layer

The atmospheric or planetary boundary layer (ABL or PBL) is the turbulent layer next to the earth's surface. The turbulence is produced by shear stresses associated with gradients in the horizontal wind and vertical motion induced by buoyant air parcels rising from the surface heated by solar radiation. The boundary layer height is about hundred meters during the night and about 1000 meters during the daytime.

The internal boundary layer (IBL) is caused by a discontinuity in surface properties, such as surface roughness or heat flux. It is a layer within which the PBL adjusts to the new surface properties.

The thermal internal boundary layer (TIBL) is associated with flow across a discontinuity in surface temperature/heat flux. It is usually related to air flow from a cool water surface to warmer land.

The urban boundary layer (UBL) is the internal boundary layer that is formed when air flows from a rural area to an urban area. The surface roughness increases from rural to urban areas, and the urban surface temperature is usually higher than the rural temperature. Figure 1.1 shows the structure of the urban boundary layer, which is adapted from Grimmond and Oke (2002).

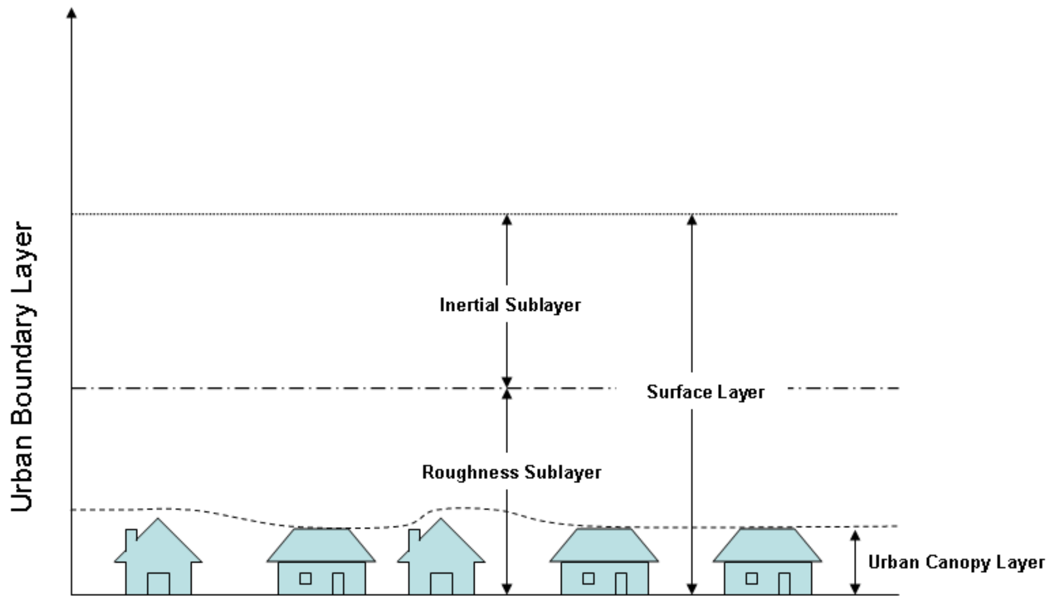

Figure 1.1: Structure of the Urban Boundary Layer (adapted from Grimmond and Oke, 2002)

The surface layer is usually defined to be the lowest 10% of the boundary layer, where turbulent fluxes vary less than 10% in magnitude with height. The Monin-Obukhov similarity theory (Monin and Obukhov, 1954) is applicable when the fluxes can be considered to be constant. The surface layer over urban areas can be divided into two sublayers: an inertial sublayer and a roughness sublayer.

The roughness sublayer (RSL) is the region where flow is directly influenced by the roughness elements. In this layer, the turbulence field is inhomogeneous and the flow is highly irregular. The depth of the RSL from laboratory and field experiments was reviewed by Roth (2000). Raupach et al. (1991) gave a range of RSL height to be 2~5 times the average roughness element height.

The inertial sublayer (ISL) is the region in which the air flow is not influenced by single roughness elements. The flow can be considered to be horizontally homogeneous and the fluxes nearly constant with height. Monin-Obukhov similarity theory usually applies to this layer. However, the RSL can be tens of meters over the urban area, while the ISL is “squeezed” or does not exist (Cheng and Castro, 2002).

The urban canopy layer (UCL) is the region below the average building height, and is the lowest part of the RSL. Some researchers, such as Rotach (1993), define the lower boundary of the RSL as the top of the UCL. The micro-scale processes within the street canyons between the buildings dominate the UCL (Oke, 1988). The mean flow and turbulence are controlled by the geometry of immediate buildings and street canyons.

1.2.2 Review of Past Studies

In the past 15–20 years, several field studies have been conducted to study the urban boundary layer and dispersion in it. Examples include the Zürich urban experiment (Rotach 1995), the Basel Urban Boundary Layer Experiment (BUBBLE) (Rotach et al. 2005; Christen 2005), the Marseille field experiment (Mestayer et al. 2005; Grimmond et al. 2004), and the London field experiment known as Dispersion of Air Pollutants and their Penetration in Local Environments (DAPPLE) (Arnold et al. 2004). A series of urban experiments were conducted and sponsored by the U.S. Department of Homeland Security (DHS) and the U.S. Defense Threat Reduction Agency (DTRA), in collaboration with other agencies and institutions in the U.S., Canada, and the U.K. The Salt Lake City (SLC) Urban 2000 (Allwine et al. 2002), the Oklahoma City Joint Urban (JU) 2003 (JU2003, Allwine et al. 2004) and the New York City Madison Square Garden 2005 (MSG05, Hanna et al. 2006) are all part of the series.

Analysis of data from these field studies have contributed to better understanding of the urban boundary layer. From the Zürich urban experimental data, Rotach (1993 I) found that the Reynolds stress is close to zero near the ground and increases with height up to about twice the average building height. Rotach (2001) also proposed a profile for the local friction velocity in the RSL as a function of the friction velocity in the ISL and the height non-dimensionalized by the RSL height. However, studies (Rotach 1993 I; Oikawa and Meng 1995; Feigenwinter et al. 1999) show that the height at which friction velocity, u_*, attains its maximum and the shape of the u_* profile vary with stability. The u_* profile is different for along canyon flow and cross canyon flow (Christen et al. 2002). Christen and Rotach (2004) examined data from one of the urban sites, Basel-Sperrstrasse, from BUBBLE experiment. They found that averaged u_* profile agrees well with that proposed by Rotach (2001), while the agreement is poor for nocturnal cold air drainage flow sector.

The RSL height is also a subject of much debate. Raupach et al. (1991) gave a range of RSL height to be 2 to 5 times average roughness element height. Roth (2000) provided a comprehensive review of more than 10 formulae for the RSL height derived from tall vegetation and rough-wall wind-tunnel studies. Relevant length scales to determine the RSL height include element heights, horizontal spacing between elements, roughness length and displacement height. However, in real urban areas when building heights are variable, the RSL might be tens of meters high and the ISL may not even exist (Rotach

1999; Cheng and Castro 2002). The uncertainties in the shape of the u_* profile within the RSL and the RSL height make it difficult to estimate u_* from routine wind measurements.

Wind and temperature profiles have been proposed for the RSL (e.g. Garratt, 1980, 1992; Harman and Finnigan, 2007). However, these profiles are functions of parameters that are dependent on stability and canopy characteristics (Garratt, 1980, 1983; Harman and Finnigan, 2007), which makes it difficult to apply them in practical applications. The wind speed profile inside the urban canopy is similar to that observed in plant canopies. Cionco (1965) showed that observations are consistent with estimates from a semi-empirical model that predicts an exponential velocity profile inside a vegetative canopy. MacDonald (2000) showed good agreement between an exponential profile and the spatially averaged velocity profile from their Building Research Establishment (BRE) wind tunnel experiment for low frontal area density of obstacles ($\lambda_f < 0.3$). He also related the attenuation parameter, a, in the exponential profile with the λ_f so that the wind speed within the canopy can be calculated if the wind speed at the building height is available.

Considering the uncertainties in the research-grade u_* profile and wind speed profile, it is difficult to apply them for practical purposes. On the other hand, there is some evidence that modified similarity functions might still be applicable in the RSL. Rotach (1999) find that Monin-Obukhov Similarity Theory (MOST) can be used to describe the wind and temperature profile in the upper part of RSL if the scaling variables such as surface friction velocity (u_*) and Obukhov length (L) are computed using local values of shear stress and heat flux. Oikawa and Meng (1995) reported good agreement with MOST at 0.77 of the canopy height for a suburban roughness sublayer. Kastner-Klein and Rotach (2003) observed that the logarithmic profile is valid above twice of the displacement height in the wind tunnel study of Nantes, France. Further studies are needed to examine whether MOST can provide useful estimates for dispersion models when the underlying surface is inhomogeneous.

Surface heat flux is another important input to dispersion models. For homogeneous surfaces, surface heat flux is usually estimated from energy balance methods, which depend on the parameterization of incoming and outgoing shortwave and longwave radiation and partitioning of the net radiation at the ground among ground heat flux, sensible heat flux and latent heat flux. A common approach to this portioning is based on assuming that the ratio of the sensible to the latent heat flux, the Bowen ratio, can be estimated from land use data. However, studies have shown that the Bowen ratio can vary substantially both spatially as well as temporarily (Ching, 1985; Roth and Oke, 1995). Besides, sensible heat can be absorbed and released from the urban canopy air, trees, buildings and the ground (Grimmond et al. 1991). This term, which is called the storage heat flux, is an important term in the surface energy balance. Prediction of the storage heat flux is required to model sensible heat flux correctly. Objective Hysteresis Models (OHM) are often used to predict the non-linear loop-like relationship between the storage heat flux and net radiation (Camuffo and Bernardi, 1982; Grimmond et al. 1991; Grimmond and Oke 1999a). The procedure to apply the OHM is time-consuming and the information is not always available: a survey of the areal coverage of different surface types is needed; a list of the model coefficients for different surface types is required (e.g. Table 4 of Grimmond and Oke 1999a). So the final coefficients for the OHM model are site specific since they are weighed according to the proportion of each surface type for that area. Alternative methods, other than the surface energy balance method, are needed to predict surface heat flux over urban areas.

Due to the drag of buildings, urban areas always experience lower wind speeds than rural areas. Low wind speed conditions are critical because pollutants build up during these conditions. During low wind speed conditions, meandering due to mesoscale motions, such as low-level jets, mesoscale wind systems, breaking gravity waves and density currents (Salmond and McKendry, 2005), can dominate dispersion in the horizontal. Meandering of the wind cannot be readily related to local measurements, and turbulent velocity fluctuations in the vertical become uncorrelated with the surface friction velocity.

Developing dispersion models dealing under low wind conditions still remains challenging. Several models have been developed since the 1970s. Sagendorf and Dickson (1974) used a segmented plume method which accounts for meander by dividing each test (1 hour) into small intervals (2 min) and calculating separately for each interval. Sharan and Yadav (1998) used variable eddy diffusivities including longitudinal diffusion in an analytical solution of the three-dimensional advection-diffusion equation. They showed that using 2-min intervals with a dependency of the eddy diffusivities on observed wind direction fluctuations gave the best results. Lagrangian particle models have been used to simulate dispersion under low wind speed conditions by various authors (Brusasca et al. 1992; Oettl et al. 2001; Anfossi et al. 2006). The success of all these methods depends on having both mean and turbulence information at short time intervals.

The growth of industry near shorelines has created a need for dispersion models that can handle the meteorology over two surfaces with different characteristics. Valuable shoreline data sets have been collected since 1970s from experiments such as the Lake Michigan experiment (Lyons, 1977), the Long Island experiment by the Brookhaven National Laboratory (Raynor et al., 1979), the Kashimaura (Japan) experiment (Gamo, 1981; Gamo et al., 1982), and the Nanticoke (Canada) experiment (Portelli, 1982).

These studies show that the thermal internal boundary layer (TIBL) grows with $x^{1/2}$, where x is the downwind distance from the shoreline (Van der Hoven, 1967; Raynor, 1975). The models (Venkatram, 1977; Plate, 1971) that have been proposed to explain this behavior assume that the heat flux that drives the growth of the TIBL varies little with distance from the shoreline. This assumption has not been evaluated with observations. Furthermore, there are no good methods of estimating the surface heat flux over the land.

Several shoreline dispersion models have been developed since the 1970s that account for the interaction between the plume and the growing TIBL. Lyons and Cole (1973) were one of the first to develop a model to account for the entrainment of an elevated plume by the growing TIBL. Van Dop et al. (1979) and Misra (1980) improved the model through a more physically realistic treatment of the entrainment process. Misra and Onlock (1982) evaluated this model using data from the Nanticoke experiment.

1.3 Motivation and Objectives

AERMOD is currently the most widely used dispersion model in the United States because the USEPA recommends it as the model of choice for regulatory applications.

AERMOD is also used for non-regulatory applications, such as risk assessment, because it incorporates the state-of-the-art in dispersion and micrometeorology, it is available at no cost and is relatively easy to use. However, the model is not designed to treat situations governed an internal boundary layer such as the one encountered at the land-water interface. There is a need for modifications to AERMOD and its meteorological processor, AERMET, to allow its application to such situations.

Wind and Reynolds stress profiles have been proposed to relate local meteorology within the RSL to those in the ISL. However, in real urban areas where building heights are variable, the RSL might be tens of meters high and the ISL may not even exist (Rotach 1999, Cheng and Castro 2002). It would be difficult or even impossible to measure variables in the ISL. Furthermore, the shapes of the profiles are dependent on stability and wind flow directions (Rotach, 1993 I; Oikawa and Meng, 1995; Feigenwinter et al., 1999; Christen et al., 2002). Siting anemometers in an urban area is difficult because no site is representative in a complex setting (Hanna et al., 2007). There is a need for methods of estimating meteorological inputs for dispersion models from local routine measurements within the RSL.

Another approach to estimate urban meteorology is from more available rural/suburban measurements. A two-dimensional internal boundary-layer (IBL) model was evaluated by Luhar et al. (2006) using data from the Basel Urban Boundary Layer Experiment (BUBBLE) conducted in the city of Basel, Switzerland (Rotach et al., 2005). It is assumed that Monin-Obukhov similarity theory is valid within the IBL over an urban area. Thus, meteorological variables estimated by the IBL model may only compare well with observation in the ISL. Combination of the IBL model and the RSL profiles is needed in order to estimate meteorology within the RSL from rural/suburban measurements.

The review shows that we can make realistic estimates of concentrations under low wind speed conditions if measurements of turbulence levels are available. Meteorology averaged about several minutes seems to be able to capture the meandering component of the flow. But such detailed measurements are not routinely available for regulatory modeling, and turbulence levels have to be estimated from mean wind speeds, usually measured at one level. Methods are needed to estimate meteorological inputs required to estimate concentrations when the surface wind speeds are low.

The specific objectives of the research described in this dissertation are:

1. Develop methods to estimate meteorological inputs for dispersion models, such as AERMOD, using measurements of wind speed and temperature on an urban tower.

2. Develop methods to estimate urban meteorology using routine measurements made in upwind rural/suburban areas. These methods are motivated by the need to apply dispersion models in locations where meteorological inputs have not been measured.

3. Develop and evaluate a steady state dispersion model that can be applied to low wind speed conditions, typical of urban areas, using routinely available meteorological inputs.

4. Modify AERMOD and its meteorological processor, AERMET, to allow its application to sources located in areas where the micrometeorology is governed by the internal boundary layer.

1.4 Structure of the Dissertation

Chapter 2 describes methods to estimate meteorological inputs for modeling dispersion during convective conditions. Chapter 3 describes research in estimating urban dispersion meteorology from suburban values. Chapter 4 examines steady-state dispersion models under low wind speed conditions. Chapter 5 presents research in the shoreline dispersion model. Chapter 6 provides the major conclusions resulting from my research.

2. USING TEMPERATURE FLUCTUATION MEASUREMENTS TO ESTIMATE METEOROLOGICAL INPUTS FOR MODELLING DISPERSION DURING CONVECTIVE CONDITIONS IN URBAN AREAS

2.1 Introduction

This study is motivated by the need for methods to estimate meteorological inputs, such as surface friction velocity and heat flux, required by the current generation of dispersion models such as AERMOD (the American Meteorological Society/Environmental Protection Agency Regulatory Model, Cimorelli et al., 2005). One can, in principle, make relatively simple measurements of mean wind and temperatures on a tower at one or preferably more levels, and derive these parameters using Monin-Obukhov similarity theory (MOST) (van Ulden and Holtslag, 1985). However, the application of MOST is generally justified when the surface roughness is relatively uniform in the upwind fetch of the tower for distances of about 100 times the measurement height (Wieringa, 1993). Such idealized conditions are rarely met in practice especially in urban areas where dispersion models still have to be applied. One way of estimating meteorological inputs for urban areas is to model the internal boundary layer that develops when rural boundary layer flows over an urban area. Luhar et al. (2006) used this approach to estimate urban parameters in Basel, Switzerland, from measurements made in relatively uniform upwind rural areas. Although such methods have undergone limited evaluation with observations, they are not yet reliable enough for routine dispersion applications. The more empirically acceptable approach is to derive the meteorological inputs from measurements made close to the location where the dispersion model is applied. Thus, the relevant question addressed in this paper is whether MOST can provide useful estimates even when the location of the measurement tower is far from ideal.

The measurements analyzed in this paper most probably lie in the roughness sublayer (RSL) of the urban area we are considering. We realize that MOST parameterizations are likely to be valid only in the inertial sublayer (ISL), where the flow can be considered in equilibrium with the underlying rough surface and turbulent fluxes are close to constant. The roughness sublayer (RSL) is about 2 to 5 times the average building height (Raupach et al., 1991), which lies below the inertial sublayer. Wind and temperature profiles have been proposed for the RSL (e.g. Garratt, 1980, 1992; Harman and Finnigan, 2007). However, these profiles are functions of parameters that are dependent on stability and canopy characteristics (Garratt, 1980, 1983; Harman and Finnigan, 2007), which makes it difficult to use them in practical applications. Furthermore, methods proposed by Rotach (1999) require measurements at the top of the RSL, which might be tens of metres high or might not even exist in an inhomogeneous urban area (Kastner-Klein and Rotach, 2004).

There is some evidence that a modified MOST might apply in the RSL. Rotach (1999) find that MOST can be used to describe the wind and temperature profile in the upper part of RSL if the scaling variables such as surface friction velocity (u_*) and Obukhov length (L) are computed using local values of shear stress and heat flux. Oikawa and Meng (1995) reported good agreement with MOST at 0.77 of the canopy height for a suburban roughness sublayer.

As far as we know, Hanna and Chang (1992) is the only study that used MOST to estimate meteorological inputs for modelling dispersion in urban areas. They estimated the sensible heat flux in several urban areas using a surface energy balance proposed by Holtslag and van Ulden (1983). Energy balance methods depend on the parameterization of incoming and outgoing shortwave and longwave radiation and partitioning of the net radiation at the ground among ground heat flux, sensible heat flux and latent heat flux. A common approach to this portioning is based on assuming that the ratio of the sensible to the latent heat flux, the Bowen ratio, can be estimated from land use data. Holtslag and Van Ulden (1983) suggest a more physically realistic method, the Penman-Monteith approach (Monteith, 1981), to account for the variation of Bowen ratio with surface moisture conditions. In urban areas, sensible heat can be absorbed and released from urban canopy structures. Several authors (Camuffo and Bernardi, 1982; Grimmond et al. 1991; Grimmond and Oke 1999) have suggested models, sometimes referred to as Objective Hysteresis Models (OHM), to predict the non-linear relationship between storage heat flux and net radiation.

Hanna and Chang (1992) found that relative errors in estimating micrometeorological parameters were about 20%, but could be much larger during stable conditions when the surface friction velocity, u_*, was less than 0.2 m s^{-1}. They show that their energy balance method is sensitive to the partitioning of sensible and latent heat fluxes (Bowen ratio), and cloud cover, information that is generally unavailable and/or unreliable.

The questions addressed by this paper are: Can measurements of mean wind speed and temperature fluctuations reduce the uncertainties associated with the energy balance method to estimate surface micrometeorology? How far can we push MOST in urban areas to estimate meteorological inputs for dispersion models?

The study described here extends earlier studies (Princevac and Venkatram, 2007; Venkatram and Princevac, 2008) on the performance of methods to estimate the surface friction velocity and turbulent velocities in unstable conditions. These estimates depend on the surface heat flux, which can be estimated with measurements of temperature fluctuations using the free convection relationship proposed by Monin and Yaglom (1971) for σ_T / T_*, where σ_T is the standard deviation of the temperature fluctuations, and the temperature scale, T_*, is the ratio of the kinematic surface heat flux to the surface friction velocity, i.e. $T_* \equiv -\overline{w'T'} / u_*$.

In the current study, we examine methods to improve these estimates using formulations such as that proposed by Tillman (1972), who showed that the free convection estimate could be improved through a function of $\zeta = z/L$, which in turn was related to the skewness of temperature fluctuations. Here L is the Obukhov length and z is the effective distance from the ground obtained by subtracting the zero-plane displacement from the measurement height.

Other investigators have also evaluated this approach for different surface types and stability ranges and proposed different forms for σ_T / T_*. Albertson et al. (1995) suggest that σ_T should be measured above the blending height (i.e. above the roughness wake layer to apply the free convection approach. Wesely (1988) and Hsieh et al. (1996) show that the free convection relationship applies over non-uniform surfaces with slight modifications to the constant in the relationship. Weaver (1990) concludes that if the flux is small or the surface is non-uniform, it is necessary to adjust the σ_T / T_* relationship for land use type.

The results presented by Lloyd et al. (1991) suggest that Tillman's (1972) correction for deviation from free convection is not necessary. On the other hand, De Bruin et al. (1993) confirmed the findings of Tillman (1972) on the usefulness of accounting for shear effects.

Most of the previous publications applied the above heat flux estimation methods for bare soil, grass, shrub or forest. This study examines the applicability of these methods to sites located in urban areas, where the assumptions that underlie them do not necessarily hold. The current study is similar to that of De Bruin et al. (1993) in that it uses measurements of wind speed and temperature fluctuations. We also examine the impact of the uncertainty in estimating heat flux on modelling concentrations associated with surface releases.

We next describe the field study used to collect the data analyzed in this paper.

2.2 Field Study

The meteorological data used in this study were measured at three sites in Riverside County, California, in 2007. The three sites lie along an east-west transect designed to make measurements of the evolution of the night-time boundary layer embedded in the easterly wind as it passed through a suburban site, an urban site, and then back to a downwind suburban site.

Site US (upwind suburban) is in a desert plain in Moreno Valley. There is a residential area to the north and east of the measurement tower. To the west and south of the site is grassland (nearly desert) up to 500 m, with sparse trees and houses further upwind.

Site DS (downwind suburban) is on top of a bluff located above the Santa Ana River in suburban Riverside. It is surrounded by mixture of bushes, grasses and sparse trees. Residential areas are at least 1 km away. However, there is one building to the west of the measurement tower. The distance between the building and the tower is about 20 m. The height, width and length of the building are about 4 m, 15 m and 15 m, respectively. As indicated later, this building might play an important role in determining the aerodynamic roughness length for the DS site.

Site CU (centre urban) is located on the street corner of Arlington and Brockton in downtown Riverside. It is surrounded by low-rise buildings that do not vary in much height in all directions up to 2 km. Sites US and CU are 18 km apart and sites CU and DS are 9 km apart.

All three measurement sites are in relatively open areas surrounded by buildings and trees. Using Google maps, we used information within a 2 km radius of the measurement site to estimate the average building height (H_B), the plan area fraction, λ_p, and the frontal area fraction, λ_f, listed in Table 2.1. These parameters have been converted into aerodynamic roughness length and zero-plane displacement, z_0 and d_h, using formulations proposed by Grimmond and Oke (1999). Because there is only one building close to the DS site, λ_p and λ_f cannot be calculated for this site.

We realize that these estimates of the aerodynamic roughness length and zero-plane displacement would have relevance to the calculation of micrometeorological variables if the measurements and the associated site met criteria for the applicability of MOST. In our case, these estimates are only meant to provide bounds on the values of z_0 and d_h obtained by fitting MOST profiles to the observed wind speeds during near neutral conditions. This fitting process is described in a later section.

Table 2.1 Morphological parameters for the three sites and z_0 and d_h based on these parameters

Sites	H_B (m)	λ_p	λ_f	z_0 (m)	d_h (m)
US	4	0.15	0.03	0.12	0.36
DS	4	NA	NA	0.02 – 0.4	0 – 2.0
CU	4	0.3	0.1	0.4	1.7

Each site was equipped with a 3 metre tower instrumented with (1) a sonic anemometer (CSAT3, Campbell Sci.), (2) two soil heat flux plates (HFP01SC-L Hukseflux), (3) an infrared thermometer (IRTS-P Apogee), (4) a krypton hygrometer (KH20, Campbell Sci.), (5) two soil temperature probes (TCAV-L, Campbell Sci.), (6) a water content reflectometer (CS616-L, Campbell Sci.), (7) two air temperature sensors (109- L, Campbell Sci.), and (8) site US had a net radiometer (CNR1, Kipp & Zonen). The sampling rate for sonics is 10 Hz. We programmed the data loggers to set warning flag high for cases of NaN, lost trigger, no data, an Synchronous Device for Measurement (SDM) error, or wrong sonic (CSAT3) embedded code. During post processing we performed data unification with additional control where all data lines flagged as suspicious (diagnostic warning flag is high) are removed (this happened in negligibly small number of cases, i.e. <0.1%).

Delays were introduced into sonic and hygrometer readings to ensure that all the measurements were made at the same instant in time. All the cross products are rotated into natural wind coordinates in post processing, as described in Kaimal and Finnigan (1994).

Data were collected from the early February through late April 2007 at Site CU. Sites US and DS were run for shorter periods of time during mid-March through late April 2007 and late March to the end of April 2007, respectively. The analysis that follows is based on 1 hour averaged data from the sonic anemometers. Under rainy conditions, some of the anemometer measurements of shear stress and sensible heat flux were unreasonably high. After excluding such conditions, there are 526, 577 and 670 hours of data for the US, DS and CU site respectively, within which we analyze 179, 215 and 247 hours corresponding to daytime (9:00 to 17:00) unstable conditions. The stability (z/L) range is -4×10^{-4} to -18 for the US site, -3×10^{-4} to -7 for the DS site and -10^{-3} to -3 for the CU site. We determined to exclude the night-time unstable conditions in this paper because stable periods intermittently mix with unstable periods, which deteriorates the performance of methods suitable for unstable conditions only. The measurement height is 3 m for all sites.

A detailed examination on the wind directions corresponding to daytime unstable conditions shows the flux footprint of each site. For the US site, the wind direction covers a wide range from 150-360 degrees, which suggests that the land use footprint of the US site might be characteristic of grassland. For the DS site, the prevailing wind sector is from 230-360 degrees, and the secondary wind sector is from 0-60 degrees, which occurs about 15% of the time. The flow at the DS site is mostly influenced by a nearby building.

Bushes, grass, and sparse trees have a secondary impact on the flow. For the CU site, the wind direction is mostly within the 260-360 degrees range. As the CU site is surrounded by buildings in all directions, the footprint of the flow at the CU site is considered to be characteristic of urban land use in cities located in the United States. However, the site is not typical of the built up downtown areas of large cities, which are often dominated by skyscrapers located within a ten block area (e.g. New York City).

Here we do not examine the relationships among measurements made at these different sites, but focus on methods for estimating micrometeorological variables using routine observations at these sites.

2.3 Analysis of Observations

In the first step in the analysis of the data, we examined the applicability of MOST to the measurements from the suburban and urban sites, which, in principle, do not meet criteria for horizontal homogeneity.

The performance of the models considered here can be described using a variety of statistics, described in Chang and Hanna (2004). We have chosen to use the geometric mean (m_g) and the standard deviation (s_g) of the ratios of the observed to modelled variable as the primary measures of model performance because they can be readily interpreted (Venkatram, 2008). They are defined as:

$$m_g = \exp\left(\langle \varepsilon_m \rangle\right) \tag{2.1a}$$

$$s_g = \exp\left(\sigma\left(\varepsilon_m\right)\right) \tag{2.1b}$$

where $\langle\ \rangle$ and σ represent mean and standard deviation respectively, and ε_m is the residual between the logarithms of model estimate and observation,

$$\varepsilon_m = \ln\left(C_p\right) - \ln\left(C_o\right) \tag{2.2}$$

where C_o and C_p are observed values and corresponding estimates respectively. The angle brackets refer to an average. The deviation of the geometric mean, m_g, from unity indicates whether the model is underpredicting or overpredicting. It is a measure of bias of the model estimate. The geometric standard deviation, s_g, is a measure of the uncertainty in the model prediction with s_g^2 being approximately the 95% confidence interval for the ratio, C_p/C_o.

The calculation of the geometric mean, m_g, and the geometric standard deviation, s_g, using Eq. (2.1) can pose problems when the observation is close to zero and the corresponding model estimate is finite; the large logarithm of the ratio dominates the calculation. This is avoided by equating m_g to the median of the ratio of the observed to predicted concentration ratio, and using the interquartile range of the ratios to estimate s_g.

2.3.1 Surface Friction Velocity

The surface friction velocity is estimated from the mean wind and heat flux measured at a single tower level using the MOST profile (Businger 1973),

$$U(z) = \frac{u_*}{\kappa}\left[\ln\left(\frac{z_r - d_h}{z_0}\right) - \psi_m(\zeta_1) + \psi_m(\zeta_0)\right], \tag{2.3}$$

where z_r is the height above the surface, d_h is the zero-plane displacement, z_0 is the aerodynamic roughness length, κ is the von-Karman constant (= 0.4), u_* is the friction velocity, $\zeta_1 = (z_r - d_h)/L$, $\zeta_0 = z_0/L$, the function ψ_m is

$$\psi_m(\zeta) = 2\ln\left(\frac{1+x'}{2}\right) + \ln\left(\frac{1+x'^2}{2}\right) - 2\tan^{-1}(x') + \frac{\pi}{2}, \text{ for } L<0 \tag{2.4}$$

where $x' = (1-16\zeta)^{1/4}$.

The aerodynamic roughness length, z_0, and zero-plane displacement, d_h, for each site are obtained by fitting the observed u_* to that estimated from the mean wind speed with MOST, as described in Princevac and Venkatram (2007). Measurements with absolute value of L larger than 200 and wind speed higher than 2 m s^{-1} were selected to reduce the effects of stability in estimating z_0. The zero-plane displacement is taken to be $d_h = 5z_0$ based on Britter and Hanna (2003).

This approach to estimating z_0 requires detailed micrometeorological measurements that are not available for routine application of dispersion models. There would be no need for the type of methods discussed in this paper if such micrometeorological measurements are available for an extended period at a site. On the other hand, it is clearly feasible to conduct a limited field study at the site of interest to obtain z_0, which can then be used to estimate micrometeorological variables over the extended period, typically several years, required in regulatory modelling. In principle, we can estimate z_0 using the correlations based on building morphology proposed by Grimmond and Oke (1999). However, as we saw earlier, this approach is difficult to apply in a horizontally inhomogeneous urban area.

We are aware that fetch conditions vary with wind sector, especially for the DS site resulting in different values of z_0 and d_h for different sectors. For the US site, z_0 for the wind direction from 0° to 90° is 0.14, while it is 0.12 for the remaining sectors; this is consistent with the existence of buildings in the 0° to 90° sector. For the DS site, z_0 varies from 0.19 for wind direction less than 250° to 0.3 for 260° to 280° and 0.25 for other directions. The building to the west of the measurement tower determines the large value of z_0 for that sector. For the CU site, the variation in z_0 is relatively small: 0.31 for wind directions less than 240°, 0.35 for 240° to 290° and 0.29 for larger than 290°. If we do not consider different fetch conditions for different sectors, only one value of z_0 is obtained for each site. We find that z_0 is 0.13, 0.27 and 0.31 metres for US, DS and CU sites, respectively.

Notice that z_0 and d_h values obtained here for the US and CU sites are consistent with those estimated from morphological parameters (Table 2.1), although this result could be fortuitous.

Routine measurements used in dispersion applications are not likely to include u_* and L used to estimate the aerodynamic roughness length. Thus, estimates of the aerodynamic roughness length in an inhomogeneous urban area are likely to be uncertain. Thus, it is useful to examine the impact of this uncertainty on estimating the surface friction velocity, u_*.

The surface friction velocity, u_*, is estimated from the observed heat flux, Q_0, and the wind speed using the approximation of MOST suggested by Wang and Chen (1980) to avoid iterative solution of Eq. (2.3),

$$u_* = \kappa u \frac{1 + d_1 \ln(1 + d_2 d_3)}{\ln(1/r_h)}, \tag{2.5}$$

where

$$r_h = \frac{z_0}{z_r - d_h} \tag{2.6a}$$

$$d_1 = \begin{cases} 0.128 + 0.005\ln(r_h), & \text{for } r_h \le 0 \\ 0.107, & \text{otherwise} \end{cases} \tag{2.6b}$$

$$d_2 = 1.95 + 32.6 r_h^{0.45} \tag{2.6c}$$

$$d_3 = \frac{Q_0 \kappa g (z_r - d_h)}{T_0 \{\kappa U / \ln[(z_r - d_h)/z_o]\}^3} \tag{2.6d}$$

where T_0 is the surface temperature and g is the gravitational acceleration.

The results shown in Figure 2.1 are based on z_0 and d_h fitted for different sectors. As expected, the estimates of u_* with MOST compare well with observed values for both urban and suburban sites; the values of m_g indicates a bias of about 10%. The 95% confidence interval for the ratio of the observed and estimated u_* is about 1.7. But the scatter is large for u_* close to 0.1 m s^{-1}.

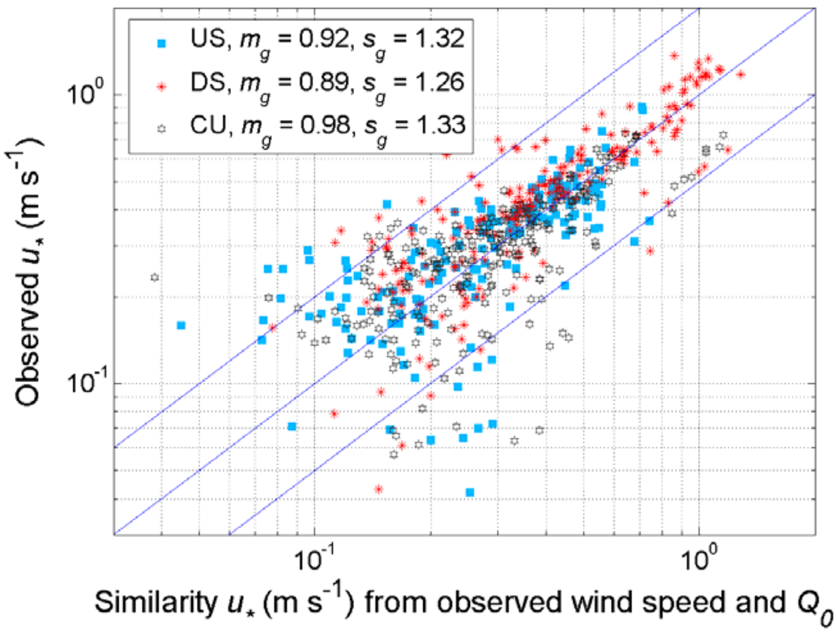

Figure 2.1: Comparison of u_* estimated from observed wind speed and heat flux using MOST with z_0 and d_h obtained for different sectors with observations for US site (solid squares), DS site (stars), and CU site (open hexagrams).

Figure 2.2 shows results when only one set of values of z_0 and d_h are used for each site, i.e. z_0 is 0.13, 0.27 and 0.31 metres for US, DS and CU sites, respectively, and $d_h = 5z_0$. The results are similar to those shown in Figure 2.1, although the scatter increases slightly for the CU site: the geometric standard deviation, s_g, increases from 1.33 to 1.36.

Figure 2.3 shows that using half of the values of z_0 and d_h results in underestimation of u_* by 40% for the CU site to 23% for the US site. However, most of the model estimates are still within a factor of two of the observations. The 95% confidence interval for the ratio of the observations and estimates is less than 1.85. Thus underestimating z_0 and d_h appears to yield acceptable estimates of u_*. However, using twice of the values of z_0 and

d_h leads to unacceptable values of u_* (not shown here). The deterioration in our particular case is caused by z_0 becoming comparable to the effective measurement height, $z_r - d_h$.

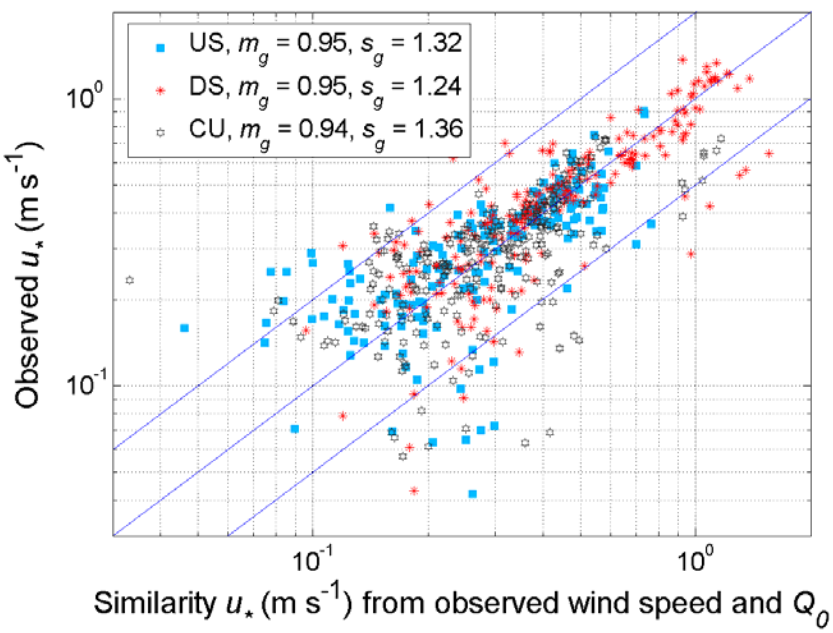

Figure 2.2: Comparison of u_* estimated from observed wind speed and heat flux using MOST with one set of values of z_0 and d_h for each site (z_0 is 0.13, 0.27 and 0.31 metres for US, DS and CU sites, respectively) with observations for US site (solid squares), DS site (stars), and CU site (open hexagrams).

These results indicate that 1) estimates of surface friction velocity are, as expected, sensitive to the estimate of aerodynamic roughness length, and 2) we might be able to obtain empirical estimates of z_0 that yield adequate estimates of surface friction velocity even when the area surrounding the measurement site is highly inhomogeneous. In the analysis of the following sections, we use the values of z_0 and d_h that were fitted for different sectors.

In the following sections, we examine the applicability of MOST in estimating the standard deviation of the horizontal and vertical turbulent velocities.

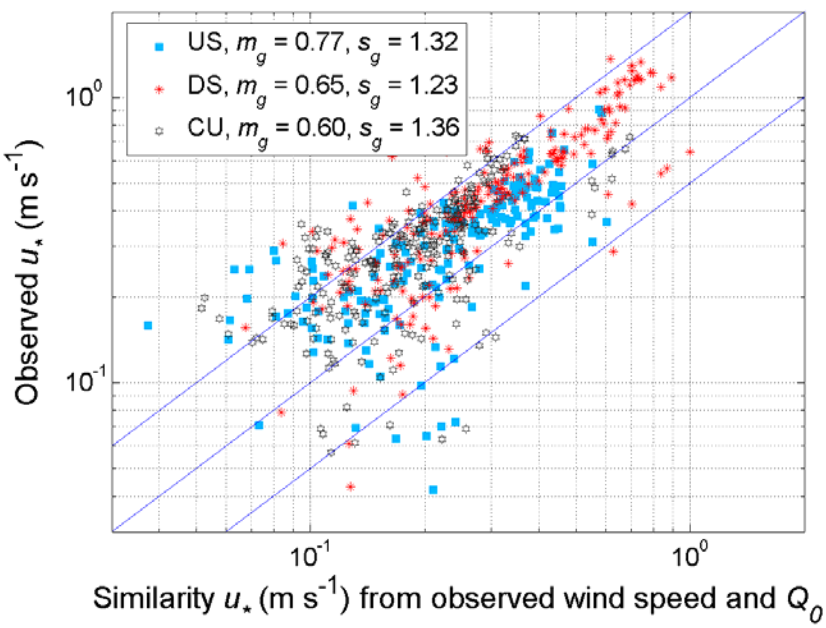

Figure 2.3: Comparison of u_* estimated from observed wind speed and heat flux using MOST with half of fitted values of z_0 and d_h for each site (z_0 is 0.065, 0.135 and 0.155 metres for US, DS and CU sites respectively) with observations for US site (solid squares), DS site (stars), and CU site (open hexagrams).

2.3.2 Vertical turbulent velocity (σ_w)

We estimate σ_w by treating the variable as a combination of a shear generated component, σ_{ws}, and a buoyancy generated component, σ_{wc}

$$\sigma_w = (\sigma_{ws}^3 + \sigma_{wc}^3)^{1/3}, \tag{2.7}$$

where the shear component, σ_{ws}, is taken to be

$$\sigma_{ws} = 1.3 u_*, \tag{2.8}$$

and the convective component, σ_{wc}, is

$$\sigma_{wc} = 1.3\left(\frac{g}{T_0}Q_0 z\right)^{1/3}, \tag{2.9}$$

where $z = z_r - d_h$ is the effective measurement height, g is the gravitational acceleration. Notice that σ_{ws} and σ_{wc} are not added directly in Eq. (2.7). Instead, their cubes are added to ensure consistency with the turbulent kinetic energy equation. Eq. (2.7) can be rearranged to obtain

$$\sigma_w = \sigma_{ws}\left[1+\left(\frac{\sigma_{wc}}{\sigma_{ws}}\right)^3\right]^{1/3} = 1.3u_*\left(1-\frac{z}{\kappa L}\right)^{1/3}. \tag{2.10}$$

where the Obukhov length is defined as:

$$L = -\frac{T_0}{g}\frac{u_*^3}{\kappa Q_0}. \tag{2.11}$$

This expression for σ_w is that presented by Panofsky et al. (1977) to fit a wide range of data.

Eq. (2.10) is used to calculate σ_w using observed u_* and L. Figure 4 (a) shows little bias in the estimates, less than 10%, relative to the σ_w observed at the US and CU sites, but σ_w is overestimated for the DS site by about 14%. The scatter at all three sites is relatively small with the 95% confidence interval of about 1.3.

Previous studies (Clarke et al, 1982; Rotach, 1993; Roth 1993; Feigenwinter, 2000; Christen, 2005) report similar results but have used smaller constants in expression (2.10).

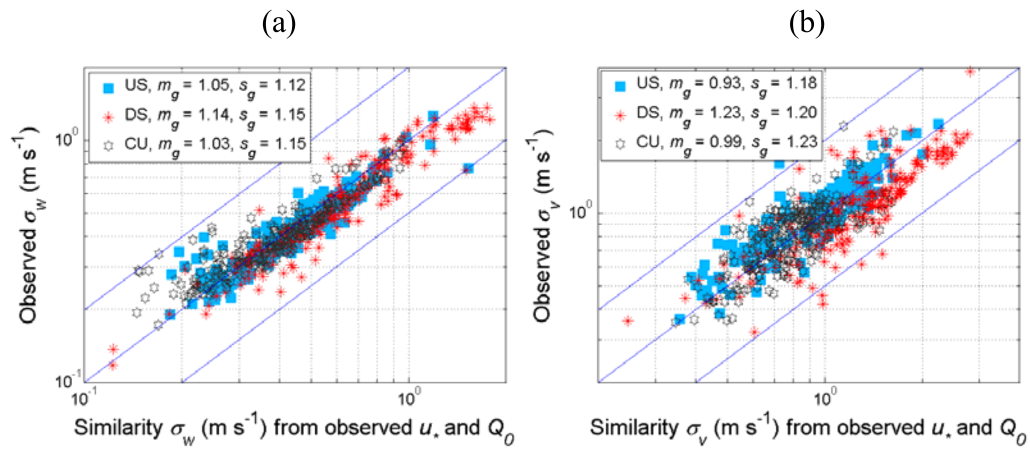

Figure 2.4: Comparison of (a) σ_w calculated from observed u_* and L using Eq. (2.10), and (b) σ_v estimated from observed u_* and Q_0 using Eqs. (2.12)-(2.14) with observations for US site (solid squares), DS site (stars), and CU site (open hexagrams).

2.3.3 Horizontal turbulent velocity (σ_v)

The standard deviation of the horizontal velocity fluctuations, σ_v, is computed from

$$\sigma_v = (\sigma_{vs}^3 + \sigma_{vc}^3)^{1/3}, \tag{2.12}$$

where the shear component is $\sigma_{vs} = 1.9u_*$ and the convective component is $\sigma_{vc} = 0.6w_*$. The convective velocity scale w_* is defined as

$$w_* = \left(gQ_0 z_i / T_0\right)^{1/3}. \tag{2.13}$$

The height of mixed layer, z_i, is calculated from a model of a mixed layer eroding a layer with a stable potential temperature gradient, γ (Carson, 1973)

$$\rho\, c_p \frac{1}{2}\gamma z_i^2 = \int_0^T H(t)dt, \tag{2.14}$$

where ρ is the air density, c_p is the heat capacity under constant pressure, H is the heat flux, t is time, and T is a time scale. The unknown potential temperature gradient, γ, above the mixed layer is taken to be a nominal value of 5 K per 1000 m. The sensitivity of the convective velocity to γ is relatively small because it is inversely proportional to the 1/6th power of γ.

Figure 2.4 (b) shows that σ_v is overestimated at the DS site by about 23%, but the bias is less than 10% at the other two sites. The 95% confidence interval of the ratio of the observed to estimated σ_v is 1.5.

The results presented here indicate that MOST provides an adequate description of the observations made in suburban and urban sites. These results motivate the application of MOST to estimate micrometeorological variables using measurements that can be made routinely. Specifically, we focus on methods that use wind speed at one level and standard deviation of temperature fluctuations, which can be measured using fast response thermistors.

2.4 Temperature Fluctuations Related to Heat Flux

The heat flux is related to the standard deviations of temperature and vertical velocity fluctuations as follows:

$$\overline{w'T'} = r_{wT}\sigma_w\sigma_T \, , \tag{2.15}$$

where σ_T is the standard deviation of temperature fluctuations (T'), and σ_w is the standard deviation of the vertical velocity fluctuations (w').

In this section, we use the data collected at all three sites to examine the behaviour of the correlation coefficient between the velocity and temperature, r_{wT}, and then formulate an expression for the heat flux that can be used in routine applications. The objective is to develop methods to estimate heat flux, surface friction velocity, and the standard deviation of vertical velocity fluctuations variables using only measurements of σ_T and wind speed at one level.

Substituting the expression of σ_w from Eq. (2.10) into Eq. (2.15), and using the definition of the temperature scale, $T_* = -\overline{w'T'}/u_*$, yields

$$\frac{\sigma_T}{T_*} = -\frac{1}{1.3 r_{wT}} (1 - z/\kappa L)^{-1/3}, \tag{2.16}$$

where the correlation coefficient, r_{wT}, is a function of z/L in general.

The proposed expression for the correlation coefficient, r_{wT}, is based on observations reported in the literature. Monin and Yaglom (1971) indicate that r_{wT} increases from about 0.35 for near-neutral conditions, to about 0.6 for Richardson number, Ri, in the range −0.3 to −0.8. Hicks (1981) also suggests that r_{wT} approaches a constant value, but this requires an unrealistic sign change across neutral conditions. As we will see, the expression presented by Tillman (1972) for σ_T/T_* implies an explicit formula for r_{wT} in terms of z/L.

The behaviour of the correlation coefficient in the free convection regime can be derived by equating Monin and Yaglom's (1971) expression for the temperature fluctuations,

$$\frac{\sigma_T}{T_*} = -C_1\left(-\frac{z}{L}\right)^{-1/3}, \tag{2.17}$$

where C_1 is a constant, to Eq. (2.16) to yield

$$r_{wT} = \frac{(-z/L)^{1/3}}{1.3C_1(1-z/\kappa L)^{1/3}}. \tag{2.18}$$

Note that r_{wT} approaches zero as L becomes large near neutral conditions.

The explicit expression for the heat flux under free convection is

$$Q_0 = \left(\frac{\sigma_T}{C_1}\right)^{3/2}\left(\frac{g\kappa z}{T_0}\right)^{1/2}. \tag{2.19}$$

Tillman's (1972) semi-empirical correction to Eq. (2.17)

$$\frac{\sigma_T}{T_*} = -C_1\left(C_2-\frac{z}{L}\right)^{-1/3} \tag{2.20}$$

yields

$$r_{wT} = \frac{(C_2-z/L)^{1/3}}{1.3C_1(1-z/\kappa L)^{1/3}}, \tag{2.21}$$

where C_1 = 0.95 and C_2 = 0.0549 are the suggested values. Here r_{wT} approaches 0.3 as L becomes large.

Note that Eq. (2.20) results in the following implicit expression for the sensible heat flux:

$$Q_0 = u_*\left(\frac{\sigma_T}{C_1}\right)\left(C_2-\frac{z}{L}\right)^{1/3}. \tag{2.22}$$

The value of Q_0 has to be obtained iteratively because both u_* and L are functions of Q_0.

In the next section, we examine observations of r_{wT} in the light of Eqs. (2.18) and (2.20). We also examine the usefulness of a constant value of r_{wT} to explain the observed heat flux using the implicit expression,

$$Q_0 = r_{wT}\sigma_w\sigma_T = r_{wT}\sigma_T 1.3u_*\left(1-\frac{z}{\kappa L}\right)^{1/3}, \tag{2.23}$$

which also has to be solved iteratively.

2.5 Evaluation with Field Observations

The left panel of Figure 2.5 shows the observed correlation coefficient, r_{wT}, as a function of $-z/L$ at the US site compared with the three alternative formulations described in the previous section. The data show that r_{wT} decreases with $-z/L$ but the scatter is large especially for near neutral conditions. The right panel shows a clear increase of σ_T / T_* with decrease in $-z/L$. However, we need to be cautious about inferring too much from the data in view of the small values of heat flux at small values of $-z/L$ and the false correlation introduced by non-dimensional variables used in the plot (see Hicks, 1981 for a discussion).

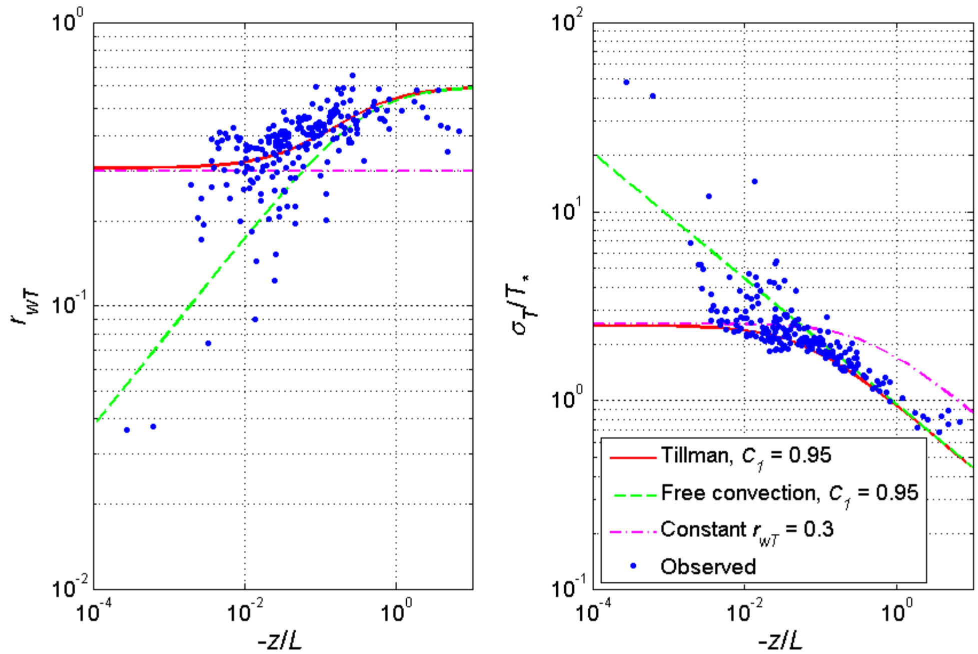

Figure 2.5: Comparison of estimates of the correlation coefficient, r_{wT} (left panel) and σ_T / T_* (right panel) as a function of $-z/L$ with observations. The solid line corresponds to Tillman's method (Eq. 2.20) with $C_1 = 0.95$, the dashed line corresponds to free convection (Eq. 2.17) with $C_1 = 0.95$, and the dash-dot line corresponds to a constant value of $r_{wT} = 0.3$. Measurements were made at US site.

The coefficient, $C_1 = 0.95$, was suggested by Tillman (1972). However, Wesely (1988) and Hsieh et al. (1996) suggest larger values for C_1 in the free convection relationship to make the results applicable to non-uniform surfaces. We will discuss this issue later in this section. We find that most of the observations of r_{wT} are best described by Tillman's method (Eq. (2.21)) when compared with the other two curves, while the free convection curve (Eq. (2.18)) follows the low values of r_{wT} near neutral conditions. Eq. (2.20) provides an adequate description of σ_T / T_* at values of $-z/L$ as low as 0.01 but approaches a constant value at neutral conditions, while the observed data continue to increase. The nominal value of $r_{wT} = 0.3$ represents the median of the data; the associated σ_T / T_* simply reflects the variation of σ_w with z/L. The plots of r_{wT} and σ_T / T_* for the DS and CU sites are similar to the results shown here for the US site, and are not shown here.

Since both the free convection formulation and Tillman's correction deviate from the data at low $-z/L$, it is reasonable to examine the utility of a constant r_{wT} in estimating the heat flux and turbulent velocities.

Figure 2.6 (a) shows the variation of the ratio of heat flux estimated from free convection formulation of Eq. (2.19) to observed heat flux with stability, $-z/L$. The statistics, m_g and s_g, for each site are also listed. As expected, the performance of the free convection formulation improves with increase in $-z/L$, as shear effects become smaller. The ratios of estimated to observed heat flux show large deviations from unity when $-z/L$ is less than 0.1. The $m_g = 0.85$, suggesting underestimation, at the DS site reflects behaviour at low $-z/L$ that cannot be readily explained. The overestimation of 24% at the CU site is more consistent with the behaviour of the free convection formulation at low $-z/L$.

Figure 2.6 (b) shows the performance of Tillman's method, Eq. (2.22), as a function of $-z/L$. We see that the underestimation at low $-z/L$ at the DS site is reduced through the correction for shear incorporated in Tillman's method. However, the heat flux is overestimated by 32% and 76% at the US and the CU site respectively. A larger value of C_1 in the free convection relationship suggested by Wesely (1988) and Hsieh et al. (1996) would decrease the overestimation of heat flux.

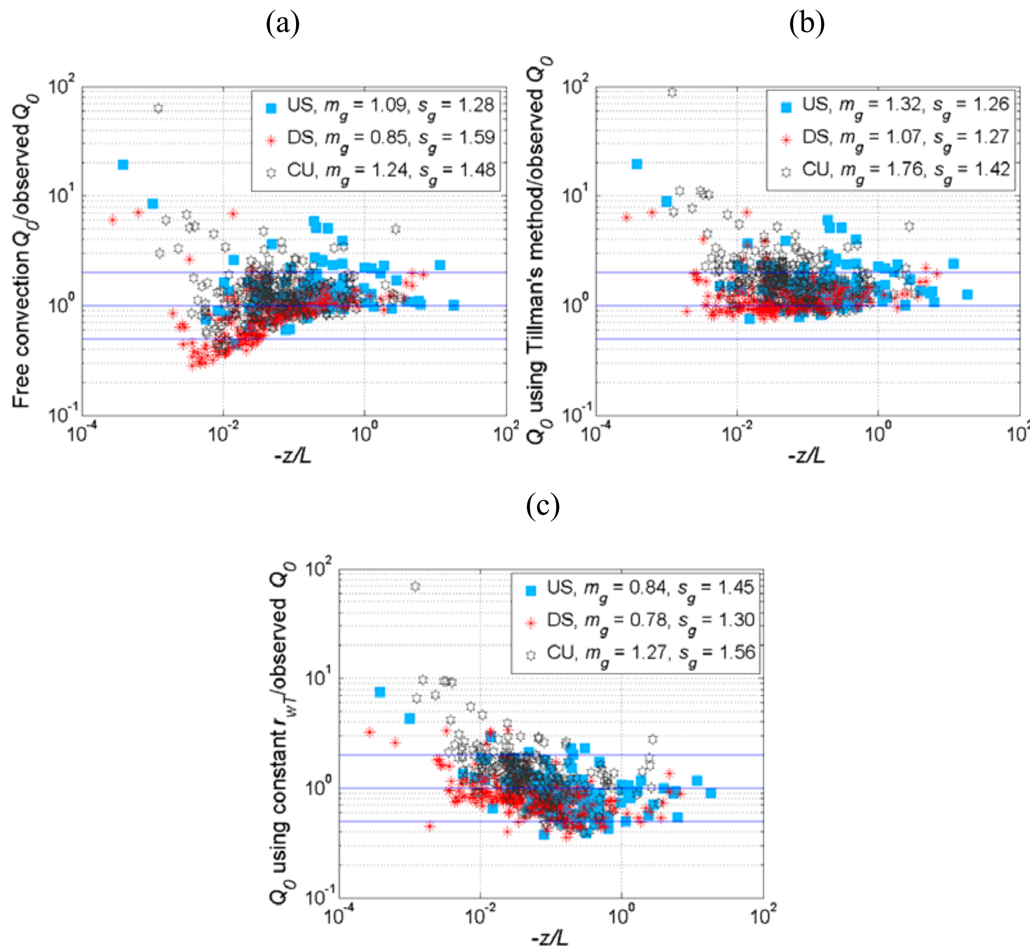

Figure 2.6: Ratio of heat flux estimates from (a) free convection, Eq. (2.19), (b) Tillman's method, Eq. (2.22), (c) using constant r_{wT}, Eq. (2.23), to observations as a function of $-z/L$ for US site (solid squares), DS site (stars), and CU site (open hexagrams).

Figure 2.6 (c) shows that using constant r_{wT} in Eq. (2.23) results in overestimation of heat flux near neutral conditions and underestimation when $-z/L$ is larger. Overall, the heat flux is overestimated by 27% for the CU site but underestimated by 16% and 22% for the US site and DS site respectively. The method has the largest scatter, measured by s_g, compared to the other two approaches.

These results indicate that in an urban area, estimates of the heat flux that account for stability effects, such as Tillman's, do lead to improvements over the simple free convection estimate at low $-z/L$. Although, the heat flux is overestimated, Tillman's correction has the smallest scatter as measured by s_g. In the sections that follow, the heat flux is estimated with this method, but C_1 is taken to be 1.25 as in Wesely (1988) to reduce the bias.

We next examine the impact of errors in estimating heat flux approximations on estimating u_*, σ_w and σ_v. The estimates of u_* in Figure 2.7 (a) are estimates based on Eq. (2.22), which requires an estimate of u_*.

The overestimation of heat flux at CU site or underestimation at the DS site has little effect on estimating u_*, as seen in Figure 2.7 (a). The geometric mean (m_g) and the geometric standard deviation (s_g) are almost identical to those when observed heat flux is used in Figure 2.1. It turns out that u_* estimates based on heat flux estimates from the free convection formulation and the constant r_{wT} approach produce comparable results. This insensitivity of u_* to heat flux errors is related to the fact that $-z/L$ is much smaller than unity (see Figure 2.5) for most of the measurements.

Figures 2.7 (b) and (c) compare estimates of σ_w and σ_v with observations from the three sites. We see that the overestimation of heat flux has little impact on estimating σ_w and σ_v: there is little bias in the model estimates and the scatter is relatively small. The next question is: How does this uncertainty in estimating micrometeorological variables affect concentration estimates?

(a)

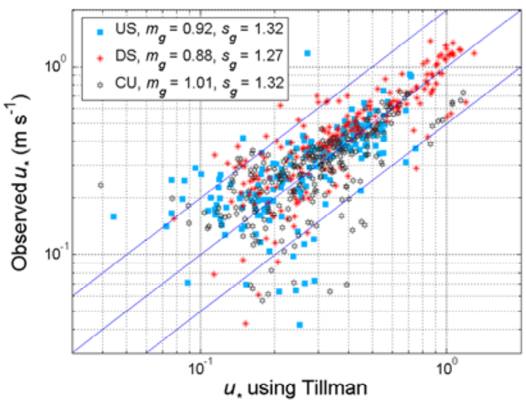

(b)

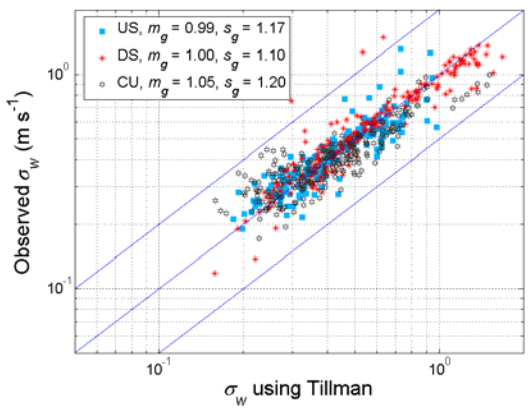

(c)

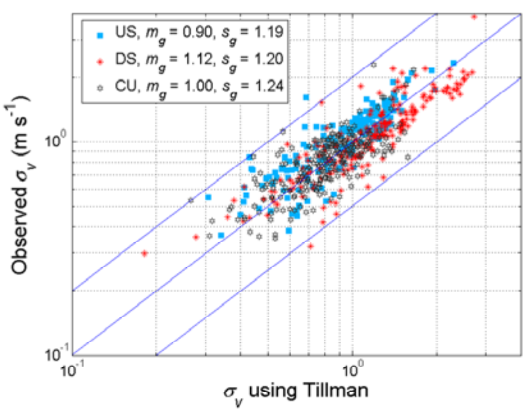

Figure 2.7: Comparison of estimated (a) u_* from Eq. (2.5), (b) σ_w from Eq. (2.10), and (c) σ_v from Eq. (2.12) with observations for US site (solid squares), DS site (stars), and CU site (open hexagrams). Heat flux is estimated from Eq. (2.22).

2.6 Impact on Dispersion Modelling

In this section, we examine the impact of the uncertainty in the estimates of heat flux and friction velocity on modelling ground-level concentrations through the following expression for the cross-wind integrated ground-level concentration associated with surface releases (Venkatram, 1992), which has been evaluated with data from the Prairie Grass experiment (Barad, 1958), and is currently incorporated in AERMOD (Cimorelli et al., 2005):

$$\overline{C}_*^y = \frac{1}{x_*\left(1+\alpha x_*^2\right)^{1/2}}, \tag{2.24}$$

where $\alpha = 6.0\times10^{-3}$, $\overline{C}_*^y = \overline{C}^y u_*\left|L\right|/Q$, and $x_* = x/\left|L\right|$. Eq. (2.24), which can be used to estimate the ground-level impact of a line source, such as a road, can be rewritten as,

$$\frac{\overline{C}^y}{Q} = \frac{1}{u_* x\left(1+\alpha\left(x/\left|L\right|\right)^2\right)^{1/2}}. \tag{2.25}$$

Note that at small $x/|L|$, the crosswind integrated concentration depends only on u_*, which is relatively insensitive to errors in estimating the surface heat flux. At large $x/|L|$, the concentration depends on u_*^2/Q_o, and thus becomes more sensitive to both the surface friction velocity and the heat flux. This sensitivity to Q_o is specific to Eq. (2.25). There are alternative expressions (see Nieuwstadt, 1980) in which the concentration depends on $Q_o^{1/2}$ rather than Q_o.

Figure 2.8 compares estimates of $\overline{C}^y/Q$ based on u_* and heat flux estimated from Tillman's correction to the free convection formulation with those based on observed values of relevant micrometeorology. The 95% confidence interval of the ratio of the observed to estimated $\overline{C}^y/Q$ at x = 10 m is only about 1.7. However, at x = 1000 m, the scatter is almost a factor of 4.

(a) (b)

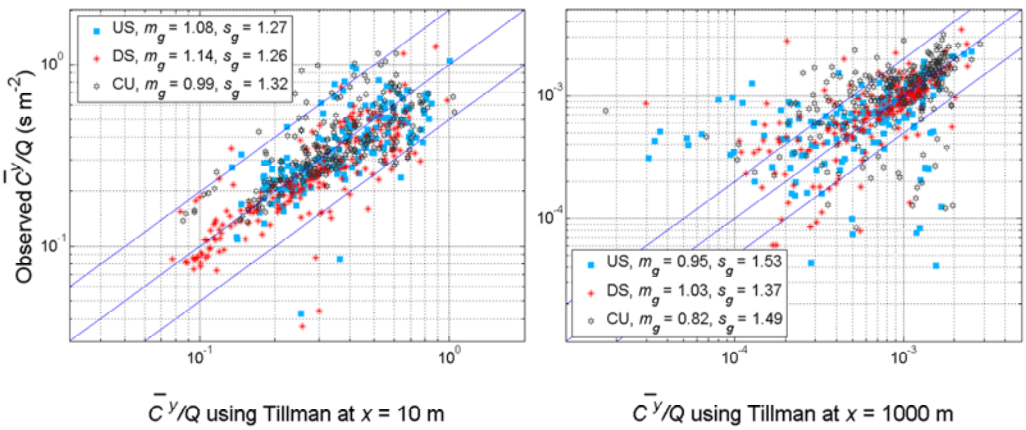

Figure 2.8: $\overline{C}^y/Q$ based on estimated heat flux and u_* from Tillman's method compared with those based on observed inputs for US site (solid squares), DS site (stars), and CU site (open hexagrams) at (a) x = 10 m and(b) x = 1000 m.

This behaviour is readily explained. At small x (Figure 2.8 (a)), the term $x/|L|$ in Eq. (2.25) plays a negligible role, and the concentration estimate is determined by $1/u_*$. The scatter in the $\overline{C}^y/Q$ estimates about those based on observations reflects the errors in estimating u_*, shown in Figure 2.7. At 1000 m (Figure 2.8 (b)), the term, $x/|L|$, becomes more important. The scatter in $\overline{C}^y/Q$ estimates is determined by the scatter in the estimated u_*^2/Q_o. Most of the lower values of $\overline{C}^y/Q$ are underestimated because u_* is underestimated while the corresponding heat flux is overestimated. There are fewer overestimated points because the effect of overestimated u_* is reduced by the overestimation of heat flux.

The uncertainty in estimating meteorological inputs can have a greater impact on concentrations from point sources because the horizontal plume spread of the point source plume is also affected by errors in estimating turbulent velocities. We examine this issue by modifying Eq. (2.25) to incorporate crosswind plume spread, σ_y

$$\frac{C}{Q} \cong \frac{1}{\sigma_y u_* x\left[1+\alpha\left(x/|L|\right)^2\right]^{1/2}} \tag{2.26}$$

where σ_y is computed using $\sigma_y \cong \sigma_v x/u$, where σ_v is estimated from Eq. (2.12), and u is the value measured at the tower level of 3 m.

Figure 2.9 shows estimates of C/Q for x = 10 m (a) and x = 1000 m (b) based on Tillman's method for heat flux plotted against those based on observed values of u_* and L. As expected, the scatter in the C/Q estimates is larger than that for $\overline{C}^y/Q$ in Figure 2.8. The comparison of Figure 2.9 (a) and (b) shows that the scatter in the concentration estimates increases with receptor distance. At x = 1000 m, the scatter in the C/Q estimates is determined by the scatter in $u_*^2/(Q_o\sigma_v)$. Most of the low values of C/Q are underestimated, which is similar to the underestimation of $\overline{C}^y/Q$ in Figure 2.8. Model performance is similar for all the three methods of estimating heat flux (not shown).

(a) (b)

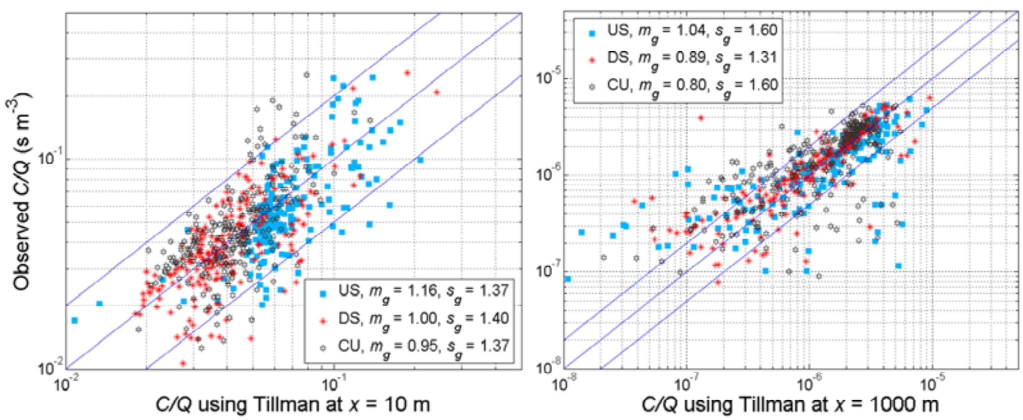

Figure 2.9: C/Q based on estimated heat flux and u_* from Tillman's method compared with those based on observed inputs for US site (solid squares), DS site (stars), and CU site (open hexagrams) at (a) x = 10 m and(b) x = 1000 m.

2.7 Comparison with Surface Energy Balance Method

This section examines whether measurements of the temperature fluctuations, σ_T can reduce the uncertainty in energy balance methods to estimate micrometeorological variables required for dispersion. Computing the components of the energy balance at the surface requires information on cloud cover, albedo, and surface temperature to estimate the incoming/outgoing solar and thermal radiation. Because such information was not available, we used radiation measurements made at the US site during daytime (from 9:00 to 17:00) when net radiation, Q_*, was positive. Notice that using the observed net radiation instead of estimates based on cloud cover and albedo reduces some of the uncertainties in the energy balance method. The sensible heat flux was computed from the energy balance equation incorporated in meteorological processors typical of the current generation of dispersion models, such as AERMOD (Cimorelli et al., 2005). The sensible heat flux (H) is estimated from

$$H = \frac{0.9Q_*}{\left(1+1/Bo\right)} \ , \tag{2.27}$$

where Bo, the Bowen ratio, is the ratio of the sensible to the latent heat flux. Here $H = Q_0 \rho c_p$, where ρ is the air density, and c_p is the specific heat of air at constant pressure. The value of Bowen ratio is highly uncertain because it depends on the moisture history of the soil. We took Bo = 1.5 by calibrating Eq. (2.27) with the maximum observed heat flux. Note that using a constant Bo cannot be readily justified because it depends on soil moisture availability, which is a function of time.

Figure 2.10 compares the sensible heat flux estimates from the energy balance method (Figure 2.10 (a)) with those from Eq. (2.22). It shows that estimates of heat flux based σ_T compares better with the observations than those derived from the surface energy balance method. The 95% confidence interval is reduced from about 2.9 (Figure 2.10 (a)) to about 1.7 (Figure 2.10 (b)).

Figure 2.11 compares estimates of u_* with observations for the US site corresponding to the heat flux estimates from Figure 2.10. As indicated earlier, variations in the heat flux estimates have little impact on estimates of u_*. Furthermore, these variations translate into less than noticeable differences in estimates of σ_w and σ_v during daytime unstable conditions.

(a) (b)

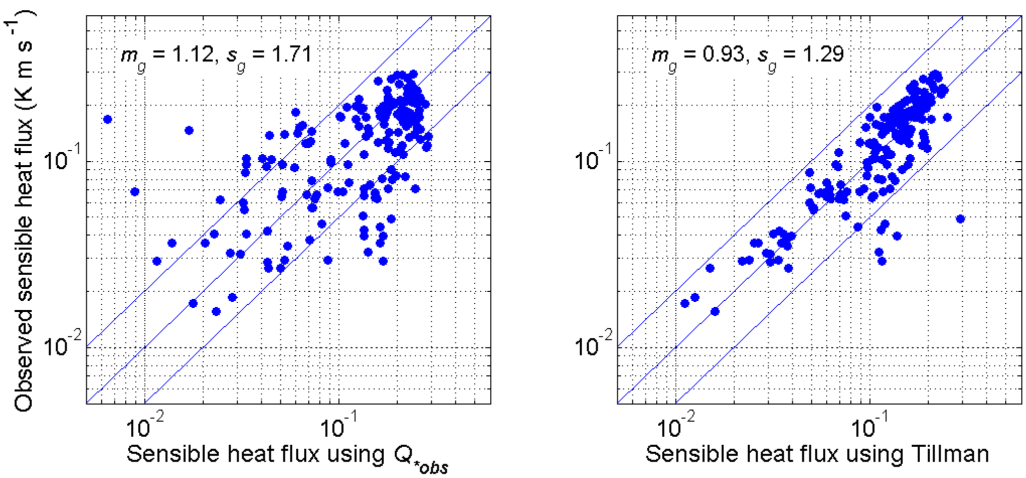

Figure 2.10: Comparison of sensible heat flux estimated from (a) observed net radiation (Eq. (2.27)), and (b) Tillman's method (Eq. (2.22)), with those based on observed inputs for US site during daytime unstable conditions.

To examine the impact of differences in the heat flux estimates on concentration calculations, we compared the computed concentrations at 1000 m where stability effects become apparent through the term, $x/|L|$ in Eq. (2.25). We see that although the scatter is large for both methods of calculating heat flux, the s_g is 1.5 for $\overline{C}^y/Q$ estimates when the heat flux is based on σ_T (Figure 2.12 (b)), while s_g, is 2.2 for $\overline{C}^y/Q$ when the surface energy balance method is used to calculate heat flux (Figure 2.12 (a)).

(a) (b)

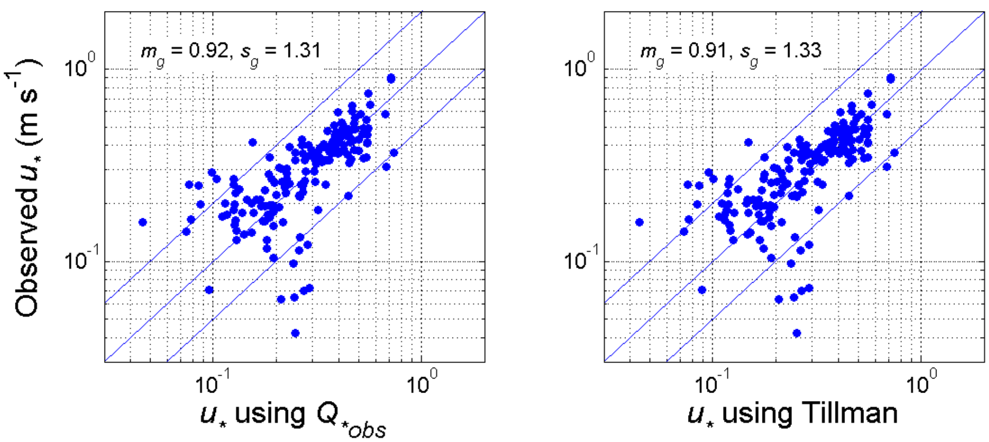

Figure 2.11: Comparison of u_* estimated from Eq. (2.5) with observations for the US site during daytime unstable conditions. Heat flux is estimated from (a) observed net radiation (Eq. (2.27)), and (b) Tillman's method (Eq. (2.22)).

(a) (b)

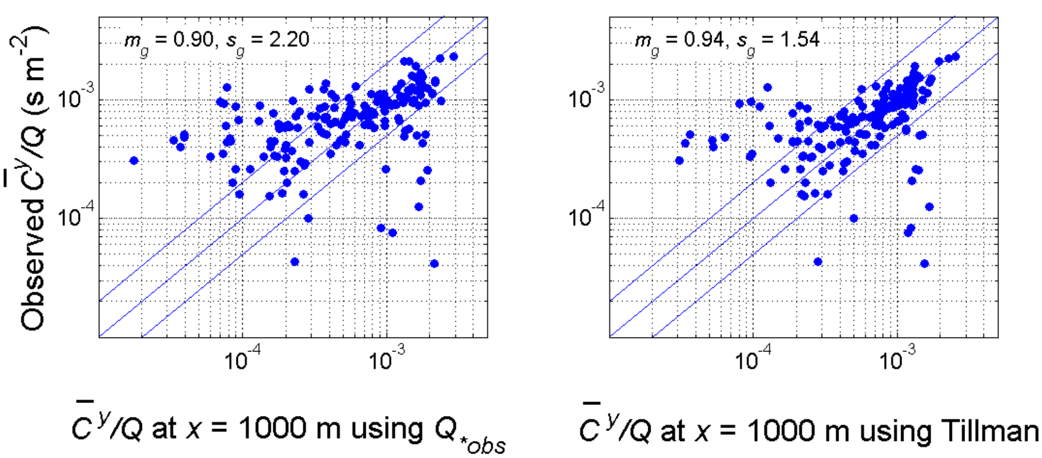

Figure 2.12: $\overline{C}^y/Q$ based on estimated heat flux and u_* from (a) observed net radiation (Eq. (2.27)), and (b) Tillman's method (Eq. (2.22)) with those based on observed inputs for US site and x = 1000 m during daytime unstable conditions.

2.8 Conclusions

The results from this study show that measurements of wind speed and standard deviation of temperature fluctuations at one level yield useful estimates of parameters required to model dispersion in both suburban and urban areas. Under unstable conditions, estimates of heat flux based on measured σ_T and wind speed at one level provide unbiased estimates of surface friction velocity and turbulent velocities. The 95% confidence interval for the ratio of the observations and estimates is about 1.7, 1.4 and 1.5 for u_*, σ_w and σ_v. However, the ability to make estimates of micrometeorological variables is crucially dependent on adequate estimates of the aerodynamic roughness length at the site of interest. We suggest using empirical methods, such as that described in this paper, to estimate the aerodynamic roughness length, although such methods have an inherent uncertainty that reflect the complexities of an urban area.

We examined two methods to account for shear effects on heat flux estimates: one proposed by Tillman (1972) and the other based on a constant value of the correlation coefficient between temperature and vertical velocity fluctuations. The results show that Tillman's method does improve upon the free convection equation, which neglects shear effects.

The scatter in the u_* and heat flux estimates leads to inevitable scatter in concentration estimates for near surface line and point sources, although the impact is less for small downwind distances relative to the Obukhov length. The scatter in the concentration estimates for a point source is larger than that for a line source, because of the additional scatter introduced by errors in estimating the horizontal turbulent velocity used to compute horizontal plume spread.

The results indicate that measurements of σ_T in addition to wind speed can reduce the uncertainty in using the energy balance method to estimate the micrometeorological variables required to apply dispersion models in urban areas. Note that energy balance method has been portrayed in the best possible light by using net radiation measurements and a calibrated value of the Bowen ratio. Even if radiation measurements are available, the energy balance method suffers from its need for an appropriate Bowen ratio (in addition to a roughness length) that can vary substantially both spatially as well as temporarily (Ching, 1985; Roth and Oke, 1995).

3. ESTIMATING URBAN DISPERSION METEOROLOGY FROM SUBURBAN VALUES

3.1 Introduction

Meteorological variables such as surface friction velocity and heat flux are critical inputs to the current generation of dispersion models such as AERMOD (the AMS/EPA Regulatory Model). Because urban measurement is usually not available, there is a need for methods that can estimate urban meteorological variables from more routinely available rural, suburban or airport measurements. A two-dimensional internal boundary-layer (IBL) model was evaluated by Luhar, Venkatram and Lee (2006) using data from the Basel Urban Boundary Layer Experiment (BUBBLE) conducted in the city of Basel, Switzerland (Rotach et al., 2005). It is assumed that Monin-Obukhov (M-O) surface similarity theory is valid within the IBL over an urban area. Assumption for the urban Obukhov length is also needed in the model.

We realize that M-O similarity parameterizations are likely to be valid only in the inertial sublayer (ISL), which refers to the layer about 2 to 5 times the average building height (Raupach et al., 1991), where the flow can be considered in equilibrium with the underlying rough surface and turbulent fluxes are close to constant. The surface friction velocity estimated by the above two-dimensional IBL model may only compare well with observation in the ISL.

On the other hand, Rotach (1993) found that Reynolds stress is not constant in the roughness-sublayer (RSL), which is below the ISL. A profile was further proposed by Rotach (2001), which calculates local friction velocity from the friction velocity at the top of RSL (or in the ISL). Meanwhile, it is found that the M-O similarity could still be valid when local values of shear stress and heat flux are used (Rotach, 1999).

The performance of the two-dimensional IBL model is re-examined here with the data observed in Riverside, 2007. The use of the local friction velocity profile together with the IBL model is also tested. We first describe the field study and analyze the observed data before application of models.

3.2 Field Study

The detailed description of the field study conducted in Riverside, CA 2007 has been given in Chapter 3. The analysis that follows is based on 1 hour averaged data from the sonic anemometers.

The Riverside suburban site was selected as the upwind suburban site in the model since it is not often enough for the wind to blow from the Moreno Valley suburban site to the urban site. The meteorological estimates for the downtown Riverside site are compared with measurements. The suburban site is located 11 km west of urban site, and wind direction range 234°~324° is selected so that the urban area is downwind of the suburban measurement site. Data from the two sites were synchronized before application of the IBL model.

3.3 Analysis of Observations

The first step of the analysis is to compare the urban and suburban observations. We separate the plots for stable (i.e. negative heat flux) and unstable (i.e. positive heat flux) suburban conditions since we assume the urban conditions are not known. Figure 3.1 shows that friction velocity, u_*, observed at the suburban site is almost twice of the urban values during both stable and unstable suburban conditions (upper panel). This difference can be explained by the difference in the wind speed for these two sites (lower panel). It can be seen that wind speed is weakened over the urban site due to existence of buildings. Besides, it is also observed that horizontal and vertical standard deviations of turbulent velocities, σ_w and σ_v, for the suburban site are also about twice as large as the urban values (not shown).

Figure 3.2 shows that turbulent intensities, i_w ($= \sigma_w/U$) and i_v ($= \sigma_v/U$), are still higher at the urban site than those at the suburban site, even though the values of σ_w, σ_v and wind speed are lower than the suburban values in Figure 3.1.

Figure 3.3 compares the kinematic sensible heat fluxes observed at the urban site with that measured at the suburban site when the suburban conditions are either stable or unstable.

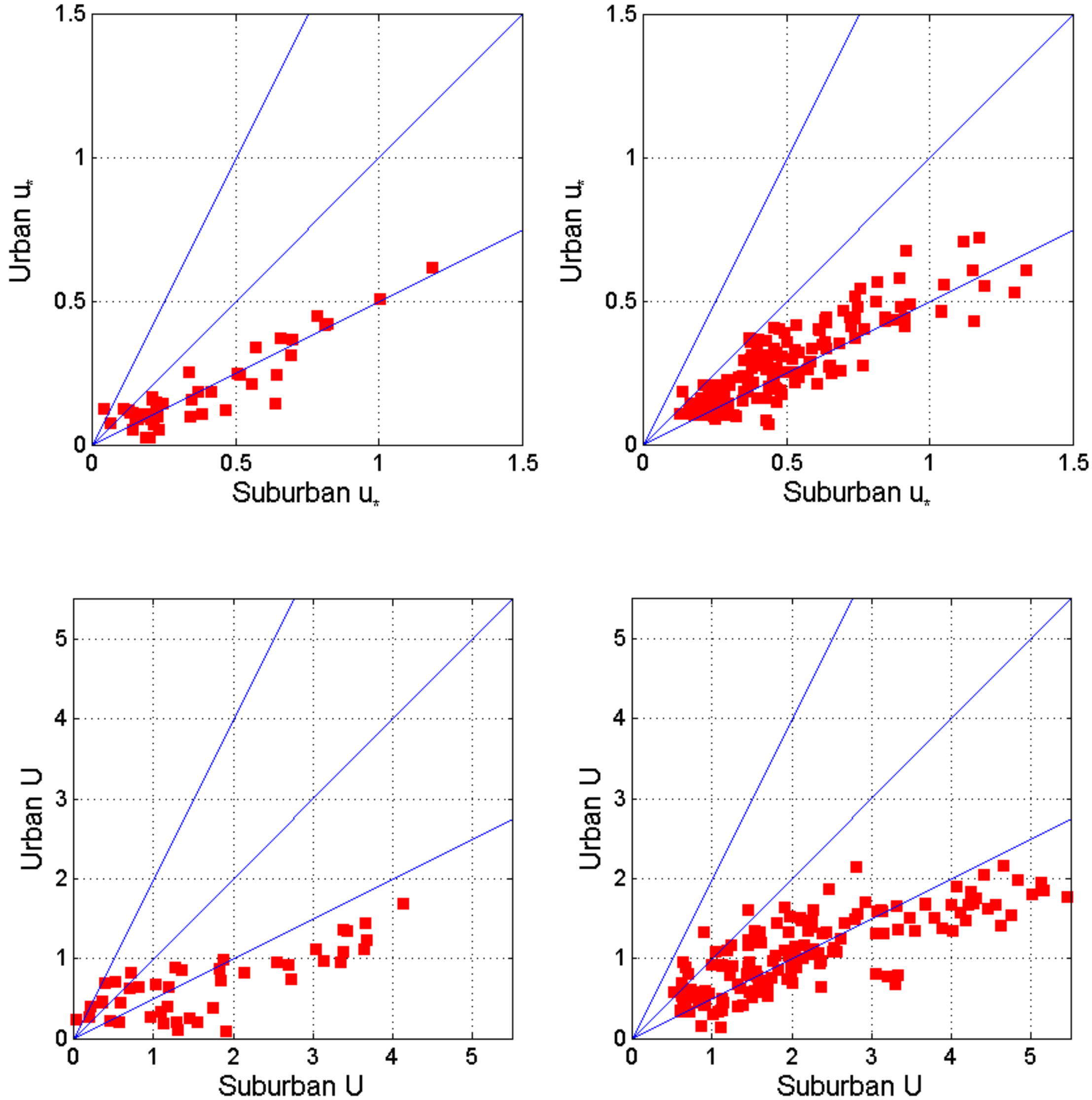

Figure 3.1: Comparison of observed suburban u_* (upper panel) and wind speed (lower panel) with urban observations during stable (left panel) and unstable (right panel) suburban conditions.

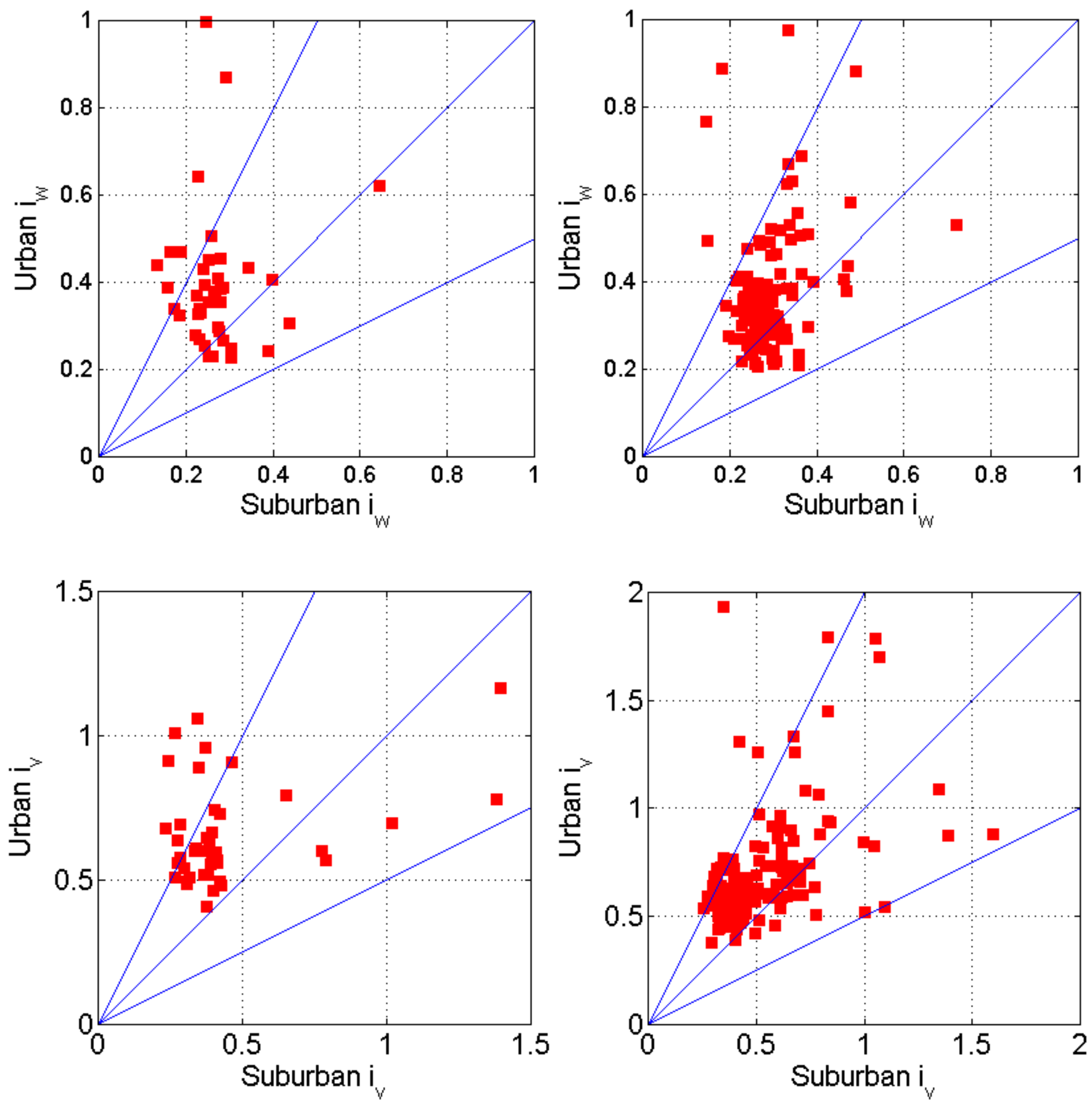

Figure 3.2: Comparison of observed suburban turbulent intensities, i_w (upper panel) and i_v (lower panel), with urban observations during stable (left panel) and unstable (right panel) suburban conditions.

When the suburban site is stable, there is no definite trend in the urban heat flux as a function of the suburban values. But it is shown that the urban site is more neutral, a consequence of the thermal properties of the urban surface and the likely presence of an anthropogenic heat flux.

When suburban site is unstable, suburban and urban fluxes are well correlated, with the suburban heat flux being almost three times as large as the urban heat flux. One possible reason for this might be that the urban site in Riverside is more irrigated than the suburban site. Besides, we are aware that the heat flux decreases with decreasing height in the street canyon from the BUBBLE study (Luhar, Venkatram, and Lee 2006). It should be noticed that since the urban observation site in Riverside is within the urban canopy, smaller heat flux observed at this site is reasonable.

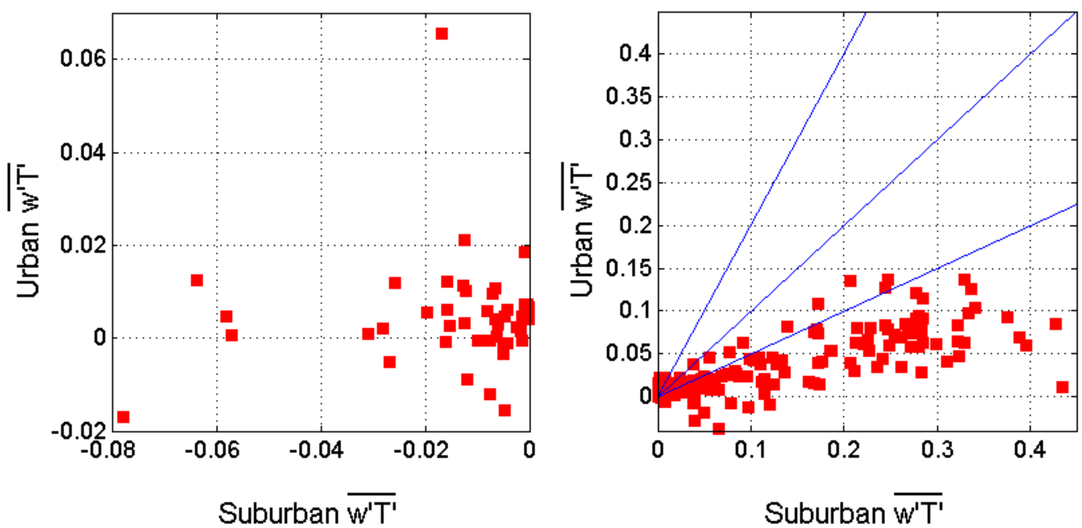

Figure 3.3: Comparison of observed suburban kinematic heat flux with urban observations during stable (left) and unstable (right) suburban conditions.

The next step in the analysis of the data consisted of examining the applicability of M-O similarity to the measurements from the suburban and urban sites, which clearly do not meet criteria for horizontal homogeneity because buildings will disturb the flow substantially.

The performance of the models is quantified by the geometric mean (m_g) and the standard deviation (s_g) of the ratios of the observed to modeled variable as in the previous chapter.

According to M-O similarity, the mean wind profile $U(z)$ in the diabatic surface layer is given as (e.g. van Ulden and Holtslag, 1985)

$$U(z) = \frac{u_*}{\kappa}\left[\ln\left(\frac{z_r - d_h}{z_0}\right) - \psi_m(\zeta_1) + \psi_m(\zeta_0)\right] \tag{3.1}$$

where z_r is the height above the surface (> d_h), κ is the von-Karman constant (= 0.4), u_* is the friction velocity, $\zeta_1 = (z_r - d_h)/L$, $\zeta_0 = z_0 / L$, the function ψ_m is

$$\psi_m(\zeta) = 2\ln\left(\frac{1+x'}{2}\right) + \ln\left(\frac{1+x'^2}{2}\right) - 2\tan^{-1}(x') + \frac{\pi}{2}, \text{ for } L < 0 \tag{3.2}$$

$$\psi_m(\zeta) = -17\left[1 - \exp\left(-0.29\zeta\right)\right], \text{ for } L \geq 0 \tag{3.3}$$

where L is the Obukhov length, and $x' = (1 - 16\zeta)^{1/4}$.

To evaluate the applicability of Equation (3.1), we used the measured heat flux, Q_0, and the surface friction velocity, u_*, to estimate the mean wind, U. The roughness length, z_0, and displacement height, d_h, for each site are obtained by fitting the M-O similarity wind speed estimated from observed u_* and L to observed wind speed, as described in Princevac and Venkatram (2007). We found in Chapter 3 that the optimal values of z_0 are 0.27 and

0.31 meters for the Riverside suburban site and urban site respectively. The displacement height is taken to be $d_h = 5z_0$ based on Britter and Hanna (2003).

We realize that stable conditions are more complex than unstable conditions. Next we examine the effects of stability on the wind profile in Figure 3.4 during stable suburban conditions. We plot the combination, $\kappa U / u_* - ln(z_r / z_0)$, which represents the deviation from neutral conditions, as a function of $(z_r - z_0)/L$. Suburban data are shown in dots, while corresponding urban data are expressed by stars.

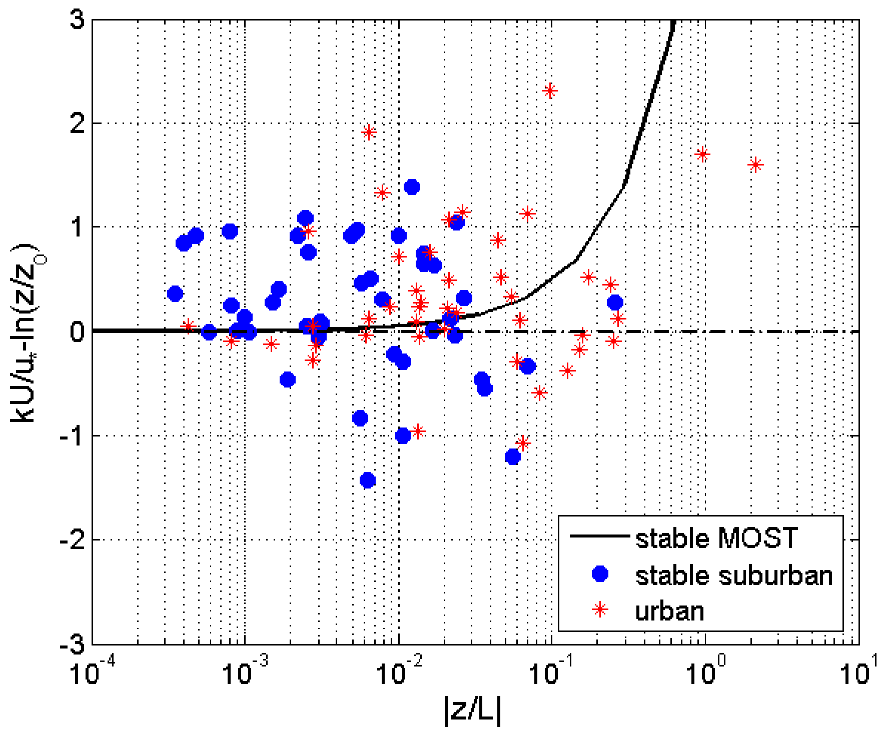

Figure 3.4: Stability correction $\beta(z_r - z_0)/L$ (solid line) compared with measured $\kappa U / u_* - ln(z_r / z_0)$ at the suburban site during stable conditions (dots), and the urban site (stars) for corresponding hours.

For simplicity, the deviation predicted by linear M-O similarity function, $\beta\left(z_r - z_0\right)/L$ ($\beta = 4.7$ by Businger, 1973), is shown as the solid line; its usefulness is not clear from the data. For both sites, the data are scattered around the zero deviation line, which suggests that the M-O stability correction might not help in estimating micrometeorological variables at urban and suburban sites. The best estimate is likely to correspond to neutral conditions with no stability correction.

On the other hand, during unstable suburban conditions, M-O surface similarity performs well at describing both the suburban and urban data as shown in Figure 3.5.

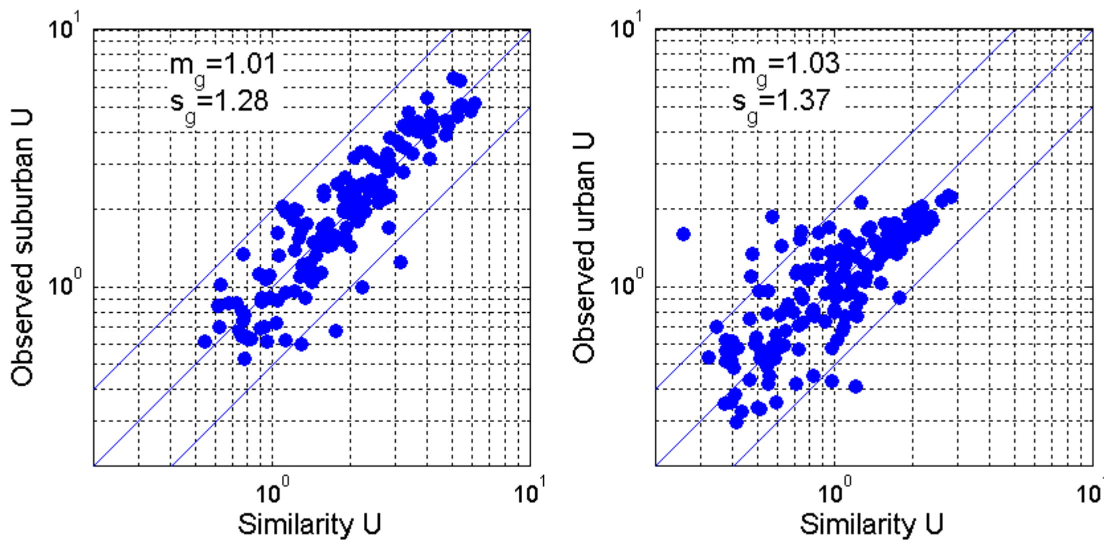

Figure 3.5: Wind speeds estimated using M-O similarity vs. the observed wind speeds over the suburban (left) and urban area (right) during unstable suburban conditions.

In the surface layer, a similarity parameterization for the standard deviation of the vertical turbulent velocity (σ_w) is (Panofsky et al., 1977)

$$\sigma_w = c_1 u_* \left(1 - \frac{z_r}{kL}\right)^{1/3}, \text{ for } L < 0 \tag{3.4}$$

$$\sigma_w = c_1 u_*, \text{ for } L \geq 0 \tag{3.5}$$

where the value of the regression constant c_1 is still uncertain. Panofsky et al. use c_1 = 1.3, Savelyev and Taylor (2005) use 1.25, and Stull (1988) gives a range of 1–1.6. In Figure 3.6, the values of σ_w are calculated using c_1 = 1.25 and plotted against measured σ_w for both suburban and urban sites. These plots show the similarity Equations (3.4) and (3.5) provide an excellent description of both the suburban and urban data.

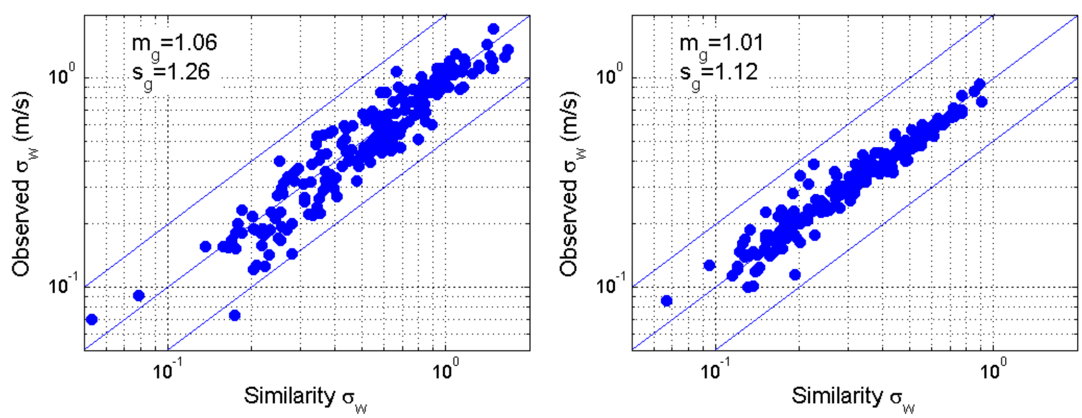

Figure 3.6: Standard deviation of the vertical turbulent velocity (σ_w) estimated using M-O similarity vs. the observed values over the suburban (left) and urban area (right).

3.4 Two-dimensional Internal Boundary Layer Model

We examined a simple scheme to estimate urban meteorological parameters in terms of suburban observations, and compare them with the Riverside data. This scheme is explained in detail by Luhar, Venkatram and Lee (2006). We are interested in the internal boundary layer (IBL) formed over an urban area due to a change in surface roughness and heat flux. One of the formulas to estimate the growth of the IBL is based on Miyake's diffusion analogy and discussed by Savelyev and Taylor (2005) as

$$U(h)\frac{dh}{dx} = A\sigma_w, \tag{3.6}$$

where h is the height of the IBL, x is the downwind distance from the roughness change, $U(h)$ is the wind speed at height h, and A is a constant ($\approx$1). We consider the values of $U(h)$ and σ_w to be those of the modified flow over the urban surface.

We assume that M-O surface similarity theory is valid within the IBL over an urban area; the similarity comparisons presented earlier provide support for this assumption. We substitute the U and σ_w expressions from Equations (3.1), (3.4), and (3.5) at $z_r = h$ into Equation (3.6). Note that u_* cancels out; however L for the urban area needs to be specified, which will be discussed later.

The assumption about the M-O length over the urban area allows us to estimate the internal boundary layer height h as a function of x from Equation (3.6). Once h is known, the micrometeorological variables over the urban area can be calculated using two assumptions: 1) the micrometeorological variables above h are the same over the urban and the suburban areas, and 2) the urban profiles below h follow M-O similarity. Then the urban friction velocity can be obtained by equating the suburban and the urban wind speeds at $z_r = h$.

$$u_{*,U} = u_{*,R} \frac{\ln\left(\frac{h-d_R}{z_{0,R}}\right) - \psi_m\left(\frac{h-d_R}{L_R}\right) + \psi_m\left(\frac{z_{0,R}}{L_R}\right)}{\ln\left(\frac{h-d_U}{z_{0,U}}\right) - \psi_m\left(\frac{h-d_U}{L_U}\right) + \psi_m\left(\frac{z_{0,U}}{L_U}\right)} \tag{3.7}$$

3.5 Results for the Riverside Data

At first, we tried assuming $L_U = L_R$, when $L_R < 0$, and L_U is infinity when $L_R > 0$ the subscripts R and U represent suburban and urban, respectively). This assumption was justified by Luhar, Venkatram, and Lee (2006) for the BUBBLE data. It turns out that urban u_* is severely overestimated during stable suburban conditions. This may due to unreasonable magnification from 'stable' suburban u_* to 'neutral' urban u_*. From Figure 3.4 we realized that during 'stable' suburban conditions, it is better to treat both sites as neutral. Thus in the following, we assume both L_U and L_R to be infinity when observed $L_R > 0$.

Figure 3.7 shows that assuming both L_U and L_R to be infinity when observed $L_R > 0$ still overestimates urban u_* (left). When the suburban conditions are unstable (right), i.e. observed $L_R < 0$, u_* is also overestimated with m_g = 1.68, but the overall performance is better than that when suburban conditions are stable.

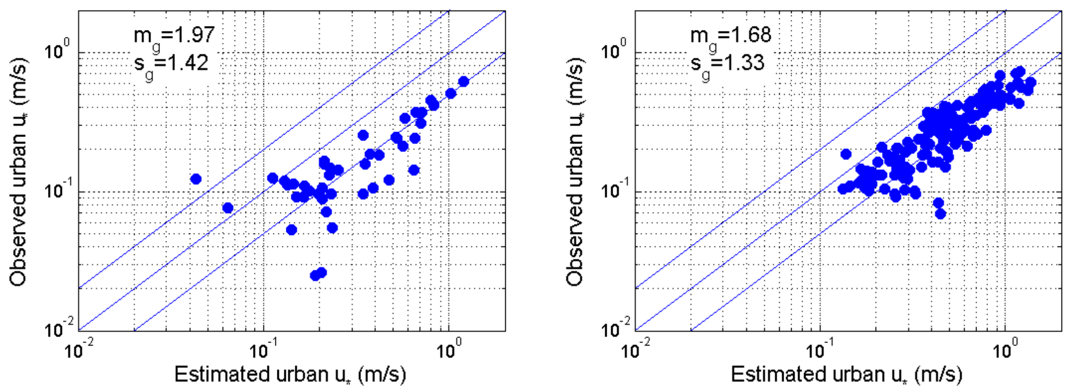

Figure 3.7: Scatter plot of u_* estimated from the IBL model when L_U and L_R are infinity when observed $L_R > 0$ (left), and $L_U = L_R$ when observed $L_R < 0$ (right) with the observed values over the urban area.

We noticed that the measurement height in the urban Riverside site is 3 m, which should be well within the roughness sublayer (RSL). As suggested by Rotach (1993), $\overline{u'w'}$ (norm of Reynolds stress) appears to increase with height within the RS before reaching an approximately constant value in the inertial sublayer (ISL). As a result, $u_{*,\mathrm{U}}$ calculated from Equation (3.7) will provide good estimation for u_* above RSL but not within the RSL.

Rotach (2001) proposed the following profile for the friction velocity within the RSL.

$$\left(\frac{u_{*,l}(z)}{u_*^{ISL}}\right)^b = \sin\left(\frac{\pi}{2}Z\right)^a \quad , \quad Z \leq 1 \tag{3.8}$$

where $u_{*,l}(z)$ is the local friction velocity, $Z = z'/z'_*$ is a non-dimensional height using $z' = z - d$ and $z'_* = z_* - d$. z_* is the RSL height. The parameters a and b are fitted to the experimental data Rotach (2001) collected to yield $a = 1.28$, and $b = 3.0$.

Estimates for z_* are often expressed as multiples of h, the average roughness element height. Raupach et al. (1991) conclude that $z_* = 2h$ - $5h$ essentially covers the range of estimates from the literature they reviewed. The average building height at the urban site is 4 m. The ratio of $u_{*,l}(z)/u_*^{ISL}$ is calculated to be 0.65 when $z_* = 2h$, and decreases to be 0.41 when $z_* = 5h$. Meanwhile, the ratio of local u_* and the peak u_* is also calculated based on the shear stress profile suggested by Kastner-Klein and Rotach (2004). The ratio is 0.75 when we use 4 m building height and $\lambda_p = 0.3$ as in Table 1. So the ratio is sensitive to the choice of z_* and u_* profile. In the following, we use Equation (3.7) to estimate the friction velocity in the ISL, and the local friction velocity at the measurement height is calculated from Equation (3.8). z_* is set to be $2.5h$ for now to get most appropriate estimation.

Figure 3.8 shows the comparison of u_* estimated from Equation (3.7) combined with Equation (3.8) with the observed values. As we have expected, the overestimation of u_* is reduced when the u_* profile within the RSL is taken into account. For the unstable suburban conditions (right), the estimates compare well with the observations. For the stable suburban conditions (left), u_* is still overestimated by 13%. It should be noticed that the simple scaling only reduces m_g, while s_g is not affected because the scatter in the data is not changed.

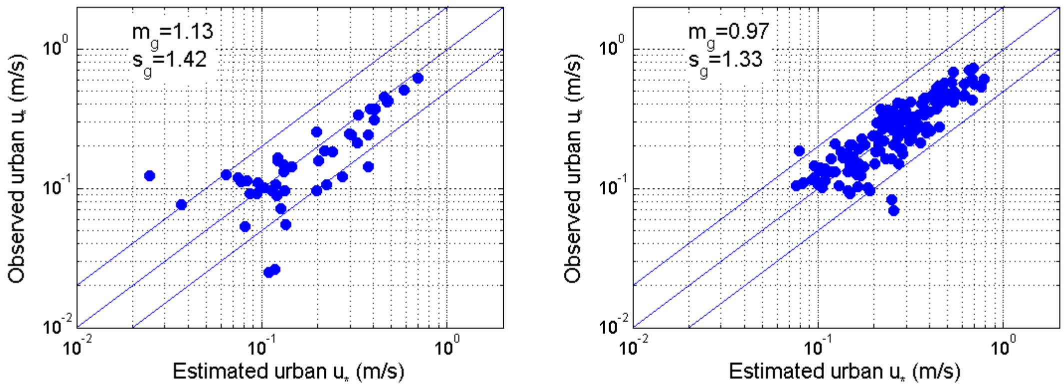

Figure 3.8: Scatter plot of u_* estimated from local u_* profile together with the IBL model when L_U and L_R are infinity when observed $L_R > 0$ (left), and $L_U = L_R$ when observed $L_R < 0$ (right) with the observed values over the urban area.

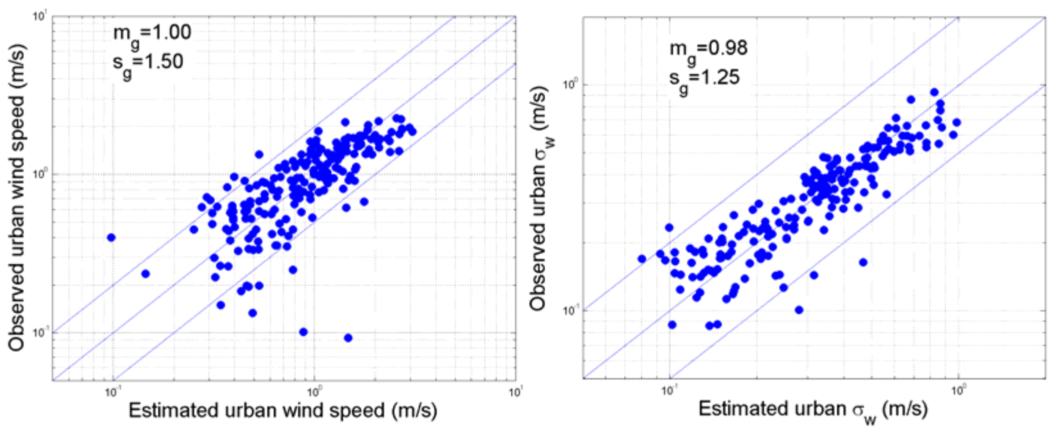

Figure 3.9: Scatter plots of estimated wind speed (left) and σ_w (right) when u_* is estimated from local u_* profile together with the IBL model when L_U and L_R are infinity when observed $L_R > 0$, and $L_U = L_R$ when observed $L_R < 0$ with the observed values over the urban area.

After u_* is estimated from the IBL model and the u_* profile in RSL, wind speed and σ_w are estimated by M-O similarity. Figure 3.9 compare the estimated similarity wind speed and σ_w with the observations. Although a portion of data is overestimated for both wind speed and σ_w, the overall performance is acceptable. The overestimation of wind speed and σ_w can be explained by the overestimation of u_* when suburban conditions are stable.

3.6 Conclusions

In this chapter, we examined a two-dimensional internal boundary-layer (IBL) model to estimate urban micrometeorology using measurements from suburban sites. This method uses Monin-Obukhov surface similarity theory and suburban variables as upwind inputs.

The comparison of urban and suburban data shows that although urban wind speed, friction velocity and turbulent velocities are lower than suburban values, the turbulent intensities are still higher at the urban site.

The IBL model itself overestimates the friction velocity for the Riverside urban site. Taking into account the u_* profile within the RSL proposed by Rotach (2001) can reduce the overestimation. The accuracy of the u_* profile depends on the z_* value, which is the RSL height. The reduction ratio can be as low as 0.41 if five times of building height is used for z_*, while we got appropriate estimates of u_* when we used 2.5 times of building height for z_* for Riverside urban site.

It turns out that during stable suburban conditions, stability function doesn't help in estimating micrometeorological variables at either urban or suburban sites. The upper panel of Figure 3.10 shows that using similarity with stability function underestimates u_* during low wind speed conditions. The best estimate is likely to correspond to neutral conditions with no stability correction (the lower panel of Figure 3.10). Assuming both urban and suburban sites to be neutral can reduce the underestimation of u_*, which can be verified by the fact that the suburban and urban sites are observed to be near neutral during the night. This leads to a further question: what is the general approach to deal with low wind stable conditions when stability condition is unknown? Next chapter is going to address this question.

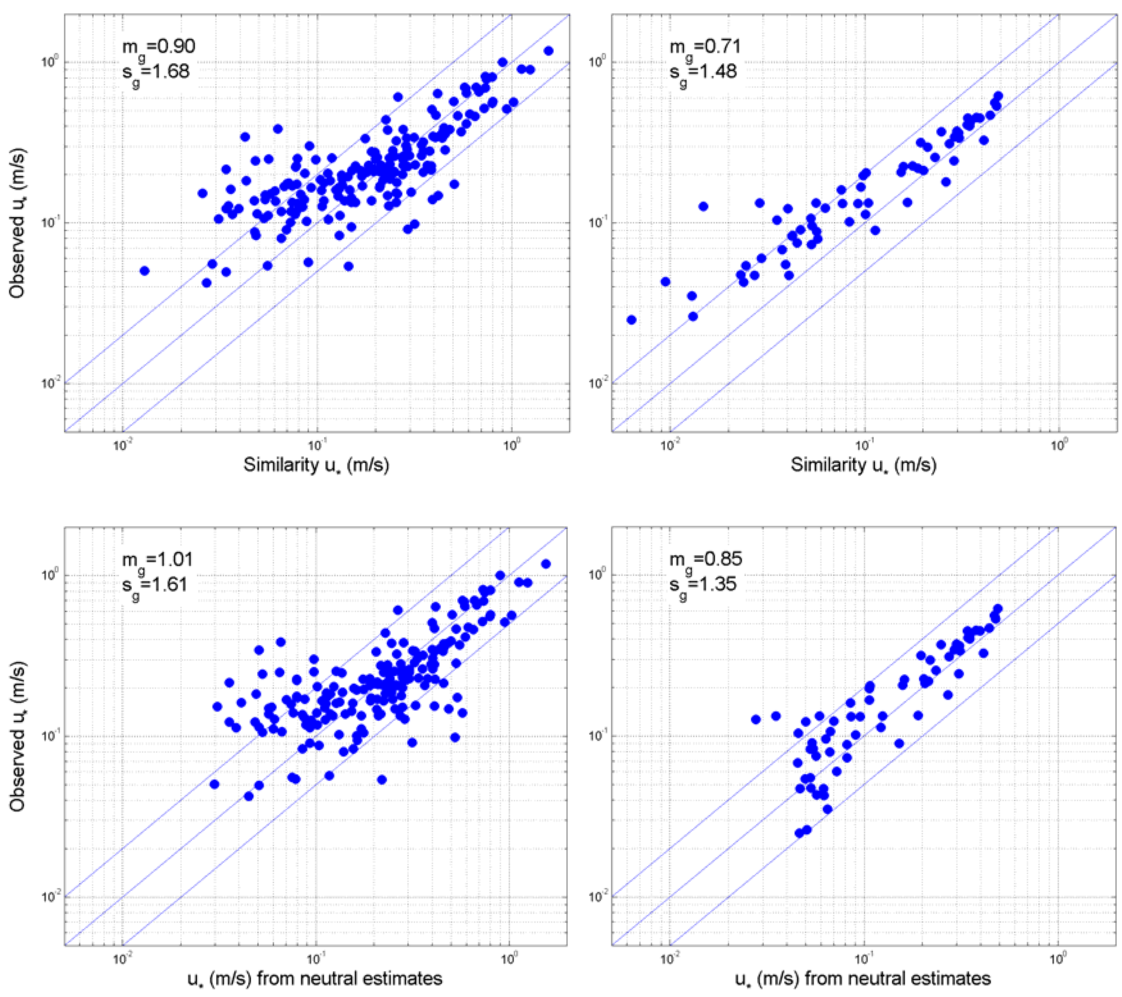

Figure 3.10: Comparison of u_* estimated from M-O similarity with observed wind speed and M-O length (upper panel) and from assuming neutral conditions (lower panel) with corresponding observations at the suburban site (left) and the urban site (right).

4. PERFORMANCE OF STEADY-STATE DISPERSION MODELS UNDER LOW WIND SPEED CONDITIONS

4.1 Introduction

It is generally believed that commonly used steady-state Gaussian dispersion models, such as AERMOD (Cimorelli et al., 2005) are not applicable to situations when the wind speeds close to the ground are comparable to the standard deviation of horizontal velocity fluctuations. Under these conditions, the time scale of wind meandering is large compared to the usual averaging time of one hour, and consequently the horizontal concentration distribution is far from Gaussian. Furthermore, routinely available mean wind measurements do not provide information on the turbulence levels required for modelling dispersion.

Other modelling approaches are considered more appropriate under these conditions. For example, Lagrangian particle models have been used to simulate dispersion under low wind speed conditions by various authors (e.g. Brusasca et al. 1992; Oettl et al. 2001; Anfossi et al. 2006). The trajectories of these particles are governed by measured wind speed and turbulence levels as a function of time. Another approach (Arya 1995; Sharan et al. 1995; Sharan and Yadav 1998) is based on modifying the three dimensional diffusion equation to include along-wind diffusion, which becomes important under low wind speeds. Venkatram et al. (2004) show that a steady state model can describe the concentration patterns under low wind speeds model if it accounts for the directional distribution of the horizontal wind speed. The main message from all these studies is that we can make realistic estimates of concentrations under low wind speed conditions if meteorological measurements are made at time intervals that are much shorter than the averaging time used for the concentration. In most applications, such highly resolved measurements are not available and it is necessary to make do with routine measurements resolved at one hour intervals. This motivates the two questions addressed in this chapter: 1) How do steady-state dispersion models perform under low wind speeds, and 2) Can we use routine meteorological measurements, such as wind speed at one or several levels, to derive inputs required by dispersion models. This section only addresses models applicable to source-receptor distances of a few kilometres. We also focus on surface releases under stable conditions when the surface wind speeds are typically low, and the concentration estimates from dispersion models can be relatively high.

To answer the first question, we consider two dispersion models. The first model is based on the numerical solution of the two-dimensional advection-diffusion equation, combined with the formulation for the horizontal plume spread proposed by Eckman (1994). This numerical solution provides an excellent description of surface layer dispersion (van Ulden, 1978, for example), and represents the best available steady state model. The performance of this model is compared with that of AERMOD (Cimorelli et al., 2005), the regulatory model recommended by the USEPA, which represents the current generation of dispersion models used in regulatory applications. The next section provides relevant details of these two models.

4.2 Description of Models

AERMOD (Cimorelli et al., 2005) uses the following formulation to estimate the ground level concentration from a surface release during stable conditions:

$$C(x,y) = \frac{Q}{\sqrt{2\pi}\sigma_z U_e} H(x,y) \left[exp\left(-\frac{(H_s - z)^2}{2\sigma_z^2} \right) + exp\left(-\frac{(-H_s - z)^2}{2\sigma_z^2} \right) \right], \tag{4.1}$$

where H_s is the effective stack height, and z is the receptor height. Under low wind speeds, horizontal meandering of the wind spreads the plume over large azimuth angles, which might lead to concentrations upwind relative to the vector averaged wind direction. AERMOD (Cimorelli et al., 2005), and other currently used regulatory models (ADMS, Carruthers *et al*., 1994), attempt to treat this situation by assuming that when the mean wind speed is close to zero, the horizontal plume spread covers 360°. Then, the concentration is taken to be a weighted average of concentrations of two possible states: a random spread state, and a plume state. In the random spread state, the release is allowed to spread radially in all horizontal directions. Then, the weighted horizontal distribution in Equation (4.1) is written as:

$$H(x,y) = f_r \frac{1}{2\pi r} + (1 - f_r) \frac{1}{\sqrt{2\pi}\sigma_y} exp\left(-\frac{y^2}{2\sigma_y^2} \right), \tag{4.2}$$

where the first term represents the random state in which the plume spread covers 2π radians, and r the distance between the source and receptor. The second term is the plume state corresponding to the Gaussian distribution.

The plume is transported at an effective velocity given by

$$U_e = \left(2\sigma_v^2 + U^2\right)^{1/2}, \tag{4.3}$$

where U is the mean velocity. Note that the effective velocity is non-zero even when the mean velocity is zero. The minimum value of the transport wind, U_e, is $\sqrt{2}\sigma_v$.

The weight for the random component in Equation (4.2) is taken to be

$$f_r = \frac{2\sigma_v^2}{U_e^2}, \tag{4.4}$$

This ensures that the weight for the random component goes to unity when the mean wind approaches zero. ADMS uses a weighting scheme based on the mean wind speed.

The success of this meandering correction in AERMOD depends on measurements of σ_v, which presumably reflect meandering when the wind speed is close to zero. If measurements are not available, we have to estimate σ_v from other meteorological variables.

The lateral dispersion, σ_y, in Equation (4.1) is calculated from

$$\sigma_y = \frac{\sigma_v x}{U_e(1+\alpha X)^p}, \tag{4.5}$$

where $X(=\sigma_v x / U_e z_i)$ is the non-dimensional distance defined in terms of the effective wind speed, U_e, and standard deviation of horizontal turbulent velocity, σ_v. The mixed layer height, z_i, is estimated to be $2300u_*^{3/2}$ (Venkatram, 1980) and $\alpha = 78$ and $p = 0.3$ are empirically determined values.

The vertical spread, σ_z, of a surface release is estimated from (Venkatram, 1992)

$$\sigma_z = \sqrt{\frac{2}{\pi}}\frac{u_* x}{U_e}\left(1 + 0.7\frac{x}{L}\right)^{-1/3}, \tag{4.6}$$

where L is the Obukhov length.

The surface friction velocity, u_*, is estimated from the wind speed measured at one level and an estimated roughness length, z_0. In the absence of measurements, σ_v is taken to be $1.9u_*$.

The second dispersion model is based on the numerical solution of the two-dimensional advection diffusion equation for crosswind integrated concentration, $\overline{C}^y$,

$$U\frac{\partial \overline{C}^y}{\partial x} = \frac{\partial}{\partial z}\left(K\frac{\partial \overline{C}^y}{\partial z}\right), \tag{4.7}$$

where horizontal diffusion is neglected.

The profiles of wind speed U and eddy diffusivity K are given by Businger (1973). During stable conditions, the wind speed at height z is given by

$$U(z) = \frac{u_*}{\kappa}\left[\ln\left(\frac{z}{z_0}\right) + 4.7\frac{(z - z_0)}{L}\right], \tag{4.8}$$

where u_* is the surface friction velocity, z_0 is the surface roughness length, and κ is the Von Karman constant taken to be 0.35 in van Ulden (1978). The Obukhov length, L, is defined by $L = -T_0 u_*^3 / (\kappa g Q_0)$, where Q_0 is the surface kinematic heat flux, g is the acceleration due to gravity, and T_0 is a reference temperature. The eddy diffusivity, K, is taken to be equal to the diffusivity for heat:

$$K = \kappa u_* z / \phi_h , \tag{4.9}$$

where

$$\phi_h = 0.74(1 + 6.3z / L) , \tag{4.10}$$

during stable conditions.

Equation (4.7) is solved numerically using the boundary conditions

$$\frac{\partial \bar{C}^y}{\partial z} = 0 \ at\ z{=}0\ and\ z{=}z_i \tag{4.11a}$$

and

$$\bar{C}^y\left(0, H_s\right) = \frac{Q}{U\left(H_s\right)} \delta\left(z - H_s\right) \tag{4.11b}$$

Surprisingly, there is little consensus on the calculation of horizontal plume spread for near surface releases. Based on results from an earlier study (Venkatram, 2004), we model the horizontal spread using Eckman's (1994) hypothesis

$$\frac{d\sigma_y}{dx} = \frac{\sigma_v}{\overline{U}} . \tag{4.12}$$

where the mean horizontal velocity of the plume, $\overline{U}$, is calculated from

$$\overline{U} \equiv \int_0^\infty U \overline{C}^y dz \Big/ \int_0^\infty \overline{C}^y dz . \tag{4.13}$$

Equation (4.12) can be integrated numerically to yield σ_y as a function of downwind distance *x*. Notice that σ_y grows rapidly close to the source where $\overline{U}$ is small and then slows down as the plume grows vertically into regions where the mean wind is larger.

Then, centreline concentration is given by

$$C(x,0,z) = \frac{\overline{C}^y}{\sqrt{2\pi}\sigma_y}. \tag{4.14}$$

In order to apply these models, measurements of u_*, σ_v and L are needed as inputs. If measurements are not available, we have to make estimates of these variables from routine meteorological variables. We examine the performance of these models in explaining concentrations measured in two field studies, Prairie Grass (Barad, 1958), and Idaho Falls (Sagendorf and Dickson, 1974), when the surface wind speeds are relatively low.

4.3 Field Studies

4.3.1 Prairie Grass Field Study

The Prairie Grass Project (Barad, 1958) provides a complete data for the analysis of surface layer dispersion. The tracer, SO_2, was released at a height of 0.46 m, for an interval of 10 min. The concentration was sampled with 5 arcs at 50, 100, 200, 400, and 800 m distance from the release. The samplers on the arcs were spaced at 2° intervals on the first 4 arcs, and at 1° on the 800 m arc. Half of the 70 experiments were conducted during stable conditions, which covered both low wind and high wind speed conditions. The data was obtained from http://www.dmu.dk/International/Air/Models/Background/ExcelPrairie.htm. Notice that the friction velocity and the Obukhov length were not measured but obtained by fitting similarity profiles to the mean wind speed and temperature measured at several levels on a tower. We focus on cases when the wind speed was less than 2 m/s at the tower level of 1 m.

4.3.2 Idaho Falls Field Study

The Idaho Falls experiment (Sagendorf and Dickson, 1974), which focuses on low wind stable conditions, was conducted at the Idaho National Engineering Laboratory (INEL) in a broad, relatively flat plain. SF_6 was released at a height of 1.5 m. Samplers were placed at intervals of 6° on arcs of radii of 100, 200, and 400 m from the release. The receptor height was 0.76 m. Wind measurements were provided by lightweight cup anemometers and bivanes at heights of 2, 4, 8, 16, 32, and 61 m on the 200-m arc.

We estimated u_* and L from the tower measurements, but this required an estimate of the aerodynamic roughness length, z_0. Brusasca et al. (1992) and Sharan and Yadav (1998) estimated z_0 to be 0.005 m for Idaho Falls. They obtained the value by fitting a neutral wind profile to observed winds at several levels for the only neutral case (Test 6) in the Idaho Falls experiment. This method might not be reliable because it is based on only one case. We recalculated z_0 by using the data from all the tests. We calculated the optimum z_0 by minimizing the coefficient of variation of u_* corresponding to the wind speeds measured at 2, 4, and 16 m. The 8 m wind measurement was questionable because it was often lower than that at 4m. The best estimate of z_0 turned out to be 0.08 m.

4.4 Model Performance

The performance of the models is quantified by the geometric mean (m_g) and the standard deviation (s_g) of the ratios of the observed to modeled variable as in Chapter 2.

The statistics of model performance also include the correlation between model estimates and observations, r^2, and the fraction of the estimates within a factor of two of the observations, *fact2*, in addition to to m_g and s_g.

We first examine the performance of the numerical model in estimating the normalized crosswind integrated concentration, $\overline{C}^y / Q$, for all the stable cases that occurred during the Prairie Grass experiment. This ensures that our results are consistent with those obtained in earlier studies (Nieuwstadt and van Ulden, 1978; van Ulden, 1978). We used a deposition velocity of 0.01 m/s in the numerical model for the SO_2. The meteorological inputs are taken from Table 2 of van Ulden (1978).

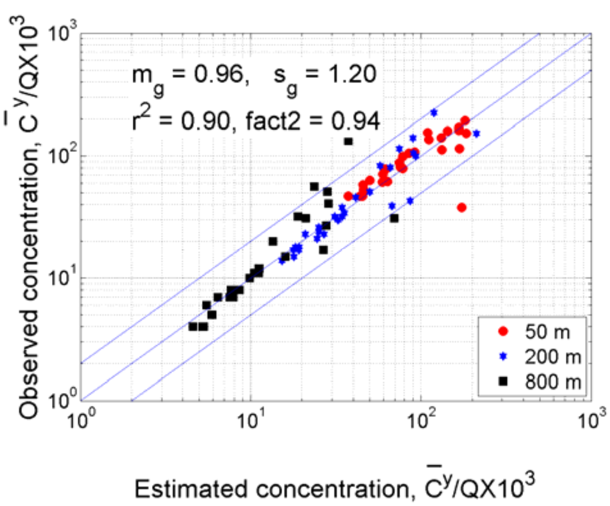

Figure 4.1: Comparison of estimated $\overline{C}^y / Q$ from the numerical method with corresponding observations during stable conditions of the Prairie Grass experiment.

Figure 4.1 shows that the performance of the numerical method is similar to that from earlier studies. The bias between the estimates and observations is only 4% and the correlation between the estimates and observations is excellent (r^2 = 0.90).

The performance of the model in explaining centreline concentrations is examined by separating the experiments into two sets: low wind set corresponding to wind speeds at 1 m of less than 2 m/s, and the high wind set to include the rest of the cases. The calculation of horizontal spread of the plume requires the standard deviation of horizontal velocity fluctuations, σ_v, which is based on σ_θ measured at 1 m. The observed values of horizontal plume spread, σ_y , are obtained by fitting Gaussian distributions to observed concentrations at each arc.

Figure 4.2 shows that during high wind stable conditions, the numerical method underestimates the observed concentrations by 39%, and overestimates the horizontal plume spread, σ_y , by 48%. But the estimates are well correlated with observations with r^2 larger than 0.89.

The underestimation of concentrations by the numerical method is clearly related to the overestimation of σ_y , which could be related to the use of a single value of σ_v measured close to surface. For the time being, we calibrated Eckman's (1994) model with the observations by multiplying the right hand side of Equation (4.12) by a 0.7 to reduce the value of σ_y. This results in the removal of most of the bias in the modeled concentration estimates.

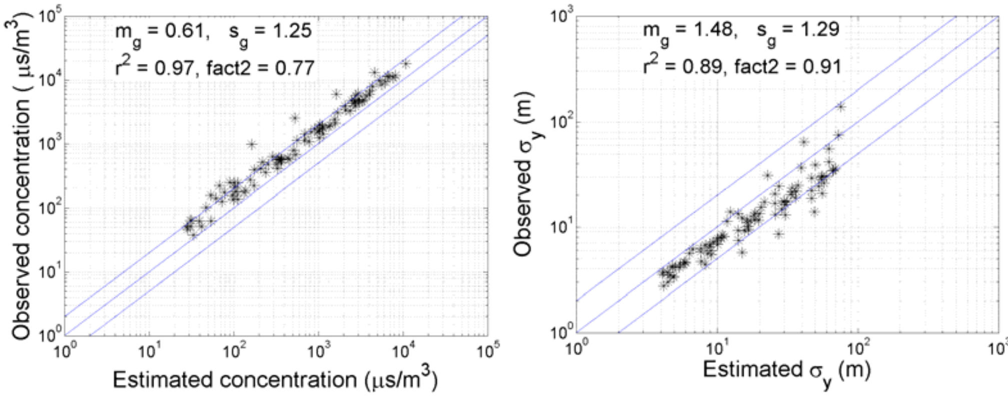

Figure 4.2: Comparison of centreline concentration (*C*/*Q*) and plume spread using the numerical method with observations from the Prairie Grass experiment during high wind stable conditions.

This calibrated model is then used to explain the concentrations observed for the low wind set. The upper panel of Figure 4.3 shows that the calibrated numerical model overestimates centreline concentrations by 42%. The correlation coefficient between the estimates and observations is only 0.55. The extreme overestimation for certain points correspond to the lowest wind speed (U = 0.66 m/s) that occurred during the Prairie Grass experiment. The overestimation of concentrations is mainly due to the underestimation of σ_y on the upper right plot of Figure 4.3.

We next use AERMOD to estimate centreline concentrations and horizontal plume spread for the same meteorological inputs. The performance of AERMOD is comparable to that of the numerical model when wind speed is higher than 2 m/s at 1 m height. AERMOD's estimates of σ_y are closer to observations because they are based on an empirical fit, Equation (4.5), to the Prairie Grass data.

The performance of AERMOD under low wind conditions is illustrated in Figure 4.3. The lower panel shows that AERMOD overestimates the concentrations by 38% and underestimates σ_y by 30% for during low wind stable conditions of the Prairie Grass experiment. The scatter in the concentration estimates (s_g = 3.05) is much larger than that of the numerical model (s_g = 1.80). The correlation between the concentration estimates and observations (r^2 = 0.12) is also smaller than that of the numerical model (r^2 = 0.55).

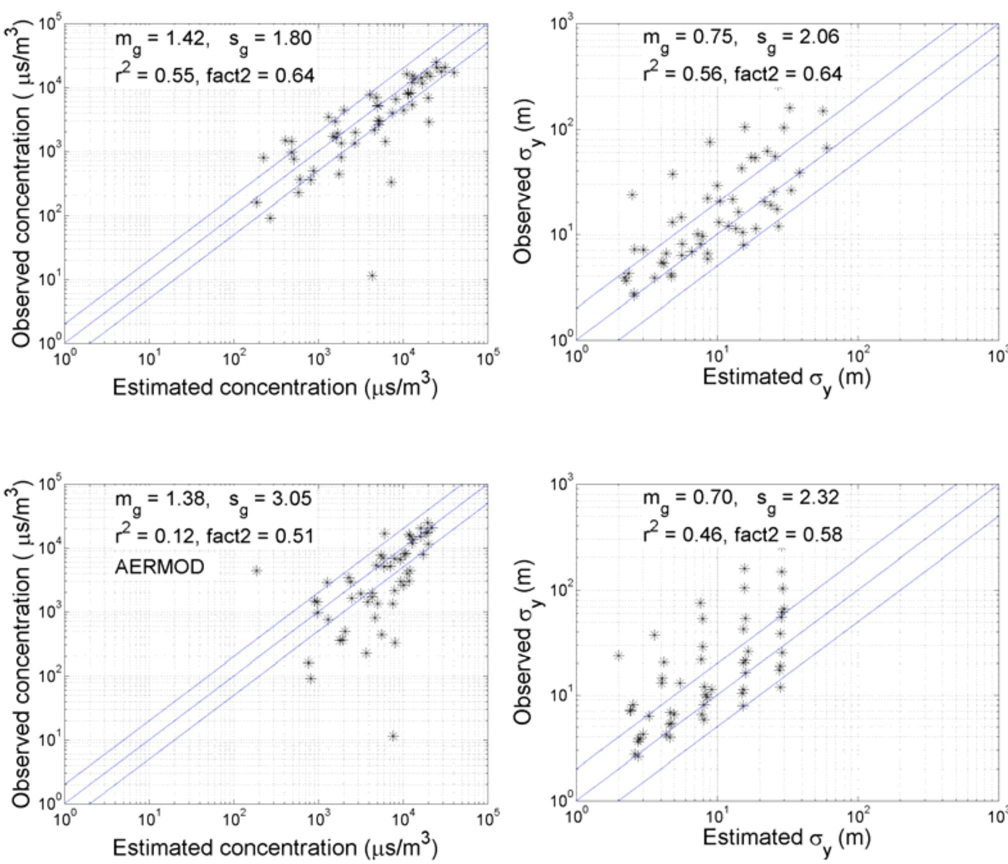

Figure 4.3: Comparison of centreline concentration (*C*/*Q*) and plume spread using the calibrated numerical model (upper panel) and AERMOD (lower panel) with observations from the Prairie Grass experiment during low wind stable conditions.

These results show that the numerical steady state model provides adequate estimates of concentrations and plume spreads because it has a justifiable description of the interaction between dispersion and the gradient of the wind speed near the surface. The meandering correction does not play a role for these cases because σ_v is small compared to the mean wind speed at 1 m. Note that Eckman's model describes horizontal plume spread even under low wind speeds as long as measured values of σ_v are used. The horizontal plume spread formula in AERMOD does not perform as well as that based on Eckman's hypothesis.

We next address how reliable are the estimates of the meteorological inputs when only routine observations at one level are available?

4.5 Estimating Meteorological Inputs

The meteorological inputs required by the models are the surface friction velocity, u_*, the Monin-Obukhov length, L, and the standard deviation of the horizontal velocity fluctuations, σ_v. We estimate these variables using the wind speed measured at one level, and an estimate of the surface roughness length, z_0.

The surface friction velocity is estimated using a method proposed in Venkatram (1980) and currently incorporated in AERMET, AERMOD's meteorological processor. It is based on M-O similarity theory for the profile of the mean wind, U, described by Equation (4.8). The temperature scale, $T_* = -\overline{w'T'}/u_*$ is taken to be 0.08 K, which is based on data from field experiments conducted in Kansas (Izumi, 1971), Minnesota (Caughey et al., 1979) and Prairie Grass (Barad, 1958). Useful estimates of L and u_* can be obtained from the following equation resulting from Equation (4.8):

$$u_* = \frac{C_{DN}U}{2}\left[1+\left(1-r^2\right)^{1/2}\right] \tag{4.15}$$

where C_{DN} is the drag coefficient during neutral conditions,

$$C_{DN} = \frac{\kappa}{\ln\left(\frac{z_r - d_h}{z_0}\right)}. \tag{4.16}$$

r is the ratio between the critical wind speed, U_{crit}, and measured wind speed, U

$$r = \frac{U_{crit}}{U} \tag{4.17}$$

where

$$U_{crit} = \frac{2u_0}{C_{DN}^{1/2}} \tag{4.18}$$

$$u_0 = \left(\frac{\beta g\left(z_r - d_h - z_0\right)T_*}{T_0}\right)^{1/2}. \tag{4.19}$$

Equation (4.15) does not have real solutions for r >1. Under such conditions, the surface friction velocity is computed as half of the neutral value,

$$u_* = C_{DN}U/2. \tag{4.20}$$

In this chapter, we approximate the offending term by

$$\left(1-r^2\right)^{1/2} \sim \exp\left(-\frac{r^2}{2}\right). \tag{4.21}$$

Then, the expression for u_* becomes

$$u_* = \frac{C_{DN} U}{2}\left[1+\exp\left(-\frac{r^2}{2}\right)\right]. \tag{4.22}$$

The vertical turbulent velocity, σ_w, which is not used directly in the models, is proportional to the surface friction velocity (Panofsky and Dutton, 1984, for example) with

$$\sigma_w = 1.3 u_*, \tag{4.23}$$

The horizontal turbulent velocity, σ_v, is related to the friction velocity through

$$\sigma_v = 1.9 u_*. \tag{4.24}$$

Assuming a constant temperature scale, T_*, results in the following expression for the Obukhov length, L,

$$L = 1100 u_*^2. \tag{4.25}$$

The observed value of σ_v is calculated as

$$\sigma_v = \operatorname{atanh}\left(\frac{\sigma_\theta}{\sigma_{\theta\max}}\right)\sigma_{\theta\max} U, \tag{4.26}$$

which defines the maximum value of σ_θ as $\sigma_{\theta\max} = \pi/\sqrt{3}$ when the wind direction distribution is uniform over 2π. When the horizontal turbulent intensity is small, it ensures that $\sigma_\theta \approx \sigma_v / U$.

We first examine the performance of Equations (4.22) and (4.24) with data from the Cardington experiment, which includes turbulence measurements during stable low wind conditions.

4.5.1 Cardington Experiment

The data analyzed here was collected at a meteorological tower operated by the U.K. meteorological office at Cardington, Bedfordshire (see http://badc.nerc.ac.uk/data/cardington/). The tower, located on a large grassy field, has sonic anemometers measuring wind and temperature measurements at 10 m, 25 m, and 50 m above ground level. That data is sampled at 50 Hz, and the vector mean winds, temperatures, turbulent fluxes and variances are averaged over 1, 10, and 30 min. We used the 30 minute averages from the 10 m in our analysis. The data set corresponds to all the stable periods (Obukhov length greater than zero) for 2005. The aerodynamic roughness length, z_0 = 0.025 m, was obtained by fitting the similarity wind speed profile to observations during near neutral conditions ($|L|$ > 200 m). This value is the same as that used by Luhar et al. (2009) in their study of low wind speed conditions.

The left panel of Figure 4.4 shows the variation of u_* / u_{*n} with U / U_{crit}, where u_{*n} is the friction velocity assuming neutral conditions. The dashed line representing Equation (4.22) follows the variation when U / U_{crit} is around 1 and higher. But when the wind speed approaches zero, the ratio of u_* / u_{*n} approaches values much larger than half of the neutral values. We propose the following tentative modification to Equation (4.22) shown by the solid line to better follow the variation when the wind speed is low:

$$u_* = \frac{C_{DN}U}{2}\frac{1+\exp\left(-r^2/2\right)}{1-\exp(-2/r)}. \tag{4.27}$$

This modification leads to a limit for u_* to be $\dfrac{C_{DN}U_{crit}}{4}$ when the wind speed approaches zero. On the right panel of Figure 4.4, we see that this limit lies in the middle of the measured values when the wind speed is close to zero, while Equation (4.22) gives much lower u_* estimates.

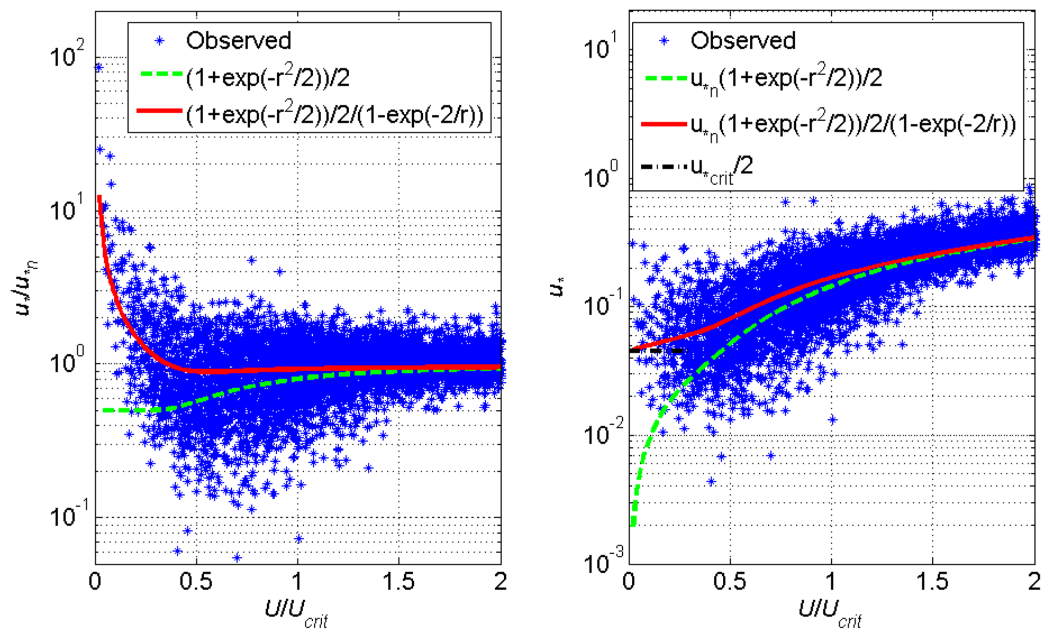

Figure 4.4: Ratio of u_*/u_{*n} (left) and u_* (right) with U/U_{crit}. Stars correspond to observations, dash lines correspond to Equations (4.22), solid lines correspond to Equation (4.27), the dash-dot line represents the limit.

The performance of Equation (4.22) and Equation (4.27) in estimating u_* is compared in the left panel of Figure 4.5. Estimates of u_* from Equation (4.22) (stars) are scattered when observed u_* are low. The modification of Equation (4.27) (dots) reduces most of the underestimation of u_*. The bias between the estimates and observations is reduced from

7% to 0% and the scatter is also reduced with s_g decreasing from 1.31 to 1.27. However, the proposed modification does not help when u_* is overestimated.

The right panel of Figure 4.5 shows the performance of Equation (4.24) in estimating σ_v based on the u_* estimates in the left panel. Because Equation (4.22) underestimates u_*, σ_v is also underestimated, as seen in the lower left plot. The modification of Equation (4.27) removes most of the underestimation of σ_v. The bias between the estimates and observations is reduced from 16% to 9%. However, a fraction of the data is still underestimated.

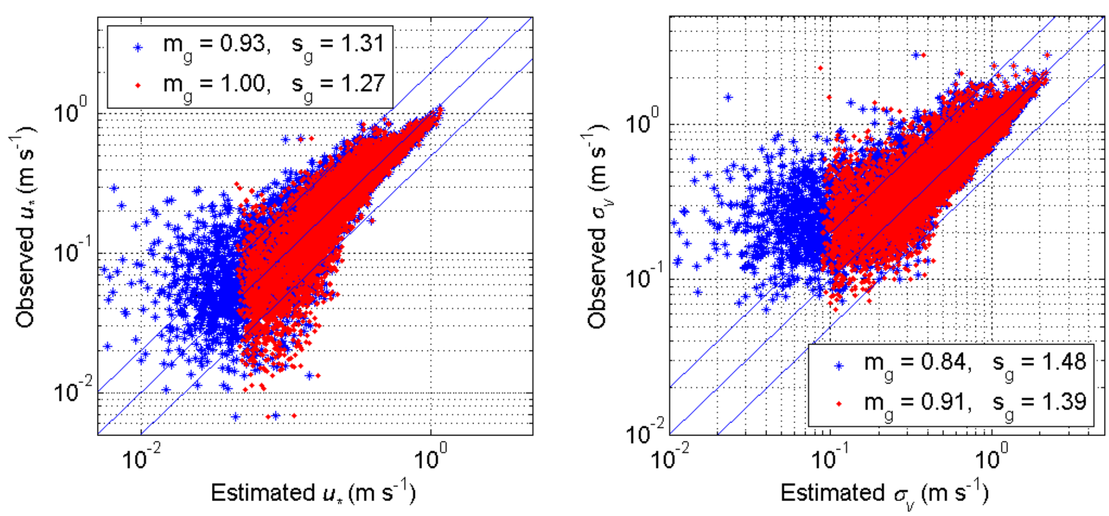

Figure 4.5: Comparison of u_* (left panel) and σ_v (right panel) estimates with observations from the Cardington site. The stars correspond to Equation (4.22) and dots correspond to Equation (4.27). σ_v is estimated from Equation (4.24) using the u_* estimates from the left panel.

4.6 Model Performance with Estimated Meteorology

We first use the numerical model to estimate the concentrations, but the meteorological inputs are based on measurements at the 1 m level. The upper panels of Figure 4.6 show estimates based on observed values of σ_v. The lower panels show concentrations based on values of σ_v related to the surface friction velocity u_* using Equation (4.27). The upper panel indicates that the bias between the concentration estimates and observations, 33%, improves upon the 42% bias corresponding to the surface friction velocity obtained from similarity used in Figure 4.3. The correlation between the estimates and observations is also better, r^2 = 0.62 here compared with r^2 = 0.55 in the upper panel of Figure 4.3. The correlation between the estimated and observed σ_y is also slightly better (r^2 = 0.58) compared with r^2 = 0.56 in the upper panel of Figure 4.3. This indicates that for this limited data set, using friction velocities based on a single wind speed yields results that are at least as good as those based on surface friction velocities derived from similarity.

However, the lower panel of Figure 4.6 shows that when σ_v is estimated from the surface friction velocity, model performance deteriorates. The centreline concentration is underestimated by 37% while σ_y is overestimated.

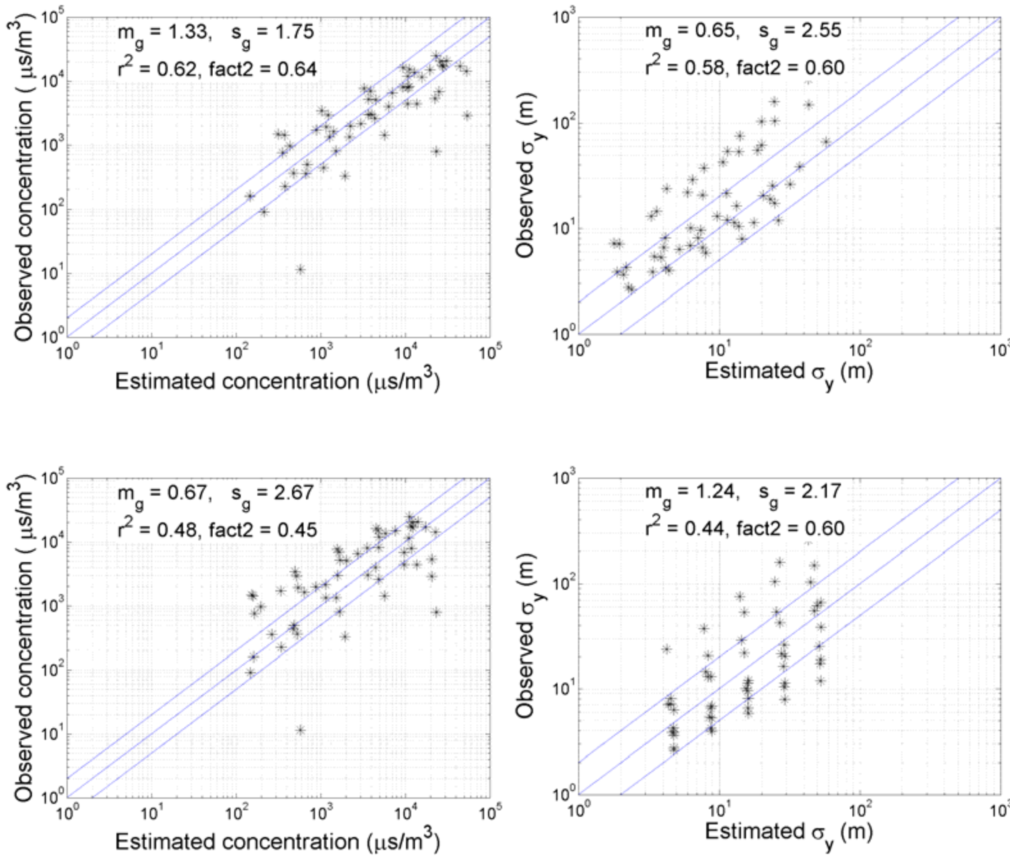

Figure 4.6: Comparison of centreline concentration (*C*/*Q*) and plume spread using the calibrated numerical method with observations from the Prairie Grass experiment during low wind stable conditions. u_* and *L* are estimated based on Equation (4.27). The upper panel uses observed σ_v, and the lower panel uses $\sigma_v = 1.9u_*$.

Figure 4.7 shows the performance of the numerical model for the Idaho Falls data. The observed σ_θ is used to calculate σ_v. The friction velocity and Obukhov length are estimated using Equations (4.27) and (4.25). The left panel shows that the centreline concentration is overestimated by 61% with the correlation coefficient between the estimates and observations, $r^2 = 0.48$.

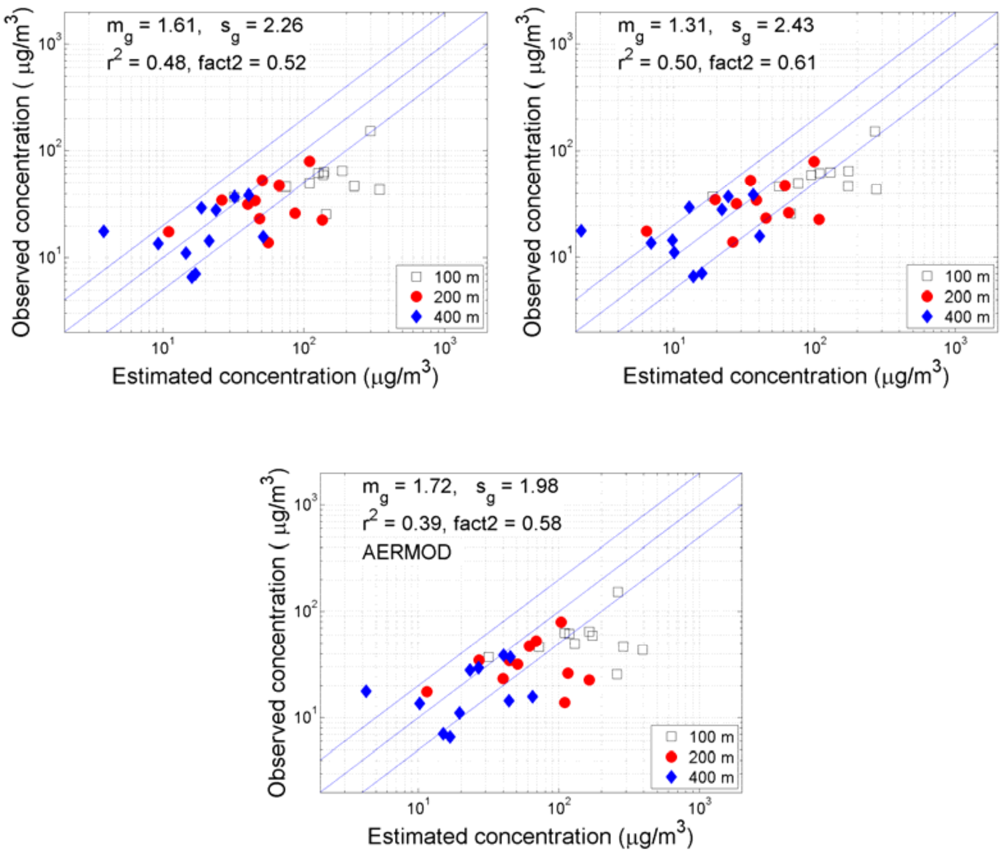

Figure 4.7: Comparison of estimates of centreline concentration using the calibrated numerical method (upper panel) and AERMOD (lower panel) with observations from the Idaho Falls experiment. Observed σ_θ is used to calculate σ_v. No meandering is considered on the upper left plot and meandering is considered on the upper right plot.

The overestimation of centreline concentration can be reduced by including meandering through the formulation in AERMOD:

$$C = \overline{C}^y \left[\frac{(1-f_r)}{\sqrt{2\pi}\sigma_y} + \frac{f_r}{2\pi r} \right]. \tag{4.28}$$

The performance of the modified numerical model is show on the right plot of Figure 4.7. The overestimation of the concentration is reduced when meandering is included in the numerical model, with m_g decreasing from 1.61 to 1.31. But the concentration is still overestimated for some cases, which is probably because the receptors did not capture the actual centreline concentrations.

The performance of the numerical method is also compared with that of AERMOD using Idaho Falls experimental data in Figure 4.7. AERMOD overestimates concentration by 72% even though it accounts for the meandering effect. The correlation coefficient between the estimates and observations is worse than that from the numerical method (r^2 = 0.39 compared with r^2 = 0.50 in the upper right plot of Figure 4.7).

The effect of meandering on the performance of the numerical model becomes apparent by examining the concentration distribution on the 50 m arc. Concentration estimates from the numerical model with and without meandering are plotted against the observations as a function of the receptor angle relative to the wind direction. The left plot of Figure 4.8 shows results for Test # 10, when the wind speed is relatively high and the random fraction is relatively low. The observed data show two peaks of concentration, which cannot be described by the steady-state model. The maximum concentration estimated from the numerical model with no meandering is higher than the observed maximum. Accounting for meandering in the model brings the maximum concentration closer to the observed value.

The right plot of Figure 4.8 shows results for Test # 8, for the wind speed when the random fraction has its highest value. We see that the concentrations are observed at large azimuth angles relative to the wind direction, indicating wind meandering. The maximum concentration from the numerical model is much larger than the observed value even when meandering is considered.

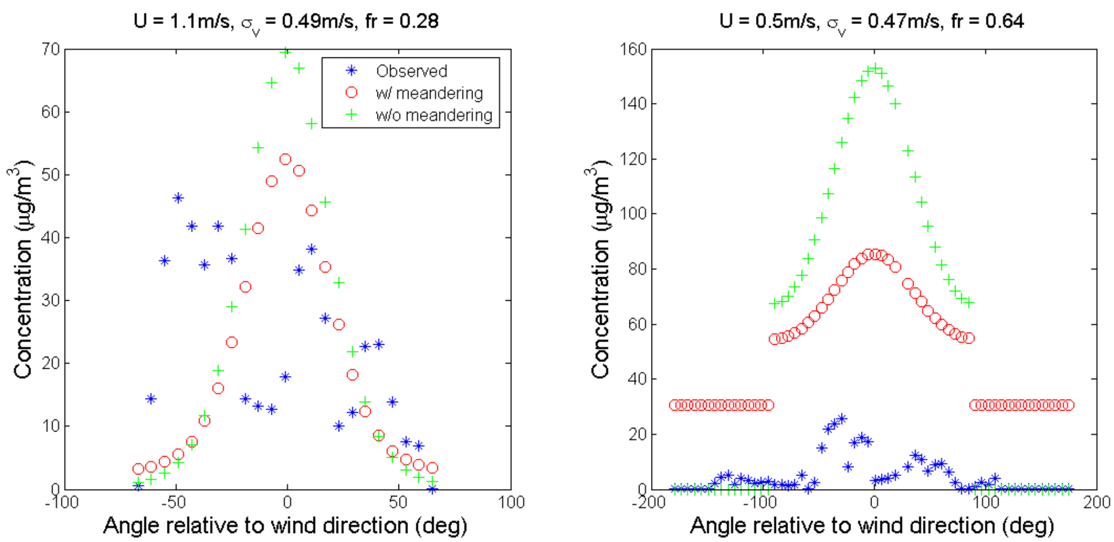

Figure 4.8: Concentration distribution with the angle relative to the wind direction for Test # 10 (left) and Test # 8 (right) of the Idaho Falls experiment. Stars represent observations, circles represent model estimates when meandering is considered, and pluses correspond to model estimates when meandering is not considered.

These results show that accounting for meandering can reduce the overestimation of maximum concentrations during low wind speed conditions. However, when meandering is large, it appears that the vertical spread is much larger than estimated using the surface friction velocity.

Figure 4.9 shows that estimating σ_v with $1.9u_*$ results in overestimation of concentrations because σ_y is underestimated. The meandering component does not help because of the underestimation of σ_v.

Limiting σ_v to be larger than 0.2 m/s reduces the overestimation to 74% from 88%. Unexpectedly, the scatter in the concentration estimates (s_g = 2.07) is smaller than that corresponding to using observed σ_v (See Figure 4.7, s_g = 2.43). The correlation between the concentration estimates and observations is also improved, with r^2 = 0.54 compared with r^2 = 0.50 in the upper right plot of Figure 4.7. These results might indicate that measurements of σ_θ may not be reliable under low wind speeds.

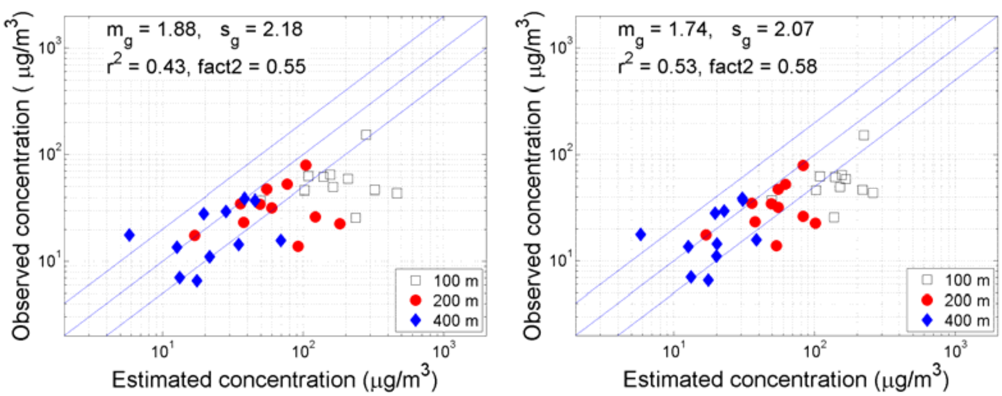

Figure 4.9: Comparison of estimates of centreline concentration using the calibrated numerical method with observations from the Idaho Falls experiment. Meandering is considered as in Equation (4.28). σ_v is estimated using Equation (4.24) (left panel) and with a lower limit of 0.2 m/s (right panel).

Finally, we examine the performance of the numerical model using several levels of wind measurements. Since the similarity relation as Equation (4.8) might not hold during low wind stable conditions, we calculate the wind speed in Equation (4.7) using the power law, $U / U_r = (z / z_r)^p$, where p is obtained by fitting to the observed winds speed at 1, 2, 4, 8, 16 m of the Prairie Grass experiment. The power, p, is obtained from the observed wind speed at 2, 4, 8, 16, 32, and 61 m of the Idaho Falls experiment.

The advantage of using several levels of wind measurements can be seen from the comparison between Figure 4.10 with the upper left plot of Figure 4.6 and the upper right plot of Figure 4.7. The overestimation of concentration is reduced using wind speed fitted to several levels of measurements. However, the correlation coefficients between the estimates and observations are comparable with those when a single level of wind measurement is used: $r^2 = 0.63$ compared with $r^2 = 0.62$ in for the Prairie Grass experiment and $r^2 = 0.51$ compared with $r^2 = 0.50$ for the Idaho Falls experiment.

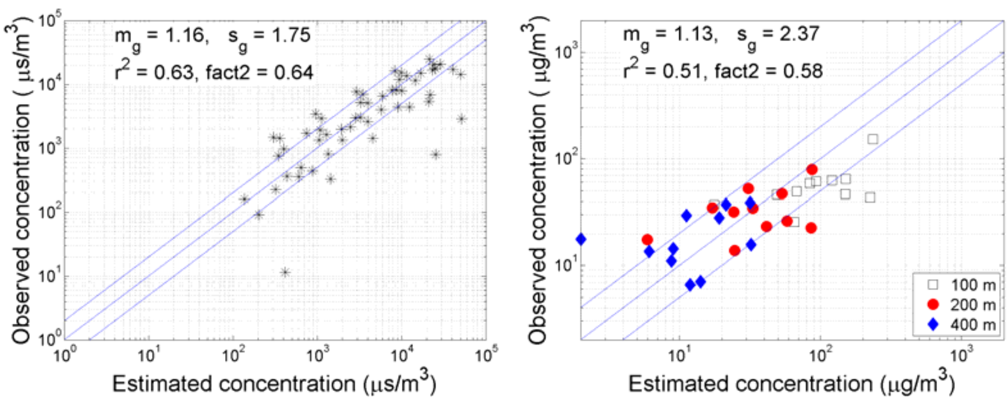

Figure 4.10: Comparison of estimates of centreline concentration using the calibrated numerical method with observations from the Prairie Grass experiment (left) and the Idaho Falls experiment (right). Wind speed is fitted from power law using several levels of measurements.

4.7 Conclusions

We evaluate the performance of two steady state models in explaining observations from two tracer studies, the Prairie Grass experiment and the Idaho Falls experiment, under stable low wind speed conditions. We find that about 50% of the concentration estimates are within a factor of two of the observations, but the scatter is large: the 95% confidence interval of the ratio of the observed to estimated concentrations is about 4. The model based on the numerical solution of the diffusion equation performs better than AERMOD in explaining the observations. Accounting for meandering of the wind reduces some of the overestimation of concentrations at low wind speeds.

The second part of the chapter examines the estimation of meteorological inputs at low wind speeds, and the impact of using these estimates in modelling. An analysis of data from the Cardington tower indicates that similarity generally underestimates the surface friction velocity at low wind speeds. These estimates can be empirically modified to reduce the underestimation. This modification leads to improvements in explaining concentrations from the Prairie Grass and Idaho Falls experiments when the observed σ_v is used to estimate horizontal plume spread.

We see that estimating concentrations associated with near surface point sources is a highly uncertain exercise when the wind speeds are low, and when only routine one-level observations are available. Even when observations of horizontal velocity fluctuations are available, there is no adequate theory to use this information to estimate horizontal spread of the plume. However, Eckman's (1994) model, based on heuristic reasoning, does provide useful estimates of horizontal spread even when the wind speeds are low.

The overall conclusion of this chapter is that the best description of dispersion of near surface point releases is provide by the combination of the two-dimensional diffusion equation and Eckman's model for horizontal dispersion; note that horizontal dispersion is not important for near surface line sources such as roads. The inclusion of a model to account for wind meandering reduces the overestimation of concentrations resulting from the Gaussian plume formulation for horizontal spread.

5. EVALUATION OF A SHORELINE DISPERSION MODEL FOR AERMOD

5.1 Introduction

Ground-level concentrations associated with sources located close to a land-water interface are affected by the thermal internal boundary layer (TIBL), which develops when stable air from the water flows onto warmer land. Vertical dispersion of near surface sources is limited by the height of the TIBL, which grows with distance from the shoreline. Elevated emissions are quickly brought down to the ground when the plume is intercepted by the TIBL. AERMOD (Cimorelli et al., 2005), the model recommended by the USEPA for regulatory applications, does not treat these processes. In view of the widespread prevalence of shoreline sources, it is important to incorporate a shoreline dispersion component in AERMOD. However, this component has to have following features: 1) It should be compatible with the current structure of AERMOD, which assumes horizontal homogeneity, and 2) It should use meteorological inputs from AERMET, AERMOD's meteorological processor.

This chapter describes a modification to AERMOD to allow its application to sources near a land-water interface. The performance of the model is evaluated with data from a tracer study conducted in the vicinity of a power plant located in Wilmington, a shoreline community in Los Angeles. It is also evaluated by the data from the Nanticoke experiments that were conducted in the vicinity of the Ontario Hydro power plant at Nanticoke on the shore of Lake Erie, Canada.

5.2 Shoreline Dispersion Model

The dispersion model presented here is based on that developed by Lyons and Cole (1973) and improved by Van Dop et al. (1979), and Misra and Onlock (1982). The model is based on the physical picture depicted in Figure 5.1.

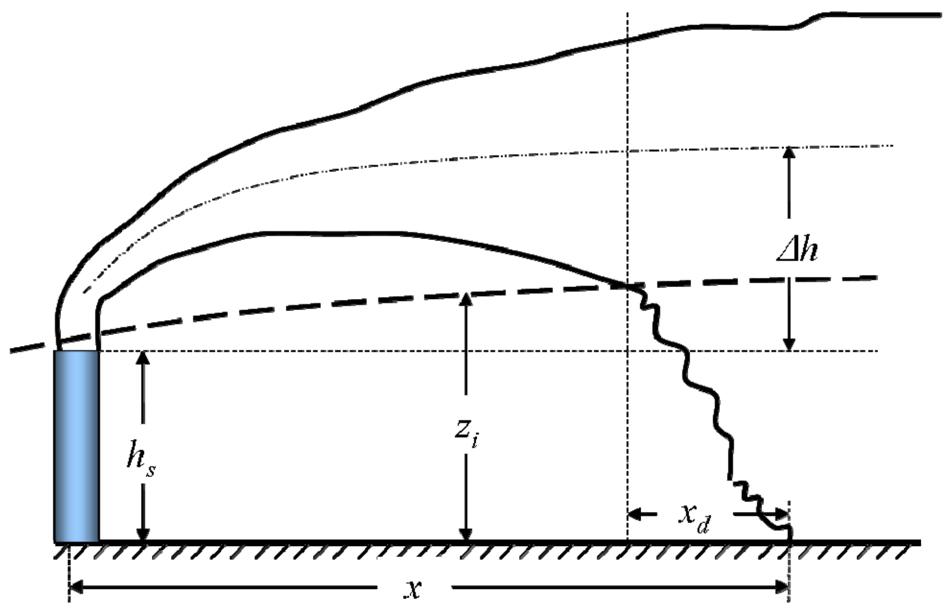

Figure 5.1: Entrainment of plume by growing internal boundary layer.

The elevated plume first travels in a stable layer before it encounters the top of the growing thermal internal boundary layer (TIBL), which develops in response to the temperature difference between land and water. As the elevated plume is transported above the internal boundary layer, it grows both horizontally and vertically due to atmospheric turbulence and turbulence generated by plume buoyancy. Because atmospheric turbulence is small above the TIBL, plume buoyancy generates most of the plume growth. This growing plume is entrained by the TIBL, whose height increases with distance from the shoreline. The entrained plume material is rapidly mixed to ground-level by the vigorous convective motions within the internal boundary layer.

The gradual entrainment of the elevated plume by the internal boundary layer is modeled by Misra (1980) as a series of point sources whose strength depends on the rate of entrainment by the TIBL and the vertical growth of the plume. Assuming that the entrained plume material is instantaneously mixed through the depth of the TIBL, the ground-level concentration is given by the sum of the contributions of all the upwind point sources. The expression for the centerline ground-level concentration is given by Misra (1980):

$$C(x,0,0) = \frac{Q}{\sqrt{2}\pi U z_i} \int_{-\infty}^{p} \frac{1}{\sigma_{yc}} \exp\left(-p^2\right) dp \tag{5.1}$$

where Q is the release rate; U is the average wind speed within the TIBL, and z_i is the height of the TIBL at the distance x, which will be discussed in detail later. The integrating variable p is related to x', the location of the point source, through

$$p = \frac{\left(z_i\left(x'\right) - h_e\right)}{\sqrt{2}\sigma_{zs}\left(x'\right)} \tag{5.2}$$

where h_e is the effective stack height, and σ_{zs} is the vertical plume spread above the internal boundary layer. The horizontal plume spread in Equation (5.1) is given by

$$\sigma_{yc}^2 = \sigma_{ys}^2\left(x'\right) + \sigma_{yu}^2\left(x - x'\right) \tag{5.3}$$

In Equation (5.3), σ_{ys} is the horizontal spread in the layer above the internal boundary layer, and σ_{yu} is the horizontal spread within the TIBL. Note that the effective horizontal plume spread combines two spreads; the plume spread in the layer above the TIBL over the distance 0 to *x'*, and then in the TIBL over the distance (*x* - *x'*).

To simplify Equation (5.1), we assume that the horizontal spread, σ_y, above the TIBL has the same value as that within the TIBL. This allows us to combine the two terms in Equation (5.3) to obtain an expression for the horizontal plume spread as a combination of that caused by turbulence and that due to plume buoyancy:

$$\sigma_{yc} = \sqrt{\sigma_y{}^2 + \sigma_s^2} \tag{5.4}$$

where σ_y is the spread caused by atmospheric turbulence, σ_v, within the thermal internal boundary layer,

$$\sigma_y = \frac{\sigma_v x / U}{\left(1 + x / L_y\right)^{1/2}} \tag{5.5}$$

The length scale, L_y, is suggested to be 2500 m by Briggs (1973) for use in urban areas on the basis of his analysis of the St. Louis experiment (McElroy and Pooler, 1968). The choice of L_y will be discussed in more detail in a later section. The term σ_s is the plume buoyancy induced spread.

The vertical spread, σ_{zs}, is taken to be

$$\sigma_{zs} = \sqrt{\left(\frac{\sigma_{ws} x}{U}\right)^2 + \sigma_s^2} \tag{5.6}$$

where the vertical turbulence above the TIBL, σ_{ws} is taken to be a nominal value of 0.001 times the value in the internal boundary layer.

Because the horizontal plume spread is not a function of p, as assumed in Equation (5.5), we can take it outside the integral in Equation (5.1) to obtain the simple expression

$$C(x,0,0)=\frac{Q f_r}{\sqrt{2\pi}U\sigma_{yc}z_i} \tag{5.7}$$

where f_r, the fraction of the plume entrained into the TIBL, is

$$f_r = \frac{1}{2}\left(1 - erf\left(\left(\frac{h_e - z_i}{\sqrt{2}\sigma_{zs}}\right)\right)\right) \tag{5.8}$$

where *erf* is the error function.

Equation (5.7) represents a minor modification of the formula that is used in AERMOD to model ground-level concentration in a well mixed boundary layer. The concentration at x is determined by the material entrained at upwind distances $x'<x$. But only a fraction of the material that is entrained into the TIBL is well mixed through the boundary layer depth at the distance x. We correct for this effect by calculating the distance x_d required for a release to become well mixed by the time it reaches x (Figure 5.1). This distance is given by

$$\sqrt{\frac{2}{\pi}}z_i = \frac{\sigma_w x_d}{U} \tag{5.9}$$

where z_i is the boundary layer height at x. Then, f_r in Equation (5.8) is evaluated at the reduced distance ($x - x_d$). Without this modification, Equation (5.7) overestimates the concentrations for the elevated release.

In Equation (5.8), the effective stack height is

$$h_e = h_s + \Delta h \tag{5.10}$$

where h_s is the physical stack and plume rise is given by the minimum of that in the neutral boundary layer and final rise in the stable boundary layer above the TIBL:

$$\Delta h = \min\left(1.6\frac{F_b^{1/3}}{U}x^{2/3}, 2.6\left(\frac{F_b}{Us}\right)^{1/3}\right) \tag{5.11}$$

where the buoyancy parameter F_b is defined as

$$F_b = gV_s\left(\frac{D_s}{2}\right)^2\frac{T_s - T}{T_s} \tag{5.12}$$

where V_s, T_s and D_s are the exhaust velocity, temperature and diameter of the stack; T is the ambient temperature. The stability parameter, s, is defined as

$$s = \frac{g}{T}\frac{d\theta}{dz} \tag{5.13}$$

Self-induced plume spread is related to plume rise through

$$\sigma_s = \frac{\beta\Delta h}{\sqrt{2}} \tag{5.14}$$

where the entrainment coefficient $\beta = 0.6$. Note that the model applies to both buoyant and non-buoyant releases.

The thermal internal boundary height, z_i, is computed using the expression (Venkatram 1977):

$$z_i = a\left(\frac{Q_0(x + x_0)}{U\gamma}\right)^{1/2} \tag{5.15}$$

where Q_0 is the average kinematic heat flux over land, x is the distance from the shoreline, U is the boundary layer averaged wind speed, and γ is the potential temperature gradient above the TIBL. The parameter x_0 is the distance of the effective shoreline from the release, which is discussed later. The parameter, a, is an empirical constant, whose value is presented later. We next describe the field study that was conducted to collect the data used in model evaluation.

5.3 Field Study

The data required to evaluate the model was collected in a field study conducted near the Harbor Generating Station of the City of Los Angeles's Department of Water and Power (LADWP) in Wilmington, a suburb of Los Angeles in 2005. The field study focused on elevated tracer releases and was conducted between June 24th and June 28th 2005.

Each experiment involved release of the tracer gas, sulfur hexafluoride (SF_6), over periods lasting from 5 to 6 hours during each day of the four day experiment. Two sets of experiments were conducted. During the studies conducted on June 24th and June 27th, SF_6 was metered at 4 g/sec (16 kg/hr) and was introduced into the base of the 67 m high stack to allow it to become well mixed with the stack exhaust. The inner diameter of the stack is 4.7 m, and the exit velocity and temperature of the exhaust gases are 23 m/s and 458 K, respectively. The plume buoyancy parameter works out to be 431 m^4/s^3, which results in a plume rise of about 175 m for the meteorological conditions observed during the field study.

During the remaining two days, June 26th and June 28th, pure SF_6 was metered with a mass flow controller and mixed with 1000 L/min of ambient air provided by a vane pump to change the buoyancy of the gas to nearly that of the surrounding air. The diluted SF_6 was released at a rate of 4 g/sec (16 kg/hr) outside the stack and about 3 m below the stack top. Figure 5.2 shows the layout of the study area and the locations of the tracer release and sampling equipments.

Integrated box samplers were deployed along three arcs with distances of 1000 m, 3000 m and 5000 m north of the source. Two sonic anemometers, with their sensors at heights of 3 and 6 meters, a minisodar, soil moisture and surface temperature sensors, temperature and relative humidity measurement systems were placed near the western fence line of the power plant, approximately 100 meters away from the plant stacks. A second minisodar was located approximately four kilometers further inland on the Los Angeles County Sanitation Districts' Joint Water Pollution Control Plant (JWPCP). A three-axis sonic anemometer with its sensors at heights of 7 meters was also located at this facility. The temperature from near surface to up to about 600 meters was measured at this facility using a remote sensing microwave temperature profiler.

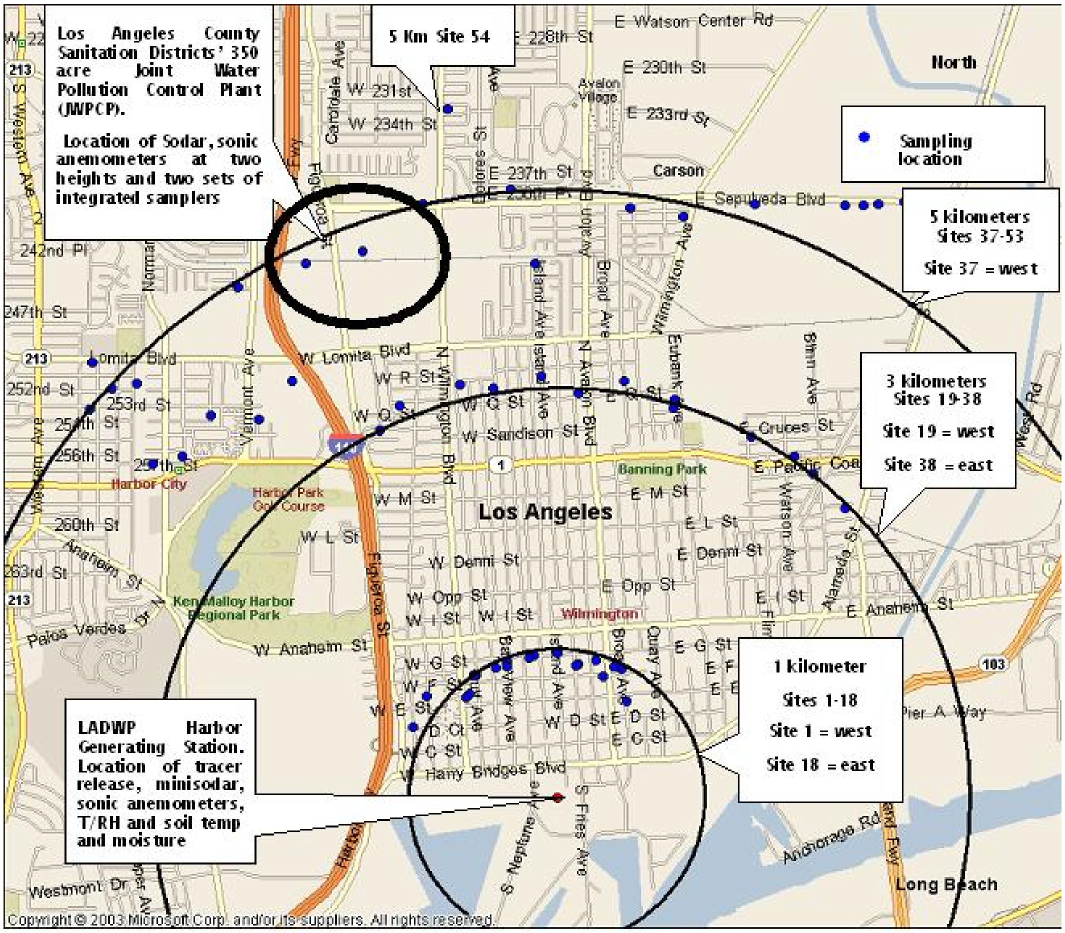

Figure 5.2: Map of Study Area and Equipment Locations for Wilmington 2005 Study.

The detailed meteorological information was used directly as inputs to the dispersion model described. It was also used to evaluate the estimates of the model inputs generated by AERMET. This information provided an opportunity to examine the change in model performance when AERMET outputs were used instead of measured values.

5.4 Meteorological Inputs

The meteorological inputs required by the model in are: 1) the turbulent velocities, σ_w and σ_v, in the TIBL, which are assumed to be uniform with height, and 2) the TIBL height as a function of distance from the shoreline. The turbulent velocities were measured using the sonic anemometer and the minisodar. The TIBL height was estimated using the measured surface heat flux in Equation (5.15). These inputs were also estimated with AERMET outputs, as described next.

AERMET, AERMOD's meteorological processor, is based on a one-dimensional boundary layer model that, in principle, cannot be applied to shorelines where surface properties vary sharply across the water-land interface. AERMET estimates the surface heat flux, Q_0, using information on latitude, surface albedo, surface temperature, and fractional cloudiness to compute net radiation, which is then partitioned between sensible and latent heat flux using the Bowen ratio. The heat flux is then used with information on the 10 m wind speed and the surface roughness length, z_0, to estimate the surface friction velocity. The surface parameters in AERMET's surface file (.sfc) are then used in AERMOD to construct vertical profiles of temperature, wind speed, and turbulence using similarity profiles (See Cimorelli et al., 2005 for details).

The AERMET surface information was used to construct inputs for the shoreline dispersion model using the following methods. The free convection contribution to the standard deviation, σ_w, of the vertical velocity fluctuations can be written as:

$$\sigma_w = \alpha w_* = \alpha \left(\frac{g}{T_0} Q_0 z_i \right)^{1/3} \tag{5.16}$$

where $\alpha = 0.6$ (Stull, 1988), and w_* is convective velocity scale. Then, an expression for the convectively generated component of turbulence in the TIBL can be obtained by combining Equations (5.15) and (5.16)

$$\sigma_{wc} = \alpha Q_0^{1/2} \left(\frac{g}{T_0} \right)^{1/3} \left(\frac{4x}{U\gamma} \right)^{1/6} \tag{5.17}$$

Note that this component is relatively insensitive to the distance, x, from the land-water interface, the wind speed, U, and the potential temperature gradient, γ. The surface heat flux is expected to vary with distance form the shoreline, with the maximum occurring close to the shoreline where the temperature difference; the square root dependence of σ_{wc} on heat flux might reduce the uncertainty associated with assuming that it does not vary with x.

The convective contribution σ_{wc} is added to the shear generated components of turbulence as follows:

$$\sigma_{\mathrm{w}} = \left(\sigma_{\mathrm{wc}}^3 + \sigma_{\mathrm{ws}}^3 \right)^{1/3} \text{ and } \sigma_{\mathrm{v}} = \left(\sigma_{\mathrm{wc}}^3 + \sigma_{\mathrm{vs}}^3 \right)^{1/3} \tag{5.18}$$

where $\sigma_{ws} = 1.3u_*$ and $\sigma_{vs} = 2.5u_*$, and u_* is the surface friction velocity from AERMET.

The AERMET surface file for Wilmington was constructed using local information that might not be available on most sites. The surface roughness, z_0, was taken to be 0.4 m based on measurements made by Princevac and Venkatram (2007) and the surface wind speed was measured using the sonic at the JWPCP site. The surface albedo of 0.3 and a cloud cover fraction of 0.7 were obtained by fitting the computed net radiation to that measured by the radiometer at the LADWP site. The Bowen ratio was obtained by calibrating the computed heat flux with the measured flux. The upper left plot of Figure 5.3 compares the estimated heat fluxes with those averaged from the measurements at the lower and upper sonics at the LADWP site and at the JWPCP site. The heat flux is generally overestimated in the morning and a little underestimated close to noon. A Bowen ratio of 1 gave the best estimates of the heat fluxes averaged over these two sites. Such calibration procedures are clearly not possible at most sites where sonic measurements are unlikely, and the surface inputs are likely to be more uncertain than those at Wilmington. A later section presents results on the effect of this uncertainty on ground-level concentrations.

We replaced the boundary layer height estimated by AERMET with the TIBL height given by Equation (5.15). We took $\gamma = 8$ K/1000 m based on temperature measurements at Wilmington. The constant a in Equation (5.15) is taken to be 2, a value which is consistent with that implied by the data presented in Table 1 of Misra and Onlock (1982).

Observations of wind speed and turbulence levels at 50 m are considered to be representative of boundary layer values. In the AERMET based model, the 50 m wind speed and turbulence levels were computed by using similarity profiles to extrapolate upwards; the inputs are the surface friction velocity, wind speed, surface heat flux, and the surface roughness length. The upper right plot of Figure 5.3 shows that the scatter in the wind speed estimates is large. The lower panel of Figure 5.3 shows that the turbulent velocities are underestimated, while the scatter in the σ_v estimates is larger than that of the

σ_w estimates. However, most of the estimates are within a factor of two of the observations of wind speed and turbulent velocities.

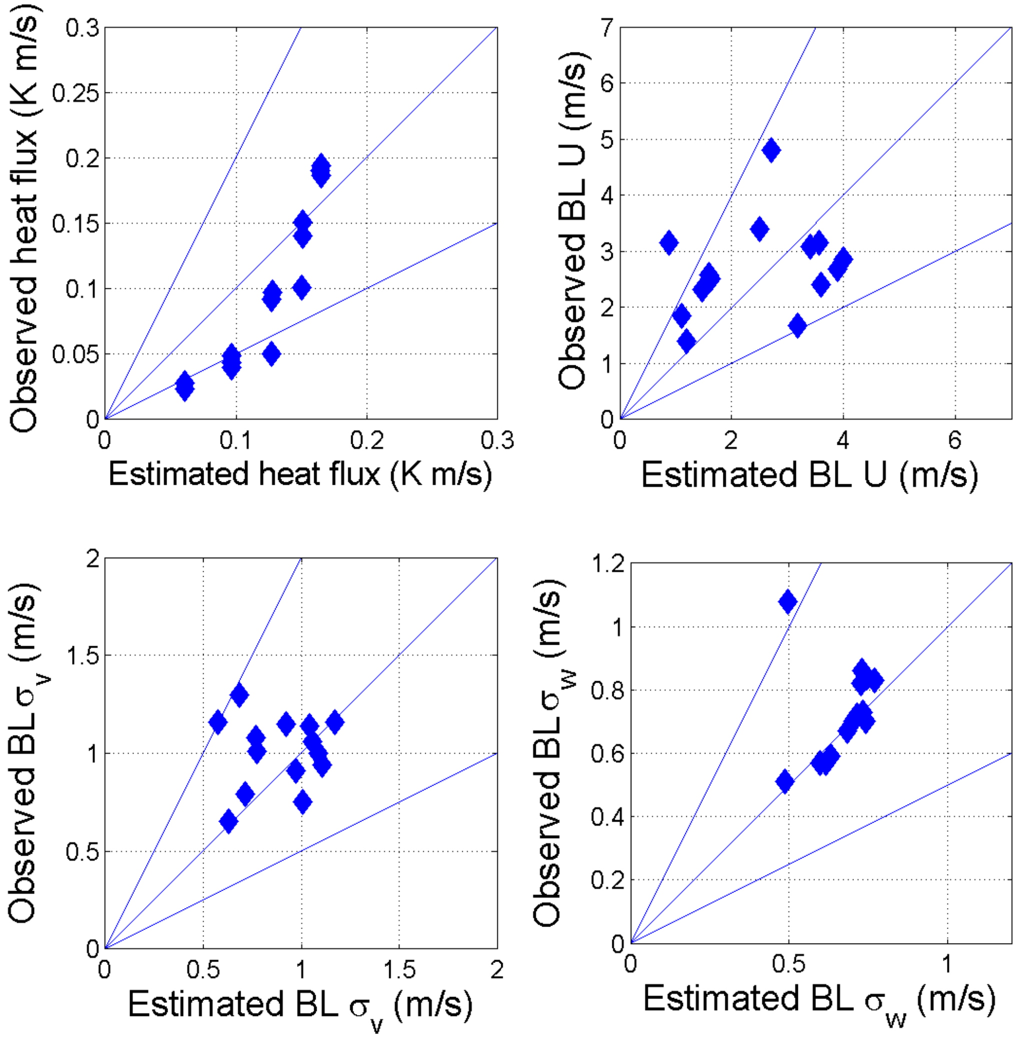

Figure 5.3: Comparison of estimated heat flux (upper left), wind speed (upper right), and turbulence levels (lower) from AERMET based model with observations for Wilmington 2005 study. Observed heat flux is averaged from measurements at both LADWP and JWPCP sites in the upper left plot. 'BL' denotes for 'boundary layer', referring to height of 50 m here.

We also estimated the 10 m meteorology as if AERMET was being used routinely. The major differences occur in the wind speed and σ_w. Both estimated wind speed and σ_w at 10 m are less than those observed at the 50 m as expected. We will examine the impact of such uncertainties in the meteorological estimates on the performance of the dispersion model in the next section.

5.5 The Length Scale L_y

During the examination of the dispersion model, we realized the importance of an appropriate choice of the length scale L_y in Equation (5.5). Briggs (1973) suggested L_y = 2500 m based on the analysis of the St. Louis experiment. It is necessary to examine the rationale behind the choice of this empirical parameter.

We start with the lateral dispersion based upon Taylor (1921)

$$\sigma_y = \frac{\sigma_v x}{U\left(1+\dfrac{x/U}{2T_{Ly}}\right)^{0.5}} \tag{5.19}$$

where T_{Ly} is the Lagrangian time scale. Equating Equation (5.19) with Equation (5.5) gives $L_y = 2T_{Ly}U$. In the convective boundary layer, it is reasonable to assume the Lagrangian time scale to be $T_{Ly} = z_i / w_*$. Substituting Equations (5.15) and (5.16) in this expression gives,

$$T_{Ly} = z_i / w_* = a^{2/3}\left(\frac{x}{UN^2}\right)^{1/3} \tag{5.20}$$

Thus the length scale L_y becomes

$$L_y = 2T_{Ly}U = 2a^{2/3}\left(\frac{xU^2}{N^2}\right)^{1/3} \tag{5.21}$$

We tested the use of Equation (5.21) in Equation (5.5) in modeling concentrations from the Wilmington field study. The results indicate that we could choose a constant value of L_y = 1000 m instead of 2500 m to obtain results similar to those from Equation (5.21). Although using L_y = 2500 m results in better concentration estimates for non-buoyant releases, we can not justify using two different values of L_y. Thus, in the following sections, we choose the empirical value of L_y = 1000 m.

5.6 Performance of the Shoreline Dispersion Model

The performance of the models is quantified by the geometric mean (m_g) and the standard deviation (s_g) of the ratios of the observed to modeled variable as in Chapter 2. r^2 is the correlation coefficient between the logarithmic values of C_o and C_p.

Figure 5.4 compares observed arc maximum concentrations with model estimates obtained using onsite meteorological inputs. The left panel indicates that concentrations are adequately estimated for the elevated buoyant releases. Most of the model estimates are within a factor of two of the observations. The model explains 80% of the observed variance. The right panel corresponds to elevated non-buoyant releases. The concentration is overestimated by 50% with m_g = 1.5, while most of the model estimates are within a factor of two of the observed values. The model explains 70% of the variance of the observations. The overestimation of concentration for non-buoyant releases could be reduced if we use L_y = 2500 m in Equation (5.5) but we used the same consistent value of L_y = 1000 m for both buoyant and non-buoyant releases.

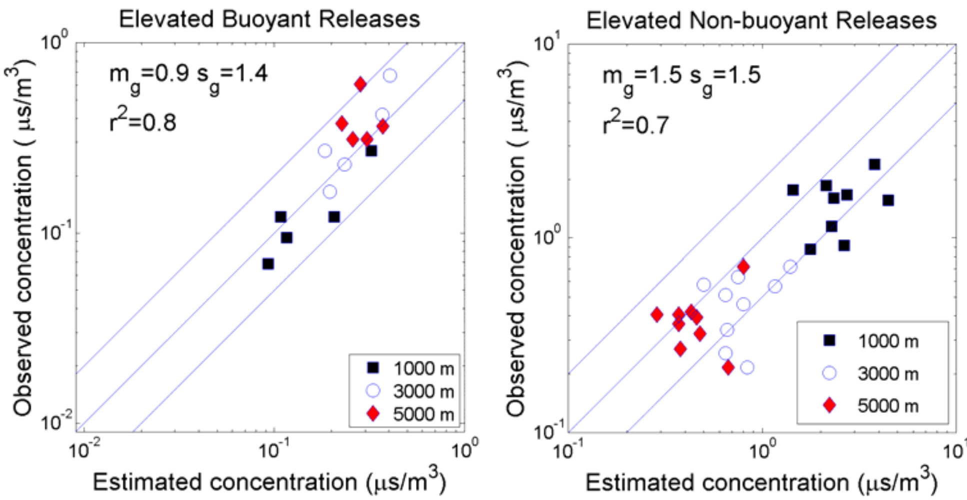

Figure 5.4: Comparison of measured arc maximum concentrations with model results for buoyant (left) and non-buoyant (right) releases for Wilmington 2005 study. The length L_y in Equation (5.5) is chosen to be 1000 m.

Figure 5.5 uses meteorology estimated at 50 m height from the AERMET based surface variables. The uncertainties in the meteorological estimates seem to have little impact on the concentration estimates. The model still explains 70% of the variance in the observations. The left panel shows that the concentration is overestimated by 10% for buoyant releases. The overestimation is explained by the overestimation of heat flux resulting in a higher TIBL, which in turn entrains more of the elevated plume. The right panel shows that the overestimation of concentration is reduced to 40% for non-buoyant releases, which is also the result of a higher TIBL. The uncertainties in the TIBL height have less impact on the concentration estimation for non-buoyant releases.

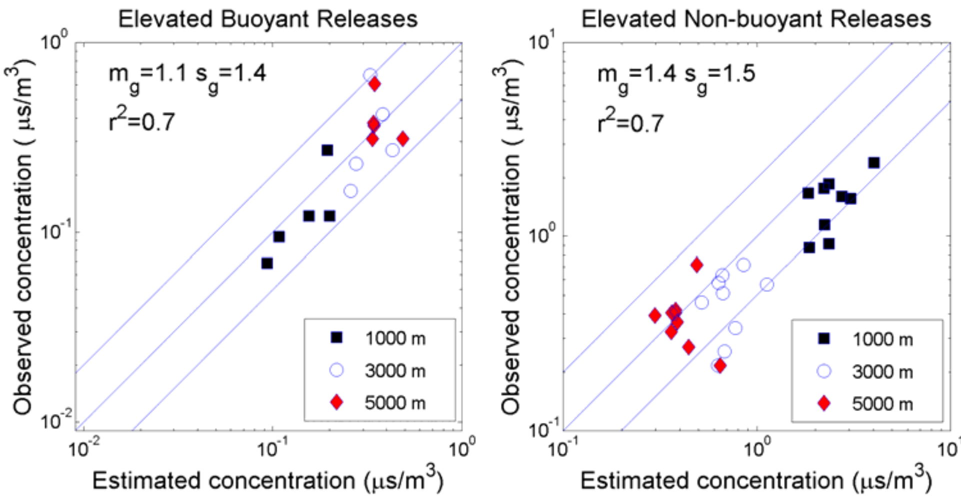

Figure 5.5: Comparison of measured arc maximum concentrations with model results for buoyant (left) and non-buoyant (right) releases for Wilmington 2005 study. Meteorology is estimated from the AERMET based values at 50 m.

This section has shown that concentration can be adequately estimated when meteorological inputs are estimated using an AERMET based model. The good model performance might be explained by the adequate estimates of heat flux using appropriate choice of parameters in the surface energy balance method. The next section examines the model performance using different choices of input parameters.

5.7 Sensitivity Studies

Figure 5.6 uses meteorology estimated at 10 m height as if AERMET were used. Concentration is still adequately estimated in spite of the fact that wind speed and σ_w estimated at 10 m are lower that those at 50 m. More than 60% of the observed variance is explained by the model. For buoyant releases, shown in the left panel, underestimation of wind speed leads to slight increase of the TIBL height. The increases in plume rise and the vertical plume spread, σ_{zs}, counteract with each other to reduce the impact on ground-level concentrations. For non-buoyant releases, shown on the right, lower wind speeds lead to higher TIBL and larger σ_{yc}. A detailed examination shows that the denominator of Equation (5.7) is proportional to $U^{-2/3}$. Thus using a lower wind speed results in lower concentrations for non-buoyant releases. The overestimation of concentration is reduced to 20% in the right panel of Figure 5.6 from 40% in the right panel of Figure 5.5.

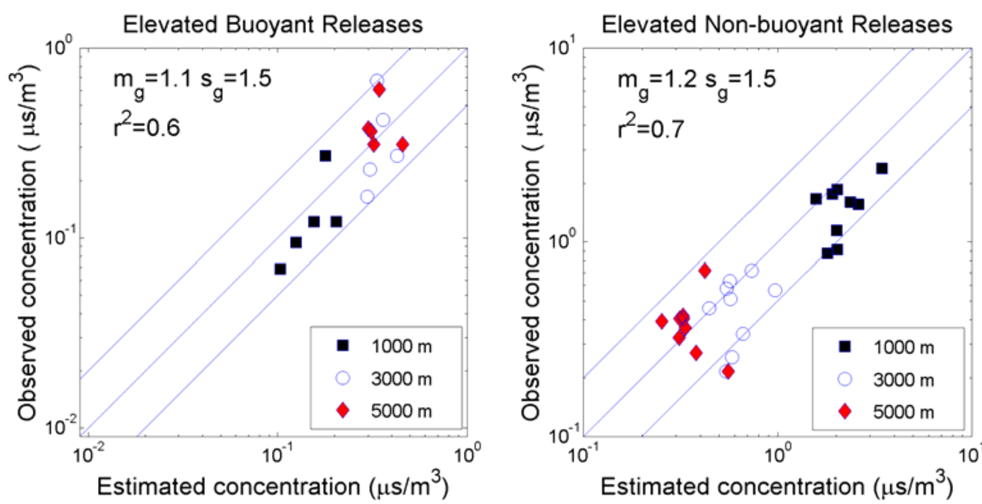

Figure 5.6: Comparison of measured arc maximum concentrations with model results for buoyant (left) and non-buoyant (right) releases for Wilmington 2005 study. Meteorology is estimated from the AERMET based model at 10 m.

The previous section shows that appropriate choice of surface parameters yields heat flux estimates that compare well with observations, which leads to appropriate estimates of TIBL height and concentrations. However, surface parameters such as cloud cover and Bowen ratio are not always available. Besides, the Bowen ratio can vary substantially both spatially as well as temporarily in urban areas (Ching, 1985; Roth and Oke, 1995). Next, we examine impact of the uncertainty in Bowen ratio on model performance.

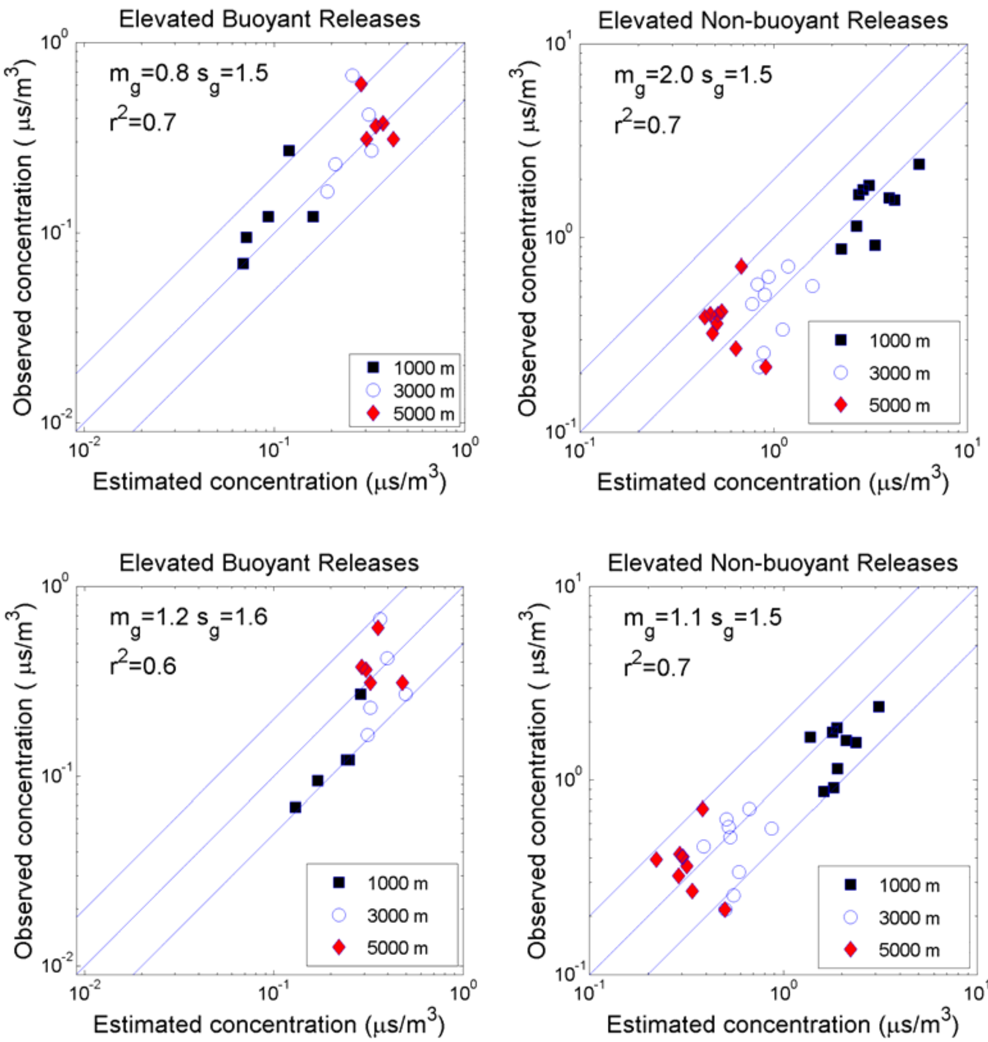

Figure 5.7: Comparison of measured arc maximum concentrations with model results for buoyant (left) and non-buoyant (right) releases for Wilmington 2005 study. Meteorology is estimated from the AERMET based values at 50 m. Bowen ratio is 0.5 in the upper panel and 2 in the lower panel.

The upper panel of Figure 5.7 uses Bowen ratio of 0.5 and the lower panel of Figure 5.7 uses Bowen ratio of 2. Comparison of Figure 5.7 with Figure 5.5 shows that larger values of Bowen ratio lead to higher heat flux and TIBL. Thus more pollutants are entrained into the TIBL for buoyant releases and concentration estimates are higher. For non-buoyant releases, concentrations become lower if larger Bowen ratio is used because pollutants are well mixed in higher TIBL.

When the Bowen ratio is chosen to be 0.5, the overestimation of concentration for non-buoyant releases increases to 100% with m_g = 2 in the upper right of Figure 5.7. When Bowen ratio is chosen to be 2 (the lower panel of Figure 5.7), concentrations are overestimated by 20% for buoyant releases. Although the model still explains more than 60% of the variance in the observations, it is clear that the bias is sensitive to the Bowen ratio.

We next examine the sensitivity of model results to the choice of roughness length. The upper and lower panels of Figure 5.8 use z_0 = 0.2 and 0.8 respectively, which are half and twice of the value obtained by Princevac and Venkatram (2007). The upper panel of Figure 5.8 shows that using a lower value of z_0 yields results comparable to those in Figure 5.5. The lower panel of Figure 5.8 shows that using a higher value of z_0 deteriorates the performance of the model: concentrations are underestimated by 40% for the buoyant releases. The underestimation of concentration can be partly explained by the overestimation of wind speed and σ_y in Equation (5.7) resulting from the higher value of z_0. The overestimation of wind speed also leads to less entrainment since the TIBL decreases faster with wind speed ($z_i \propto U^{-1/2}$ in Equation (5.15)) than the plume rise ($\Delta h \propto U^{-1/3}$ in Equation (5.11) once the final plume rise is reached). The results shown here are compatible with the findings by Qian et al. (2010), who showed that using a higher value of z_0 deteriorated the friction velocity estimation since z_0 becomes comparable to the effective measurement height, $z_r - d_h$. Concentration estimates for non-buoyant releases are less sensitive to the choice of z_0 because the increase of wind speed and σ_y counteract each other with the decrease in TIBL height.

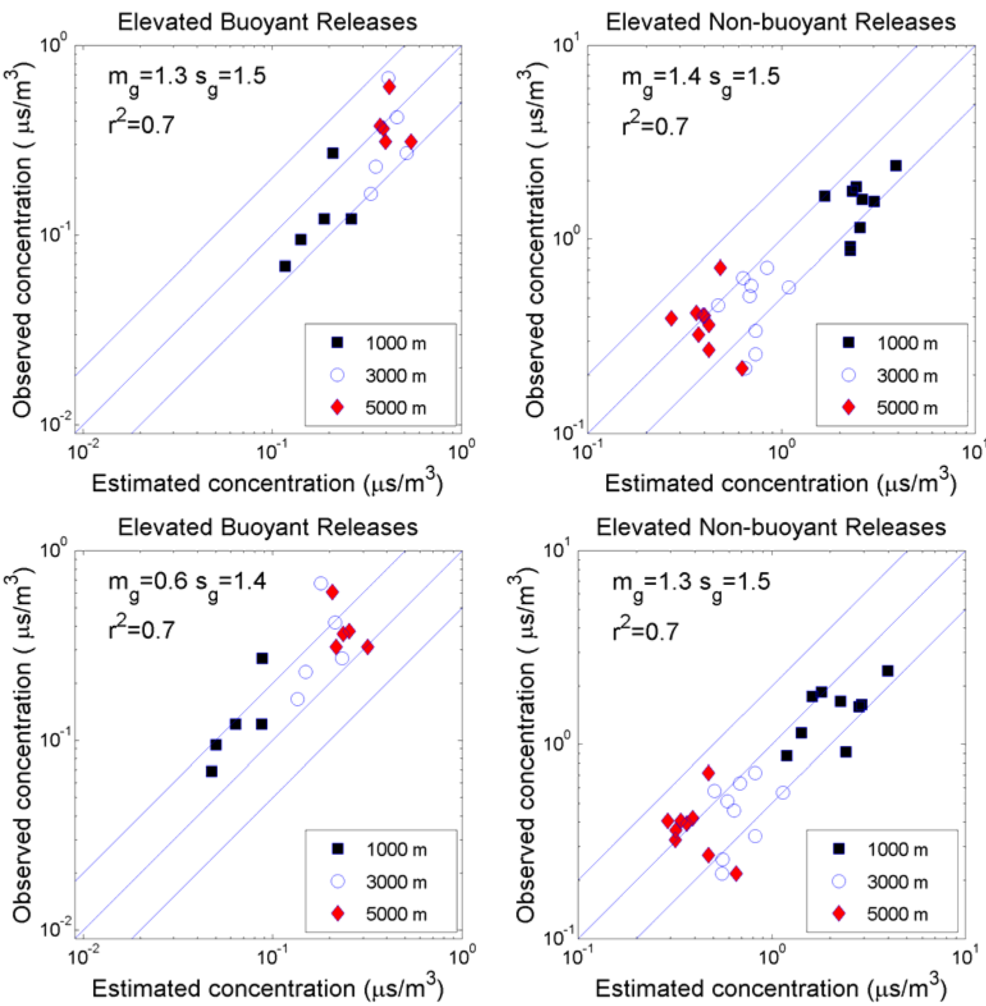

Figure 5.8: Comparison of measured arc maximum concentrations with model results for buoyant (left) and non-buoyant (right) releases for Wilmington 2005 study. Meteorology is estimated from the AERMET based values at 50 m. surface roughness length, z_0, is 0.2 m in the upper panel and 0.8 m in the lower panel.

5.8 Nanticoke Experiments

The performance of the shoreline dispersion model is also examined using the Nanticoke experiments during May 9 – June 16, 1978 and May 28 – June 14, 1979 (Portelli, 1979; Misra and Onlock, 1982), designated as EXP I and EXP II respectively. Nanticoke is on the northern shore of Lake Erie, Canada. A TIBL develops over land for onshore/lakebreeze flow in the lakeshore environment. The electric power generating station of Ontario Hydro at Nanticoke has two 198 m stacks at the shoreline with a separation of 273 m. Plumes from these two stacks are observed to merge within a short downwind distance to form one plume.

Observations of meteorology and concentrations for Nanticoke experiments can be found from Tables 1-3 of Misra and Onlock (1982). The measurements of TIBL in the Nanticoke experiment make it possible to check the formulation of Equation (5.15). The coefficient $a = 2$ is consistent with that implied by the data presented in Table 1 of Misra and Onlock (1982). The turbulent velocity, σ_w and σ_v, are taken to be $0.6w_*$ (Panofsky et al., 1977), where w_* was measured. The total buoyancy parameter, F_b, is taken to be the sum of the buoyancies from each of the two stacks. A default value of 1500 m^4/s^3, based on other measured values, is assigned wherever it is missing in the table. The Brunt–Väisälä frequency, N, was listed in Table 2 for EXP II of Nanticoke in Misra and Onlock (1982), while it is not given for EXP I. We assume $N = 0.0135\ s^{-1}$ from Table 2 also applies to EXP I. Then the stability parameter, s, is calculated to be $(0.0135)^2\ s^{-2}$. The length scale, L_y, in Equation (5.5) is also taken to be 1000 m determined for the Wilmington experiment.

Figure 5.9 shows the performance of the shoreline dispersion model described earlier in estimating concentrations for EXP I (left panel) and EXP II (right panel) of the Nanticoke experiments. Most of the concentration estimates are within a factor of two of the observations. The bias between the estimates and observations is less than 20%. The extreme underestimation of concentrations at two points in the left panel of Figure 5.9 might be due to the uncertainty in the determination of crosswind positions as mentioned by Misra and Onlock (1982). On the other hand, the right panel of Figure 5.9 shows that the crosswind concentrations in each case of EXP II are adequately estimated. The good performance also proves indirectly that L_y = 1000 m in Equation (5.5) is a reasonable empirical value. The small difference between the ground level concentration of case 2 (dots) and the concentration measured by a helicopter at 100 m (squares) indicates that concentration is indeed well mixed within the TIBL.

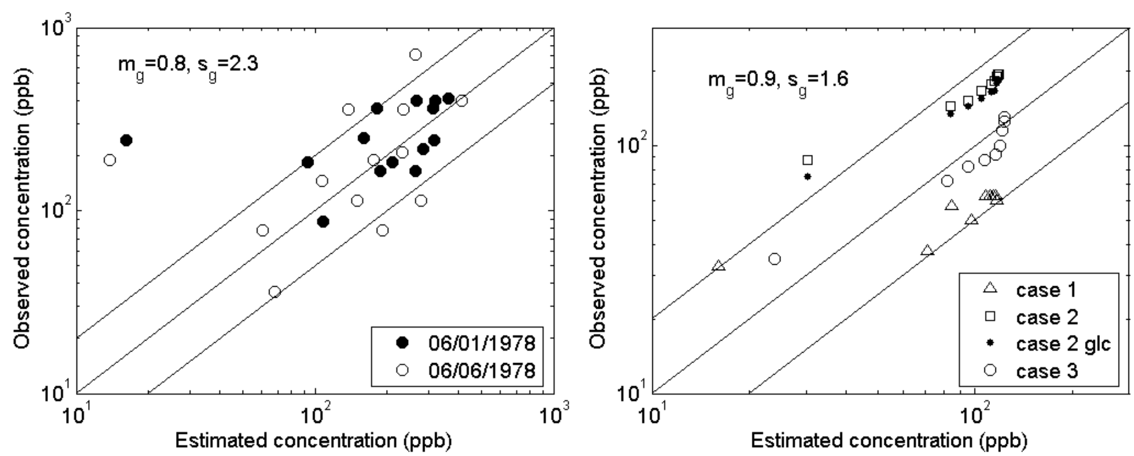

Figure 5.9: Comparison of estimated concentration with corresponding observations in Nanticoke experiments. The left panel corresponds to EXP I and the right panel corresponds to EXP II.

5.9 Conclusions

This chapter evaluates the performance of semi-empirical dispersion model applicable to shoreline sources. The model is a simplified version of a model developed earlier by Lyons and Cole (1973) and improved by Van Dop et al. (1979) and Misra and Onlock (1982). This version is designed to be compatible with the one-dimensional structure of AERMOD, and can use the meteorological outputs from AERMET. The model incorporates the entrainment of an elevated plume by the thermal internal boundary layer (TIBL), whose height increases with distance from the shoreline.

Concentration estimates from the model are compared with observations made in two field studies, one in Wilmington, CA. and the other in Nanticoke, Ontario, Canada. The model performs well when onsite measurements are used to derive meteorological inputs for the model. These inputs have also been constructed by processing of the meteorological outputs from AERMET using a two-dimensional TIBL model. Model performance using meteorological inputs estimated from this method is comparable to that based on onsite measurements. Sensitivity studies show that adequate estimates of heat flux are critical in determining the performance of the shoreline dispersion model in estimating concentrations especially for buoyant releases above the TIBL. Parameters such as cloud cover, albedo and Bowen ratio need to be chosen appropriately to yield adequate estimates of heat flux. Because these parameters are likely to be uncertain, it might be important to use measurements that can provide indirect estimates of heat flux. Using measurements of temperature fluctuations to infer heat fluxes (as in Chapter 2) is one approach.

Results also show that choosing an appropriate roughness length is important for the good performance of the dispersion model because the roughness length is used to estimate the boundary layer wind speed from the surface wind measurement. Near surface releases within the TIBL are affected by the roughness length through the surface friction velocity. These results suggest the need for paying attention to estimating the roughness length under spatially inhomogeneous conditions.

6. CONCLUSIONS

The research reported in this dissertation is motivated by the need to apply dispersion models in spatially inhomogeneous surfaces such as urban areas. The first part of my thesis deals with methods to estimate micrometeorological inputs in urban areas. The second part of my thesis describes the development and evaluation of dispersion models that can be applied to sources located close to the land-water interface on coastlines.

The methods to estimate micrometeorological inputs from tower measurements are based on the concept of local homogeneity, which assumes that methods developed for spatially homogeneous conditions, such as Monin-Obukhov similarity theory (MOST), can be applied to estimate variables in the vicinity of the measurement location. The major conclusions from my research are:

1. During unstable conditions, measurements of standard deviation of temperature fluctuations can provide adequate estimates of local heat flux using free convection theory. However, these estimates are generally higher than the observations.
2. The bias in heat flux estimates can be reduced through a stability correction that based on the measured wind speed.
3. MOST provides unbiased estimates of surface friction velocity and turbulent velocities, σ_w and σ_v, using heat flux estimates and measured wind speeds as inputs.

4. The ability to make estimates of micrometeorological variables is crucially dependent on adequate estimates of the aerodynamic roughness length at the site of interest.
5. Discrepancies between estimated and observed surface friction velocity and heat flux estimates leads to inevitable scatter in concentration estimates for near surface line and point sources, although the impact is less for small downwind distances relative to the Obukhov length.

A two-dimensional internal boundary-layer (IBL) model was used to estimate urban meteorological variables from suburban measurements. This model assumes that meteorological variables over the suburban and urban sites are the same at the height of the internal boundary layer, and Monin-Obukhov similarity theory is applicable below the IBL height over the urban site. The major conclusions of this research are:

1. During stable suburban conditions, the best estimates of meteorological variables correspond to neutral conditions without stability correction.
2. The IBL model overestimates the friction velocity measured within the roughness sublayer (RSL) of the urban site.
3. Using a friction velocity profile (Rotach, 2001) within the RSL reduces the overestimation. However, the accuracy of this method depends on the appropriate estimates of both surface roughness parameters and the RSL height.

The second part of my thesis focuses on the development and testing of dispersion models during low wind speed stable conditions, which frequently occur over urban areas. The first model is based on the numerical solution of the steady state mass conservation equation in which the wind speed and eddy diffusivity follow vertical profiles consistent with .MOST. The second model, incorporated in AERMOD (Cimorelli et al., 2005), is a steady state Gaussian dispersion model, which accounts for wind meandering under low wind speed conditions. These models were evaluated with data from the Prairie Grass experiment (Barad, 1958) and the Idaho Falls experiment (Sagendorf and Dickson, 1974). The results from this evaluation are:

1. The model based on advection-diffusion equation performs better than AERMOD during low wind stable conditions through a justifiable description of the interaction between dispersion and the gradient of the wind speed near the surface.
2. Accounting for the meandering effect in the numerical model leads to improvements in model performance when meandering cannot be neglected. However, steady-state models can not explain the concentration distribution when the meandering effect is large.

This study also examined the estimation of surface micrometeorology under low wind stable conditions. The major conclusions are:

1. MOST leads to underestimation of friction velocity during low wind speed conditions.
2. This underestimation is reduced through a modification in the formula to estimate the friction velocity during such conditions.
3. Estimates of horizontal turbulent velocity based on linear proportionality with friction velocity do not compare well with observations.

4. The modified friction velocity leads to better concentration estimates as long as the observed horizontal turbulent velocity is used.
5. Uncertainties in estimates of horizontal turbulent velocities result in errors in horizontal plume spread estimates, which in turn lead to scatter in concentration estimates.

The last part of my thesis evaluates a shoreline dispersion model that is modified to be compatible with the one-dimensional structure of AERMOD, the USEPA recommended model. The shoreline dispersion model accounts for entrainment of an elevated plume by the growing thermal internal boundary layer (TIBL) through a simple modification of the stable dispersion equation in AERMOD. The model was evaluated with data from field studies conducted in Wilmington (Yuan, et al. 2006; Princevac and Venkatram, 2007; Venkatram and Princevac, 2008) and Nanticoke (Misra and Onlock, 1982). The major conclusions from this evaluation are:

1. The model performs well when meteorological inputs are derived from onsite measurements at Wilmington and Nanticoke experiment.
2. AERMET, AERMOD's meteorological processor, was modified with the two-dimensional TIBL model to produce meteorological inputs for the shoreline dispersion model. Model performance using meteorology estimated with this method is comparable to that using onsite measurements. Surface parameters such as cloud cover, albedo and Bowen ratio need to be chosen appropriately to yield adequate estimates of heat flux.

3. The performance of the shoreline dispersion model is not sensitive to Bowen ratio varying from 1 – 2 as long as net radiation is available.
4. Results also show that choosing an appropriate roughness length is also important to the good performance of the dispersion model.

7. REFERENCES

Aditi and M. Sharan, (2007) Analysis of weak wind stable conditions from the observations of the land surface processes experiment at Anand in India, Pure Appl. Geophys. 164, pp. 1811–1837.

Albertson JD, Parlange MB, Katul GG, Chu CR, Stricker H, Tyler S (1995) Sensible heat flux from arid regions using a simple flux-variance method, Water Resour. Res. 31, 969–973.

Allwine, K.J., and J.E. Flaherty: 2006, Joint Urban 2003: Study Overview and Instrument Locations. PNNL-15967, Pacific Northwest National Laboratory, Richland, WA.

Allwine, K. J., M. J. Leach, L. W. Stockham, J. S. Shinn, R. P. Hosker, J. F. Bowers, and J. C. Pace, 2004: Overview of Joint Urban 2003—An atmospheric dispersion study in Oklahoma City. Symp. on Planning, Nowcasting, and Forecasting in the Urban Zone, Seattle, WA, Amer. Meteor. Soc.

Allwine, K.J., J.H. Shinn, G.E. Streit, K.L. Clawson and M. Brown, (2002) Overview of URBAN 2000: a multiscale field study of dispersion through an urban environment, Bulletin of the American Meteorological Society 83, pp. 521–536.

Anfossi, D., Alessandrini, S., Trini Castelli, S., Ferrero, E., Oettl, D., 2006. Tracer dispersion simulation in low wind speed conditions with a new 2D Langevin equation system. Atmospheric Environment 40, 7234–7245.

Anfossi, D., D. Oettl, G. Degrazia and A. Goulart, (2005) An analysis of sonic anemometer observations in low wind speed conditions, Boundary Layer Meteorology 114, pp. 179–203.

Arnold, S., H. ApSimon, J. Barlow, S. Belcher, M. Bell, D. Boddy, R. Britter, H. Cheng, R. Clark, R. Colvile, S. Dimitroulopoulou, A. Dobre, B. Greally, S. Kaur, A. Knights, T. Lawton, A. Makepeace, D. Martin, M. Neophytou, S. Neville, M. Nieuwenhuijsen, G. Nickless, C. Price, A. Robins, D. Shallcross, P. Simmonds, R. Smalley, J. Tate, A. Tomlin, H. Wang and P. Walsh, Dispersion of air pollution and penetration into the local environment, DAPPLE, Science of the Total Environment 332 (2004), pp. 139–153.

Arya, S. P. (1995) Modelling and parameterization of nearsource diffusion in weak winds. Journal of Applied Meteorology 34, 1112-1122.

Arya, S.P. (1999) Air Pollution Meteorology and Dispersion. Oxford University Press, New York, 320pp.

Barad ML (Ed.) (1958) Project Prairie Grass. A field program in diffusion, Geophysical Research Paper No. 59, vols. I (300 pp.) and II (221 pp.), AFCRF-TR-58-235, Air Force Cambridge Research Center, Bedford, MA.

Basu S, Porté-Agel F, Foufoula-Georgiou E, Vinuesa J-F, Pahlow M (2006) Revisiting the local scaling hypothesis in stably stratified atmospheric boundary-layer turbulence: an integration of field and laboratory measurements with large-eddy simulations. Boundary-Layer Meteorol 119:473–500

Beljaars, A.C.M., and A.A.M. Holtslag, (1991) Flux parameterization over land surfaces for atmospheric models. Journal of Applied Meteorology 30, pp. 327–341.

Bornstein, R.D., 1968 Observations of the urban heat island effect in New York City, J. appl. Met. 7, pp. 575–582.

Britter RE, Hanna SR (2003) Flow and dispersion in urban areas. Ann. Rev. Fluid Mech. 35, 469–496.

Briggs, G.A., 1973: Diffusion estimation for small emissions. ERL, ARL USAEC Report ATDL-106, US Atomic Energy Commission, Oak Ridge, TN.

Briggs, G.A. (1992), Stagnation diffusion observed in a deeply pooling valley during STAGMAP. Preprints, Tenth Symposium on Turbulence and Diffusion, September 29 - October 2, 1992, Portland, Oregon. American Meteorological Society, Boston, 155-162.

Brusasca, G., Tinarelli, G., Anfossi, D., 1992. Particle model simulation of diffusion in low windspeed stable conditions. Atmospheric Environment 26A, 707– 723.

Businger JA (1973) Turbulent Transfer in the Atmospheric Surface Layer, in D. H. Haugen (ed.), Workshop on Micrometerology, Am. Meteorol. Soc., Boston, MA, pp. 67–100.

Businger, J. A., Wyngaard, J. C., Izumi, Y., and Bradley, E. F.: 1971, Flux– profile Relationships in the Atmospheric Surface Layer, J. Atmos. Sci. 28, 181-189.

Camuffo D, Bernardi A (1982) An Observational Study of Heat Fluxes and Their Relationship with Net Radiation, Boundary-Layer Meteorol. 23, 359–368.

Carruthers DJ, Holroyd RJ, Hunt JCR, Weng W-S, Robins AG, Apsley DD, Thompson DJ, and Smith FB, (1994) UK-ADMS: A new approach to modelling dispersion in the earth's atmospheric boundary layer. J Wind Eng Ind Aerodyn 52, 139-153.

Carson DJ (1973) The development of a dry inversion-capped convectively unstable boundary layer, Q. J. Roy. Meteorol. Soc. 99, 450–467.

Carson, D.J., and P.J.R. Richards, Modelling surface turbulent fluxes in stable conditions. Boundary-Layer Meteorology 14 (1978), pp. 67–81.

Caughey, S. J., Wyngaard, J. C., and Kaimal, J. C., (1979), Turbulence in the Evolving Stable Boundary Layer, Journal of the Atmospheric Sciences 36, 1041-1052.

Chang JC, Hanna SR, (2004), Air quality model performance evaluation. Meteorol. Atmos. Phys. 87, 167–196.

Cheng, H. and Castro, I. P.: 2002, Near Wall Flow over Urban-Like Roughness, Boundary-Layer Meteorol. 104, 229–259.

Ching, JKS (1985) Urban-scale variations of turbulence parameters and fluxes, Boundary-Layer Meteorol. 33, 335–361.

Christen A, (2005) Atmospheric turbulence and surface energy exchange in urban environments. PhD-Thesis in Meteorology. Institute of Meteorology, Climatology and Remote Sensing University of Basel, 142 pp.

Christen A, Rotach MW (2004) Estimating wind speed at an urban reference height. Fifth Symposium on the Urban Environment (AMS), Vancouver, Canada, 23–28 August 2004.

Christen, A., R. Vogt, M.W. Rotach and E. Parlow, First results from Bubble, Partitioning of turbulent heat fluxes and urban surfaces. AMS Conference on the Urban Environment (2002) pp. 105–106.

Cimorelli, J. A., Perry, G. S., Venkatram, A., Weil, C. J., Paine, J. R., Wilson, B. R., Lee, F. R., Peters, D. W., Brode, W. R., 2005: AERMOD: A Dispersion Model for Industrial Source Applications. Part I: General Model Formulation and Boundary Layer Characterization. J. Appl. Met., 44, pp. 682–693.

Cionco, R.M, A mathematical model for air flow in a vegetative canopy, J. Appl. Meteorol. 4 (1965), pp. 517–522.

Clarke JF, Ching JKS, and Godowitch JM (1982) An experimental study of turbulence in an urban environment. Tech. Rep. EPA 600/3-82-062, U.S. Environmental Protection Agency, Research Triangle Park, NC, 150 pp.

Deaves, D. M. and Lines, I. G.: 1998. The Nature and Frequency of Low Wind Speed Conditions, J. Wind Eng. Ind. Aerodyn. 73, 1– 29.

De Bruin, H.A.R., and A.A.M. Holtslag, 1982: A Simple Parameterization of the Surface Fluxes of Sensible and Latent Heat During Daytime Compared with the Penman-Monteith Concept. , 21, 1610–1621.

De Bruin HAR, Kohsiek W, Van Den Hurk BJJM (1993) A Verification of Some Methods to Determine the Fluxes of Momentum, Sensible Heat and Water Vapour Using Standard Deviation and Structure Parameter of Scalar Meteorological Quantities, Boundary-Layer Meteorol. 63, 231–257.

Doll, D., Ching, J. K. S. and Kaneshire, J.: 1985, Parameterization of Subsurface Heating for Soil and Concrete using New Radiation Data, Boundary-Layer Meteorol. 32, 351–372.

Doran, J. C., J.D. Fast & J. Horel: The VTMX 2000 Campaign, Bull. American Meteor. Soc., 83(4), 537–551, 2002.

Dyer, A. J. and Hicks, B. B.: 1970, Flux– Gradient Relationships in the Constant Flux Layer, Quart. J. Roy. Meteorol. Soc. 96, 715-721.

Dyer, A. J.: 1974, A Review of Flux-Profile-Relationships, Boundary-Layer Meteorol. 7, 363-372.

Eckman RM, (1994) Re-examination of empirically derived formulas for horizontal diffusion from surface sources. Atmos Environ 28, 265-272.

Feigenwinter C (2000), The vertical structure of turbulence above an urban canopy, PhD thesis, University of Basel, Institue of Meteorology, Climatology and Remote Sensing, 84 pp.

Feigenwinter, C., R. Vogt, and E. Parlow, 1999: Vertical Structure of Selected Turbulence Characteristics above an Urban Canopy. Theoretical and Applied Climatology, 62, 51-63.

Foken T (2006) 50 years of the Monin–Obukhov similarity theory. Boundary-Layer Meteorol 119:431–447

Gamo, M. S.: 1981, A Study on the Structure of the Free Convective Internal Boundary Layer During the Sea Breeze. Report of the National Research Institute for Pollution and Resources (Japan) # 19, 89 pp.

Gamo, M., Yamamoto, S., and Yokoyama, O.: 1982, ‘Airborne Measurements of the Free Convective Internal Boundary Layer During the Sea Breeze’, J. Meteorol. Sot. Japan 60, 1284-1298.

Garratt JR (1980) Surface Influence Upon Vertical Profiles in the Atmospheric Near-Surface Layer, Q. J. Roy. Meteorol. Soc. 106, 803–819.

Garratt JR (1983) Surface influence upon vertical profiles in the nocturnal boundary layer. Boundary-Layer Meteorol. 26, 69–80.

Garratt, J. R. 1990, The Internal Boundary Layer – A Review, Boundary-Layer Meteorol. 50, 171–203.

Garratt JR (1992) The Atmospheric Boundary Layer, Cambridge University Press, Cambridge, 316 pp.

Gifford, F. A.: 1960, Peak to Average Concentration Ratios According to a Fluctuating Plume Dispersion Model, Int. J. Air Pollut. 3, 253–260.

Grimmond CSB, Cleugh HA, and Oke TR (1991) An objective urban heat storage model and its comparison with other schemes, Atmos. Environ. 25B, 311–326.

Grimmond CSB, Oke TR (1999a) Heat storage in urban areas: local-scale observations and evaluation of a simple model, J. Appl. Meteorol. 38, 922-940.

Grimmond CSB, Oke TR (1999b) Aerodynamic properties of urban areas derived from analysis of surface form, J. Appl. Meteorol. 38, 1261–92.

Grimmond C. S. B., Oke TR 2002: Turbulent heat fluxes in urban areas: Observations and local-scale urban meteorological parameterization scheme (LUMPS). *J. Appl. Meteor.*, 41, 792–810.

Grimmond, C. S. B., Salmond, J. A., Oke, T. R., Offerle, B. and Lemonsu, A., 2004. Flux and turbulence measurements at a dense urban site in Marseille: Heat, Mass (water, carbon dioxide) and Momentum. Journal of Geophysical Research, 109, D24101, 19p.

Hanna, S. R., 1983: Lateral turbulence intensity and plume meandering during stable conditions. J. Climate Appl. Meteor., 22, 1424–1430.

Hanna, S. R.: 1990, Lateral Dispersion in Light-Wind Stable Conditions, Nuovo Cimento 13, 889– 894.

Hanna, S.R., Briggs, G.A., Hosker, R.P., 1982. Handbook on Atmospheric Diffusion. DOE/TIC-11223 (DE82-002045), NTIS/USDOC, Springfield, VA, 102pp.

Hanna S.R., Britter R.E., (2002), Wind Flow and Vapor Cloud Dispersion at Industrial Sites. New York: Am. Inst. Chem. Eng.

Hanna, S.R., Britter, R.E., and Franzese, P., 2003: A baseline urban dispersion model evaluated with Salt Lake City and Los Angeles Tracer data, Atmospheric Environment, 37, 5069–5082.

Hanna, S.R., M.J. Brown, F.E. Camelli, S. Chan, W.J. Coirier, O.R. Hansen, A.H. Huber, S. Kim and R.M. Reynolds, Detailed simulations of atmospheric flow and dispersion in urban downtown areas by computational fluid dynamics (CFD) models – an application of five CFD models to Manhattan, Bull. Am. Meteorol. Soc. 87 (2006), pp. 1713–1726.

Hanna SR, Chang JC (1992) Boundary layer parameterizations for applied dispersion modeling over urban areas, Boundary-Layer Meteorol. 58, 229–259.

Hanna, S.R. and R.J. Paine, 1989: Hybrid Plume Dispersion Model (HPDM) development and evaluation. J. Appl. Meteorol., 28, 206–224.

Hanna, S.R., J. White and Y. Zhou, (2007) Observed winds, turbulence, and dispersion in built-up downtown areas in Oklahoma City and Manhattan, Bound-Lay. Meteorol. 125, pp. 441–468.

Harman IN, Finnigan JJ (2007) A simple unified theory for flow in the canopy and roughness sublayer, Boundary-Layer Meteorol. 123, 339–363.

Hicks B (1981) An examination of turbulence statistics in the surface boundary layer, Boundary-Layer Meteorol. 21, 389–402.

Högström, U.: 1988, Non-dimensional Wind and Temperature Profiles in the Atmospheric Surface Layer: A Re-evaluation, Boundary-Layer Meteorol. 42, 55-78.

Holtslag, A.A.M., and H.A. de Bruin, Applied modelling of the nighttime surface energy balance over land. *Journal of Applied Meteorology* 27 (1988), pp. 689–704.

Holtslag AAM, van Ulden AP (1983) A simple scheme for daytime estimates of the surface fluxes from routine weather data, J. Clim. Appl. Meteorol. 22, 517–529.

Howell, J. F. and Mahrt, L.: 1997, 'Multiresolution Flux Decomposition', Boundary-Layer Meteorol. 83, 117–137.

Howell, J.F., and J. Sun, (1999) Surface-layer fluxes in stable conditions. Boundary-Layer Meteorology 90, pp. 495–520.

Hsieh CI, Katul GG, Scheildge J, Sigmon JT, Knoerr KR (1996) Estimation of Momentum and Heat Fluxes Using Dissipation and Flux-Variance Methods in the Unstable Surface Layer, Water Resour. Res. 8, 2453–2462.

Izumi, Y.: 1971, Kansas 1968 Field Program Data Report. Bedford, MA, Air Force Cambridge Research Papers, No. 379, 79 pp.

Kastner-Klein P, Rotach MW (2004) Mean flow and turbulence characteristics in an urban roughenss sublayer. Boundary-Layer Meteorol. 111, 55–84.

Kaimal JC, and Finnigan JJ (1994) Atmospheric Boundary Layer Flows, Their Structure and Measurement, Oxford University Press, New York, 289 pp.

Kasten, F., Czeplak, G.: (1980) Solar and Terrestrial Radiation Dependent on the Amount and Type of Cloud. Solar Energy*24*, 177–189.

Kerman, B. R., Mickle, R. E., Portelli, R. V., Trivett, N. B., and Misra, P. K.: 1982, 'The Nanticoke Shorelme Diffusion Experiment, June 1978, II. Internal Boundary Layer Structure', Aimos. Environ. 16,423-437.

Lloyd CR, Culf AD, Doman AJ, Gash JH (1991) Estimates of sensible heat flux from observations of temperature fluctuations, Boundary-Layer Meteorol. 57, 311–322.

Luhar AK, Hurley PJ, Rayner KN (2009) Modelling near-surface low winds over land under stable conditions: sensitivity tests, flux–gradient relationships, and stability parameters. Boundary-Layer Meteorology 130, 249–274.

Luhar, A.K., Venkatram A., Lee SM., 2006, On relationships between urban and rural near-surface meteorology for diffusion applications, Atmospheric Environment 40, 6541-6553.

Lyons, W. A., 1977: Mesoscale Air Pollution Transport in Southeast Wisconsin, EPA 600/4-77-010. U.S. Environmental Protection Agency.

Lyons, W. A., and H. S. Cole, 1973: Fumigation and trapping on the shores of Lake Michigan during stable onshore flow. J. Appl. Meteor., 12, 494–510.

Macdonald, R.W., (2000) Modeling the mean velocity profile in the urban canopy layer. Bound. Layer Meteorol. 97, 25–45.

Mahrt, L., 1998: Stratified atmospheric boundary layers and breakdown of models. J. Theor. Comp. Fluid Dyn., 11, 263-280.

Marht, L., 1999: Stratified atmospheric boundary layer. Bound.-Layer Meteor., 90, 375–396.

McElroy, J.L., Pooler, F., 1968a. The St. Louis Dispersion Study - Instrumentation, Procedures, and Data Tabulations, vol. I. National Air Pollution Control Administration, Pub. No. APTD-68-12, US DHEW, Arlington.

McElroy, J.L., Pooler, F., 1968b. The St. Louis Dispersion Study - Analysis, vol. II. National Air Pollution Control Administration, Pub. No. AP-53, US DHEW, Arlington.

Mestayer PG, Durand P, Augustin P, Bastin S, Bonnefond J-M, Bénech B, Campistron B, Coppalle A, Delbarre H, Dousset B, Drobinski P, Druilhet A, Fréjafon E, Grimmond CSB, Groleau D, Irvine M, Kergomard C, Kermadi S, Lagouarde J-P, Lemonsu A, Lohou F, Long N, Masson V, Moppert C, Noilhan J, Offerle B, Oke TR, Pigeon G, Puygrenier V, Roberts S, Rosant J-M, Sanid F, Salmond J, Talbaut M, Voogt J (2005) The urban boundary-layer field campaign in marseille (ubl/clu-escompte): set-up and first results. Boundary-Layer Meteorol 114:315–365

Misra, P. K., 1980: Dispersion from tall stacks into a shore line. Atmos. Environ., 14, pp. 397-400.

Misra, P.K. and S. Onlock, 1982: Modelling continuous fumigation of Nanticoke generation station plume. Atmospheric Environment 16 3, pp. 479–489.

Mitchell, J.M. Jr., 1961: The temperature of cities, Weatherwise 14, pp. 224–229.

Monin, A. S. and Obukhov, A. M.: 1954, Osnovnye zakonomernosti turbulentnogo peremeshivanija v prizemnom sloe atmosfery (Basic Laws of Turbulent Mixing in the Atmosphere Near the Ground), Trudy geofiz. inst. AN SSSR 24(151), 163-187.

Monin AS, Yaglom AM (1971) Statistical fluid mechanics: mechanics of turbulence, Vol. 1, MIT Press, Cambridge, Massachusetts, 769 pp.

Monteith JL (1981) Evaporation and Surface Temperature, Q. J. Roy. Meteorol. Soc. 107, 1–27.

Nieuwstadt FTM (1980) Application of Mixed-Layer Similarity to the Observed Dispersion from a Ground-Level Source. J. Appl. Meteorol. 19, 157–162.

Nieuwstadt, F. T. M.: 1984, The Turbulent Structure of the Stable Nocturnal Boundary Layer, *J. Atmos. Sci.* 41, 2202–2216.

Nieuwstadt FTM, and van Ulden AP, (1978) A Numerical Study on the Vertical Dispersion of Passive Contaminants from a Continuous Source in the Atmospheric Surface Layer, Atmos Environ 12, 2119–2124.

Obukhov, A. M.: 1946, Turbulentnost’ v temperaturnoj – neodnorodnoj atmosfere (Turbulence in an Atmosphere with a Non-uniform Temperature), Trudy Inst. Theor. Geofiz. AN SSSR 1, 95–115.

Oettl, D., Almbauer, R.A., Sturm, P.J., 2001. A new method to estimate diffusion in stable, low wind conditions. Journal of Applied Meteorology 40, 259-268.

Oikawa S, and Meng Y (1995) Turbulence characteristics and organized motion in a suburban roughness sublayer. Boundary-Layer Meteorol. 74, 289–312.

Oke, T. R.: 1978, Surface Heat Fluxes and the Urban Boundary Layer, WMO Symp. Bound. Layer Physics Appl. Specific Problems Air Poll., WMO No. 510, World Meteorol. Organiz., Geneva, pp. 63–70.

Oke, T. R. (1988), Boundary layer climates, Routledge, London, pp. 464.

Oke, T. R. and Cleugh, H. A.: 1987, Urban Heat Storage Derived as Energy Balance Residuals, Boundary-Layer Meteorol. 39, 233–245.

Paltridge, G. W. and Platt, C. M. R.: 1976, Radiative Processes in Meteorology and Climatology, Elsevier Scientific Publishing Company, Amsterdam. 318 pp.

Panofsky, H.A., and Dutton, J.A., (1984), Atmospheric Turbulence, Wiley, New York, 397pp.

Panofsky HA, Tennekes H, Lenschow DH, Wyngaard JC (1977) The characteristics of turbulent velocity components in the surface layer under convective conditions, Boundary-Layer Meteorol. 11, 355–359.

Plate, E. J.: 1971, Aerodynamic Characteristics of Atmospheric Boundary Layers, United State Atomic Energy Commission, 190 pp.

Portelli, R.V. (1979) The Nanticoke Study: Experimental Investigation of Diffusion from Tall Stacks in a Shoreline Environment, Presented at the NATO-CCMS Conference Rome, Italy.

Portelli, R. B.: 1982, 'The Nanticoke Shoreline Diffusion Experiment, June 1978 1, Experimental Design and Program Overview', Atmos. Env. 16, 413-421.

Princevac M, Venkatram A (2007) Estimating micrometeorological inputs for modeling dispersion in urban areas during stable conditions, Atmos. Environ. 41, 5345–5356.

Qian, W., M., Princevac, and A., Venkatram, 2010, Using Measurements in Suburban and Urban Areas to Estimate Meteorology for Modeling Dispersion during Convective Conditions, Boundary-Layer Meteorology 135, p269-289.

Raupach, M. R., Antonia, R. A., and Rajagopalan, S.: 1991, Rough-Wall Turbulent Boundary Layers, Appl. Mech. Rev. 44, 1–25.

Raupach MR, Thom AS. 1981. Turbulence in and above plant canopies. Annual Review of Fluid Mechanics. 13: 97-129.

Raynor, G. S., Michael, P., Brown, R. M., and SethuRaman, S.: 1975, Studies of Atmospheric Diffusion From a Nearshore Oceanic Site', J. App. Meteorol. 14, 1080-1094.

Raynor, G. S., SethuRaman, S., and Brown, R. M., 1979: Formation and Characteristics of coastal Internal Boundary Layers During Onshore Flows, Boundary Layer Meteorol. 16, 487-514.

Rotach, M. W.: 1993, Turbulence Close to a Rough Urban Surface Part I: Reynolds Stress, Boundary-Layer Meteorol. 65, 1–28.

Rotach MW (1993), Turbulence Close to a Rough Urban Surface, Part II: Variances and Gradients, Boundary-Layer Meteorol. 66, 75–92.

Rotach MW. 1995. Profiles of turbulence statistics in and above an urban street canyon. Atmospheric Environment 29: 1473–1486.

Rotach MW (1999) On the Influence of the Urban Roughness Sublayer on Turbulence and Dispersion, Atmos. Environ. 33, 4001–4008.

Rotach, M.W.: 2001, Simulation of urban-scale dispersion using a lagrangian stochastic dispersion model, Boundary Layer Meteorology 99, pp. 379-410

Rotach, M.W., Vogt, R., Bernhofer, C., Batchvarova, E., Christen, A., Clappier, A., Feddersen, B., Gryning, S.-E., Martucci, G., Mayer, H., Mitev, V., Oke, T.R., Parlow, E., Richner, H., Roth, M., Roulet, Y.-A., Ruffieux, D., Salmond,,J.A., Schatzmann, M., Voogt, J.A., 2005: BUBBLE – an Urban Boundary Layer Meteorology Project. Theoretical and Applied Climatology 81, 231–261.

Roth M (1993), Turbulent transfer relationships over an urban surface. II. Integral statistics, Q. J. Roy. Meteorol. Soc. 119, 1105–1120.

Roth M. 2000. Review of atmospheric turbulence over cities. Quarterly Journal of the Royal Meteorological Society 126: 941-990.

Roth M, and Oke TR (1995) Relative efficiencies of turbulent transfer of heat, mass and momentum over a patchy urban surface. J. Atmos. Sci. 52, 1863-1874.

Sagendorf, J. F. and Dickson, C. R.: 1974, Diffusion under Low Windspeed, Inversion Conditions, NOAA Technical Memorandum ERL ARL-52, 89 pp.

Salmond, J.A. and McKendry, I.G. (2005) Turbulence in the very stable nocturnal boundary layer: Implications for air pollution, Progress in Physical Geography. Vol. 29, No. 2, p171-188

Savelyev, S.A., Taylor, P.A., 2005: Internal boundary layers: I. Height formulae for neutral and diabatic flows. Boundary-Layer Meteorology 115, 1–25.

Sharan, M., Rama Krishna, T.V.B.P.S., Aditi, 2003. Surface layer characteristics in strong and weak wind stable boundary layers. Boundary Layer Meteorology 108, 257–288.

Sharan, M. Yadav, A. K. and Singh, M. P. (1995) Comparison of sigma schemes for air pollutant dispersion in low winds. Atmospheric Environment 29, 2051-2059.

Sharan, M. and Yadav, A.K., 1998. Simulation of experiments under light wind, stable conditions by a variable K-theory model. Atmospheric Environment 32, pp. 3481–3492.

Smith, F.B., 1992. Low wind speed meteorology. In: *For Cambridge Atmospheric Dispersion Modelling Course, 6/7 July 1993 based on the paper presented at Riso in May 1992 and at ECCOMAS*.

Stull, R.B., 1988: An Introduction to Boundary-Layer Meteorology. Kluwer Academic Publishers, Dordrecht, pp. 666.

Swinbank, W. C., 1963: Long-wave radiation from clear skies. Quart. J. Roy. Meteor. Soc. 89, 330–348.

Swinbank, W. C.: 1964, The Exponential Wind Profile, Quart. J. Roy. Meteorol. Soc. 90, 119-135.

Taylor, G. I., 1921: Diffusion by continuous movements, Proc. London math. Soc., 20, pp. 196–212.

Tillman JE (1972) The indirect determination of stability, heat and momentum fluxes in the atmospheric boundary layer from simple scalar variables during dry unstable conditions, J. Appl. Meteorol. 11, 783–792.

Van der Hoven, I.: 1967, ‘Atmospheric Transport and Diffusion at Coastal Sites’, Nut. Safety 8,490-499.

van Dop, H., Steenkist, R., Nieuwstadt, F. T. M., 1979: Revised Estimates for Continuous Shoreline Fumigation, J. Appl. Met. 18, pp. 133-137.

van Ulden, A.P., 1978. Simple estimates for vertical dispersion from sources near the ground. Atmospheric Environment 12, 2125– 2129.

van Ulden, A. P. and A. A. M. Holtslag, 1985: Estimation of atmospheric boundary layer parameters for diffusion applications. J.Climate Appl.Meteor., 24, 1196-1207.

Venkatram, A., 1977: A model of internal boundary-layer development, Boundary-Layer Meteorology 11, pp. 419-437.

Venkatram, A., (1980), Estimating the Monin-Obukhov length in the Stable Boundary Layer for Dispersion Calculations. Boundary-Layer Meteorology 19, 481-485.

Venkatram, A.: 1986, An Examination of Methods to Estimate the Height of the Coastal Internal Boundary Layer, Boundary-Layer Meteorol. 36, 149–156.

Venkatram A (1992) Vertical dispersion of ground-level releases in the surface boundary layer, Atmos. Environ. 26, 947–949.

Venkatram, A., 2004: The role of meteorological inputs in estimating dispersion from surface releases. Atmospheric Environment 28, 2439-2446.

Venkatram A (2008), Computing and displaying model performance statistics, Atmos. Environ. 24, 6862-6868.

Venkatram, A., Isakov, V., Yuan, J., Pankratz, D., 2004: Modeling dispersion at distances of meters from urban sources, Atmospheric Environment, 38, 4633-4641.

Venkatram, A, and Princevac, M., 2008: Using measurements in urban areas to estimate turbulent velocities for modeling dispersion, Atmospheric Environment, 42, 3833–3841.

Vickers D., Mahrt L. (2003). The Cospectral Gap and Turbulent Flux Calculations. J. Atoms. Oceanic. Tech. 20:660–672.

Vickers D, Mahrt L. 2006. A solution for flux contamination by mesoscale motions with very weak turbulence. Boundary-Layer Meteorol. 118: 431-447.

Wang IT, Chen PC (1980) Estimation of Heat and Momentum Fluxes Near the Ground, Proc. 2nd Joint Conf. on Applications on Air Poll. Meteorol., AMS, 45 Beacon St., Boston, MA 02108, 764–769.

Weaver HL (1990) Temperature and humidity flux-variance relations determined by one-dimensional eddy correlation, Boundary-Layer Meteorol. 53, 77–91.

Webb, E. K.: 1970, Profile Relationships: The Log-Linear Range, and Extension to Strong Stability, Quart. J. Roy. Meteorol. Soc. 96, 67-90.

Wesely ML (1988) Use of variance techniques to measure dry air-surface exchange rates, Boundary-Layer Meteorol. 44, 13–31.

Wieringa J (1993) Representative roughness parameters for homogeneous terrain, Boundary-Layer Meteorol. 63, 323-393.

Yuan, J., Venkatram, A., Isakov, V., 2006: Dispersion from Ground-level Sources in a Shoreline Urban Area. Atmos. Environ. 40, pp. 1361-1372.

Zilitinkevich SS, Essau I. 2007. Similarity theory and calculation of turbulent fluxes at the surface for stably stratified atmospheric boundary layers. Boundary-Layer Meteorol. 125: 193-205.